Materials perspective on Casimir and van der Waals interactions

L. M. Woods*

Department of Physics, University of South Florida, Tampa, Florida 33620, USA

D. A. R. Dalvit

Theoretical Division, MS B213, Los Alamos National Laboratory, Los Alamos, New Mexico 87545, USA

A. Tkatchenko

Fritz-Haber-Institut der Max-Planck-Gesellschaft, D-14195 Berlin, Germany and Physics and Materials Science Research Unit, University of Luxembourg, L-1511 Luxembourg

P. Rodriguez-Lopez

Laboratoire de Physique Théorique et Modèles Statistiques and GISC, CNRS UMR 8626, Bât. 100, Université Paris-Sud, 91405 Orsay cedex, France

A. W. Rodriguez

Department of Electrical Engineering, Princeton University, Princeton, New Jersey 08540, USA

R. Podgornik

Department of Physics, University of Massachusetts, Amherst, Massachusetts 01003, USA, Department of Theoretical Physics, Jozef Stefan Institute, SI-1000 Ljubljana, Slovenia, and Department of Physics, Faculty of Mathematics and Physics, University of Ljubljana, SI-1000 Ljubljana, Slovenia

(published 2 November 2016)

Interactions induced by electromagnetic fluctuations, such as van der Waals and Casimir forces, are of universal nature present at any length scale between any types of systems. Such interactions are important not only for the fundamental science of materials behavior, but also for the design and improvement of micro- and nanostructured devices. In the past decade, many new materials have become available, which has stimulated the need for understanding their dispersive interactions. The field of van der Waals and Casimir forces has experienced an impetus in terms of developing novel theoretical and computational methods to provide new insights into related phenomena. The understanding of such forces has far reaching consequences as it bridges concepts in materials, atomic and molecular physics, condensed-matter physics, high-energy physics, chemistry, and biology. This review summarizes major breakthroughs and emphasizes the common origin of van der Waals and Casimir interactions. Progress related to novel *ab initio* modeling approaches and their application in various systems, interactions in materials with Dirac-like spectra, force manipulations through nontrivial boundary conditions, and applications of van der Waals forces in organic and biological matter are examined. The outlook of the review is to give the scientific community a materials perspective of van der Waals and Casimir phenomena and stimulate the development of experimental techniques and applications.

DOI: 10.1103/RevModPhys.88.045003

CONTENTS

I. Introduction 2
II. *Ab Initio* Methods for van der Waals Forces 3
A. Exact nonrelativistic treatment of microscopic van der Waals interactions 4
B. Response functions and polarization waves 4
C. Approximate microscopic methods for van der Waals interactions 5
1. Two-point density functionals for van der Waals interactions 6
2. Fragment-based methods for van der Waals interactions 6
3. Beyond pairwise additivity: Improved accuracy and efficiency via many-body van der Waals methods 7
D. Applications of atomistic van der Waals methods to materials 7

*Corresponding author.
lmwoods@usf.edu

 © 2016 American Physical Society

1. Finite and periodic molecular systems 8
2. Condensed materials 9
3. Interfaces between molecules and solids 9
III. Dirac Materials beyond Atomic Scale Separations 10
A. Lifshitz formalism 10
B. Basic properties of graphene nanostructures 11
C. Casimir interactions and graphene nanostructures 13
1. Graphene 13
2. Quasi-1D graphene nanostructures 16
D. Materials with topologically nontrivial phases 17
E. Possibility of Casimir repulsion in topological materials 18
IV. Structured Materials 20
A. Metamaterials 20
B. Photonic crystals 22
C. Plasmonic nanostructures 23
V. Nontrivial Boundary Conditions 25
A. Scattering methods 26
B. Stress-tensor methods 27
C. Casimir interactions in complex geometries 28
VI. Soft and Biological Materials 30
A. The importance of aqueous solvent 31
B. Lipid membranes 32
C. van der Waals torques 34
D. Electrostatic fluctuations 36
VII. Experiments Probing Materials Aspects of van der Waals and Casimir Interactions 37
VIII. Future Outlook 38
IX. Conclusions 39
Acknowledgments 39
References 39

I. INTRODUCTION

Phenomena originating from electromagnetic fluctuations play an important role in many parts of science and technology. The Casimir effect, first predicted as an attractive force between neutral perfect metals (Casimir, 1948), has made an especially large impact. This nonclassical electromagnetic force is typically associated with the coupling between objects with macroscopic dimensions. The same type of interaction known as a Casimir-Polder force concerns atom-surface configurations (Casimir and Polder, 1948). The conceptual realization of the Casimir and Casimir-Polder effects, however, is much more general. The connection of such interactions with broader definitions of "dispersion forces" establishes a close relationship with the van der Waals (vdW) force (Mahanty and Ninham, 1976; Barton, 1999; Parsegian, 2006). The common origin of vdW and Casimir interactions is directly related to their fluctuations nature, since at thermodynamic equilibrium the electromagnetic energy of dipoles (associated with the vdW force) can also be associated with the energy stored in their corresponding fluctuating electromagnetic fields (typically associated with the Casimir regime), as illustrated schematically in Fig. 1. The fact that these constitute the same phenomenon has been known for several decades. Specifically, Barash and Ginsburg (1984) write "The fluctuation nature of the van der Waals forces for macroscopic objects is largely the same as for individual atoms and molecules. The macroscopic and microscopic aspects of the theory of the van der Waals forces are therefore intimately related."

This ubiquitous force, present between any types of objects, has tremendous consequences in our understanding of interactions and stability of materials of different kinds, as well as in the operation of devices at the microscales and nanoscales. The Casimir force becomes appreciable for experimental detection at micron and submicron separations. After the first experimental confirmation (Sparnaay, 1958), subsequent and more precise measurements using torsional pendulum (Lamoreaux, 1997), atomic force microscope (AFM) (Mohideen and Roy, 1998), and micromechanical systems (MEMS) (Chan *et al.*, 2001; Decca *et al.*, 2003) were reported. It was realized that this interaction is especially relevant for nanomechanical and micromechanical devices, such as most electronic gadgets we use every day, where stiction and adhesion appear as parasitic effects (Serry, Walliser, and Maclay, 1995, 1998; Buks and Roukes, 2001).

van der Waals interactions are recognized to play a dominant role in the stability and functionality of materials with chemically inert components, especially at reduced dimensions. The most interesting recent example has been graphene and its related nanostructures (Novoselov *et al.*, 2004). The graphene Dirac-like spectrum together with the reduced dimensionality is responsible for novel behaviors in their Casimir and vdW forces. The graphene explosion in science and technology has stimulated discoveries of other materials, including 2D dichalcogenides, 2D oxides or other honeycomb layers, such as silicene, germanene, or stanene, where dispersive forces are of primary importance. Engineering heterostructures by stacking different types of layers via vdW assembly is an emerging field with many technological applications (Geim and Grigorieva, 2013). Other materials with Dirac spectra are also being

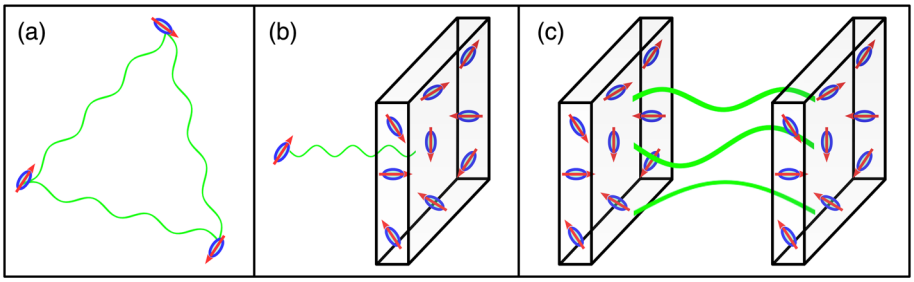

FIG. 1. Schematic representation of dispersive interactions induced by electromagnetic fluctuations for (a) the dipolar vdW force between atoms and molecules, (b) the Casimir-Polder force between atoms and large objects, and (c) the Casimir force between large objects. For small enough separations one can neglect retardation effects due to the finite speed of light c, which corresponds to the vdW regime. For large enough separations, retardation effects become important, which is characteristic for the Casimir regime.

investigated. For example, topological insulators, Chern insulators, and Weyl semimetals are very interesting for the Casimir or vdW field as the surface of such materials has a distinct nature from the bulk.

The importance of the vdW interaction extends to organic and biological matter. Perhaps the adhesion of the gecko, a type of lizard from the *Gekkota* infraorder, has become a pop-cultural poster child for such interactions after Autumn and co-workers (Autumn *et al.*, 2002) in a series of experiments showed that complex hierarchical nanomorphology of the gecko's toe pads (Lee, 2014) allow them to adhere to hydrophobic substrates (Autumn and Peattie, 2002). Dispersion forces play an important role in the organization of other biosystems, such as cellulose, lignin, and proteins. The stability of biological matter via an array of lipid membranes coupled through the vdW force is a fundamental problem of much current interest in soft matter physics.

The stability of many hard materials, including composites and heterostructures, is also closely related to their Casimir and vdW interactions. Its electromagnetic nature makes this phenomenon inherently long ranged as it depends in a complicated manner upon the electromagnetic boundary conditions and response properties of the materials. Metallic and dielectric structures of nontrivial shapes lend themselves as a platform where this aspect can be investigated in order to tailor this force in terms of its magnitude and sign. The payoff is highly beneficial in the context of being able to reduce the unwanted stiction and adhesion in nano-electro-mechanical and micro-electro-mechanical devices and improve their performance. Structured materials, including metamaterials, photonic crystals, and plasmonic nanostructures, on the other hand, allow the engineering of the optical density of states and magnetic response, which is also useful for manipulating the Casimir force.

Research published in the past decade has shown that the role of materials can hardly be overestimated when it comes to the description and understanding of dispersive interactions. In addition to recent books discussing basic concepts (Parsegian, 2006; Bordag, Klimchitskaya *et al.*, 2009; Dalvit *et al.*, 2011; Buhmann, 2012a, 2012b; Simpson and Leonhardt, 2015), there are several existing topical reviews on the Casimir effect with different emphasis. Aspects such as the quantum field theory nature (Bordag, Mohideen, and Mostepanenko, 2001; Milton, 2004), the quantum electrodynamics (QED) method (Buhmann and Welsch, 2007), experimental progress (Lamoreaux, 2005), the Lifshitz theory and proximity force approximation (PFA) with related experiments (Klimchitskaya, Mohideen, and Mostepananko, 2009), nontrivial boundary conditions (Dalvit *et al.*, 2011; Rodriguez, Capasso, and Johnson, 2011; Buhmann, 2012b; Reid, Rodriguez, and Johnson, 2013; Rodriguez *et al.*, 2015), and nanoscale aspects of long-ranged interactions (French *et al.*, 2010) have been summarized. Much of the research in these works has focused on utilizing the Lifshitz approach and its variations on the interplay between optical properties, thermal effects, and geometrical configurations in typical metals, semiconductors, and dielectrics.

A broader materials perspective of vdW and Casimir interactions has not been considered so far. With recent advances in materials science, especially in novel low-dimensional materials, composites, and biosystems, this field has become a platform for bridging not only distance scales, but also concepts from condensed-matter, high energy, and computational physics. There is an apparent need for discussing progress beyond the existing topical reviews via a materials perspective and give a broader visibility of this field. The purpose of this article is to summarize advances in the development and application of theoretical and computational techniques for the description of Casimir and vdW interactions guided and motivated by progress in materials discoveries. Each section of this review describes a separate direction defined by the type of systems, length scales, and applications of vdW and Casimir phenomena. An important goal of this review is to provide a succinct presentation of first-principles and coarse-grained computational methods, highlighting how the distance scale is interconnected with adequate microscopic and macroscopic descriptions of the materials themselves. We consider vdW and Casimir phenomena under equilibrium conditions, leaving aside other important effects including nonequilibrium or critical Casimir forces, which arguably warrant a separate review.

We begin the discussion with the vdW regime (Sec. II). The most significant advances in the past decade have been in the development of novel first-principles methods for vdW calculations. Much of this progress has been motivated by the need for an accurate description of vdW interactions in materials as well as relevant experimental measurements. In the next section (Sec. III), we move on to larger separation scales and focus on emerging materials with Dirac-like spectra, such as graphene and systems with nontrivial topological phases. By summarizing results obtained via the Lifshitz theory, QED approach, and perturbative Coulomb interaction calculations, we discuss how the Dirac spectra affect various characteristics of the vdW and Casimir forces. The following two sections are devoted to Casimir interactions in structured materials. We discuss how the force can be manipulated by engineering the response properties of materials and by the presence of nontrivial boundary conditions. For this purpose, we summarize important work in metamaterials, photonic crystals, and plasmonic nanostructures in Sec. IV. Progress in the development and application of brute-force computational techniques based on macroscopic electromagnetism for dealing with complex geometries in typical materials is presented in Sec. V, along with recent comparisons of exact predictions against well-established but *ad hoc* approximations, including the proximity-force and pairwise-additive approximations. Biological materials are included in Sec. VI by highlighting results obtained via the Lifshitz and Hamaker theory calculations. Fluctuation phenomena for biosystems are also discussed in light of other, Casimir-like phenomena. Much of this review is focused on the rapid expansion of theoretical and computational advances applied to the vdW and Casimir interactions, although key experiments giving us unprecedented insight into vdW and Casimir interactions are reviewed throughout the paper as well as in Sec. VII. In the last section, we give our outlook for the future by discussing open problems in this field.

II. *AB INITIO* METHODS FOR VAN DER WAALS FORCES

Noncovalent interactions between materials at separations on the Å to a few nm scale, especially those arising from

correlated electron fluctuations, play a key role in understanding their stability and organization. In recent years, important advances have been made toward computational methods for calculating vdW interactions with sufficient accuracy. These state-of-the-art methods are firmly based on a microscopic description of vdW interactions. Based on the treatment of the electron degrees of freedom of the atomistic system, we distinguish between two types of approaches: exact and approximate formulations of the many-body correlation energy. We discuss the essentials in terms of the adiabatic connection fluctuation-dissipation theorem (ACFDT), as both approaches rely on it. Based on the substantial evidence accumulated over the last few years, we argue that ubiquitous many-body effects in the vdW energy are crucial for accurate modeling of realistic materials. The inclusion of these effects in first-principles calculations and comparative performance evaluation for a wide range of materials, including finite and periodic molecular systems, (hard) insulating and semiconducting solids, and interfaces between organic and inorganic systems are also discussed.

A. Exact nonrelativistic treatment of microscopic van der Waals interactions

The exact energy of a microscopic system obtained via the solution of its Schrödinger equation seamlessly includes the vdW contribution. Explicitly solving the Schrödinger equation for more than a few electrons, however, is still a prohibitive task due to the complexity of the many-body problem. Therefore, first-principles modeling of realistic materials often starts with more tractable mean-field models, such as the Hartree-Fock approximation (HFA), or density-functional approximations (DFAs), which utilize the three-dimensional electron charge density $n(\mathbf{r})$ in lieu of the more complicated many-electron wave function. Unfortunately, these commonly utilized approximations are unable to describe the long-range electronic correlation energy and therefore fail to treat vdW interactions.

The vdW energy is directly related to the electron correlation energy E_c, which can be constructed exactly by invoking the ACFDT (Gunnarsson and Lundqvist, 1976; Langreth and Perdew, 1977)

$$E_c = -\frac{\hbar}{2\pi}\int_0^\infty d\omega \times \int_0^1 d\lambda \mathbf{Tr}\{[\chi_\lambda(\mathbf{r},\mathbf{r}',i\omega)-\chi_0(\mathbf{r},\mathbf{r}',i\omega)]v(\mathbf{r},\mathbf{r}')\}, \quad (1)$$

where $\chi_\lambda(\mathbf{r},\mathbf{r}',i\omega)$ and $\chi_0(\mathbf{r},\mathbf{r}',i\omega)$ are, respectively, the interacting at Coulomb coupling strength λ and bare (noninteracting) response functions. Here ω is the frequency of the electric field, $v(\mathbf{r},\mathbf{r}')=|\mathbf{r}-\mathbf{r}'|^{-1}$ is the Coulomb potential, and $\mathbf{Tr}$ denotes the spatial trace operator (six-dimensional integral) over the spatial electronic coordinates $\mathbf{r}$ and $\mathbf{r}'$. The essential idea is that Eq. (1) is an adiabatic connection between a reference noninteracting mean-field system with $\lambda=0$ and the fully interacting many-body system with $\lambda=1$. The vdW contribution can be found from E_c in a tractable manner provided that a set of single-particle orbitals computed with DFAs or HFA can be used to construct $\chi_0(\mathbf{r},\mathbf{r}',i\omega)$. This is still a formidable computational task for systems with thousands of electrons. In addition, approximations are needed to obtain $\chi_\lambda(\mathbf{r},\mathbf{r}',i\omega)$ for $0<\lambda\leq 1$.

The power and significance of the ACFDT approach is that essentially all existing vdW modeling methods can be derived from approximations to Eq. (1). For example, the widely employed pairwise approximation is obtained by truncating the ACFDT expression to second order in the perturbative expansion of the Coulomb interaction. The simple addition of interatomic vdW potentials that is used to compute the vdW energy in classical force fields and DFA calculations can be recovered from Eq. (1) by further approximating the response function as a sum of independent dipole oscillators located at every nucleus in a given material (Tkatchenko, Ambrosetti, and DiStasio, 2013). The vdW-DF approach originated by Langreth, Lundqvist, and collaborators (Dion *et al.*, 2004; Cooper, Kong, and Langreth, 2010; Lee *et al.*, 2010) that has become widely used to correct semilocal DFAs can also be derived from Eq. (1) by making a local approximation to the response function in terms of the electron density and then employing second-order perturbation theory. However, the main shortcoming of all these rather efficient approximations is that they are unable to capture the nontrivial many-body effects contained in the interacting response function $\chi_\lambda(\mathbf{r},\mathbf{r}',i\omega)$ as well as the infinite-order nature of the ACFDT expression in Eq. (1).

B. Response functions and polarization waves

The interacting response function is defined self-consistently via the Dyson-like equation

$$\chi_\lambda = \chi_0 + \chi_0(\lambda v + f_\lambda^{xc})\chi_\lambda, \quad (2)$$

which contains the exchange-correlation kernel $f_\lambda^{xc}(\mathbf{r},\mathbf{r}',i\omega)$, an unknown quantity which must be approximated in practice. Neglecting the explicit dependence of f_λ^{xc} on the coupling constant allows for an analytic integration over λ in Eq. (1) and forms the basis for the most widely employed approximation, namely, the random-phase approximation (RPA) (Bohm and Pines, 1953; Gell-Mann and Brueckner, 1957).

The noninteracting response function can be obtained using the Adler-Wiser formalism (Adler, 1962; Wiser, 1963), given a set of occupied and unoccupied electronic orbitals $\{\phi_i\}$ with corresponding energies $\{\epsilon_i\}$ and occupation numbers $\{f_i\}$ determined from semilocal density-functional theory (DFT), Hartree-Fock, or hybrid self-consistent field calculations, i.e.,

$$\chi_0(\mathbf{r},\mathbf{r}',i\omega)=\sum_{ij}(f_i-f_j)\frac{\phi_i^*(\mathbf{r})\phi_i(\mathbf{r}')\phi_j^*(\mathbf{r}')\phi_j(\mathbf{r})}{\epsilon_i-\epsilon_j+i\omega}. \quad (3)$$

This mean field χ_0 can exhibit relatively long-range fluctuations (polarization waves), the extent of which is determined by the overlap between occupied and rather delocalized unoccupied electronic states used in Eq. (3). In this framework, the fluctuations in χ_1 may be shorter ranged than in χ_0, especially in 3D solids where the Coulomb interaction leads to significant screening effects. The situation is generally very

different in anisotropic nanostructured materials, where the Coulomb interaction might lead to so-called *antiscreening* effects, i.e., significantly farsighted polarization waves [see Fig. 2(a)].

So far, the general understanding of polarization waves comes from coarse-grained approximations to the density-density response function. For example, Dobson, White, and Rubio (2006) found that the asymptotic vdW interaction between two low-dimensional metallic objects differs qualitatively from the commonly employed sum-over-pairs expressions. Another example is the vdW graphene-graphene interaction energy decays as d^{-3}, instead of the conventionally expected d^{-4} power law. Here, however, many-body renormalization of the Dirac graphene carriers beyond the RPA might lead to a vdW interaction power law between d^{-3} and d^{-4} (Dobson, Gould, and Vignale, 2014) (also discussed in Sec. III.C). This is a matter of ongoing debate.

For some time it was assumed that complete delocalization of fluctuations is required to identify interesting deviations from the otherwise pairwise-additive behavior. However, Misquitta *et al.* (2010, 2014) demonstrated that semiconducting wires also exhibit unusual asymptotics, which becomes more pronounced with the decrease of the band gap. In this case, the vdW interaction exhibited a power law of d^{-2} at large but finite distances, converging to the standard d^{-5} behavior for large interwire separations. Ambrosetti *et al.* (2016) analyzed the spatial extent of dipole polarization waves in a wide range of systems and demonstrated a continuous variation of the power law for finite distances between 1D wires and 2D layers with visibly enhanced nonlocal responses due to the collective many-body effects. Such relative *farsightedness* of vdW interactions provides an avenue for appropriately tuning the interactions between complex polarizable nanostructures.

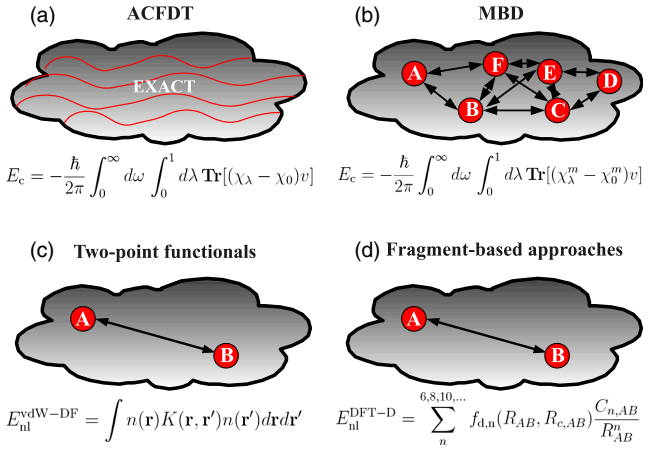

FIG. 2. Schematic representation of first-principles methods for the (a) exact formulation of the electronic correlation energy E_c from the adiabatic connection fluctuation-dissipation theorem; (b) formulation based on coupled dipolar fluctuations, such as the many-body dispersion (MBD) methods (Tkatchenko, DiStasio *et al.*, 2012; Ambrosetti, Reilly *et al.*, 2014); (c) E_c using two-point functionals obtained by approximating the nonhomogeneous system with a homogeneouslike response; and (d) fragment-based correlation energy obtained from multipolar expansions.

Another way to understand polarization waves in materials consists of studying the renormalization (nonadditivity) of polarizability and vdW coefficients for different systems as a function of their size and topology. Ruzsinsky *et al.* (2012) modeled the polarizability of fullerenes employing a hollow shell model with a finite thickness. They demonstrated that the polarizability scales superlinearly as a function of fullerene size. This leads to a superquadratic increase in the vdW C_6 coefficients, clearly demonstrating the importance of long-range fluctuations. Tao and Perdew (2014) extended these findings to a wide range of nanoclusters. Recently, Gobre and Tkatchenko (2013) studied the dependence of carbon-carbon vdW coefficients for a variety of carbon nanomaterials and they found that vdW C_6 coefficients could change from 20 to 150 hartree bohr^6 depending on the dimensionality, topology, and size of the carbon nanostructure. This demonstrates the extreme nonadditivity of vdW interactions in low-dimensional materials and highlights the need to include collective effects in vdW interactions when modeling the self-assembly of such nanostructures.

C. Approximate microscopic methods for van der Waals interactions

Since the vdW energy is a small part of the total energy of a many-electron system, vdW methods have to be coupled to an underlying electronic structure method that provides an adequate treatment of hybridization, charge transfer, electrostatics, and induced polarization, among other electronic structure effects. DFT with approximate exchange-correlation functionals provides an optimal approach in this regard. DFT is able to correctly describe short-range quantum-mechanical interactions and also treats classical electrostatic and polarization effects rather accurately. The total energy E_t of a many-electron system is

$$E_t = E_{\mathrm{kin}} + E_{\mathrm{es}} + E_x + E_c, \tag{4}$$

where E_{kin} is the electronic kinetic energy (corresponding to mean-field kinetic energy in the Kohn-Sham framework), E_{es} is the electrostatic energy (including nuclear repulsion, electron-nucleus attraction, and Hartree electron-electron repulsion), and E_x and E_c are the nonclassical exchange and correlation terms, respectively. Most DFT methods utilize semilocal approximations by using information about the electron density (local density approximation) and its gradients (generalized gradient approximation, GGA). Other approaches are based on the Laplacian of the electron density in the so-called meta-GGA functionals (Zhao and Truhlar, 2008; Sun *et al.*, 2013). It may also be advantageous to include a certain amount of exact Hartree-Fock exchange in the DFA, leading to so-called hybrid functionals.

We note that from ACFDT E_x and E_c are nonlocal [Eq. (1)]. The correlation energy E_c, which is of relevance to the vdW interaction, can be written as $E_c = E_{\mathrm{sl}} + E_{\mathrm{nl}}$, where E_{sl} is the semilocal correlation energy and E_{nl} is the nonlocal part. The fact that such partition is not unique has led to a flurry of heuristic approaches that aim to construct a reliable approximation to the full electronic correlation energy. The different classes of methods for the nonlocal correlation energy are

schematically shown in Fig. 2 and are summarized in what follows.

1. Two-point density functionals for van der Waals interactions

Obtaining an exact expression for $\chi_\lambda(\mathbf{r},\mathbf{r}',\omega)$ in general is not possible. However, for a 3D homogeneous electron gas the correlation energy can be written *exactly* in terms of the electron density $n(\mathbf{r})$. Approximating the polarization of a nonhomogeneous system assuming an homogeneouslike response is possible in certain situations (Rapcewicz and Ashcroft, 1991; Dobson and Dinte, 1996). These ideas have led to the derivation of the vdW-DF approach. In addition to the approximation of the interacting polarizability as a local quantity, one also takes a second-order approximation in Eq. (1) assuming $\chi_\lambda = \chi_1$. Thus the nonlocal correlation energy is obtained as

$$E_{\mathrm{nl}}^{\mathrm{vdW\text{-}DF}} = \int n(\mathbf{r}) K(\mathbf{r},\mathbf{r}') n(\mathbf{r}') d\mathbf{r} d\mathbf{r}', \tag{5}$$

where $K(\mathbf{r},\mathbf{r}')$ is a "vdW propagator" [Fig. 2(c)]. Note that Eq. (5) constitutes a great simplification over the exact Eq. (1) since only $n(\mathbf{r})$ and its gradient (utilized in K) are required.

The original implementation of this additive nonlocal correlation energy to the total DFT energy was proposed to couple $E_{\mathrm{nl}}^{\mathrm{vdW\text{-}DF}}$ to a revised Perdew-Burke-Ernzerhof functional (Zhang and Yang, 1998), the rationale being that this functional yields repulsive binding energy for prototypical vdW-bound systems, such as rare-gas dimers (Dion *et al.*, 2004). A follow-up implementation using the DFT functional PW86 (Lee *et al.*, 2010) has generated a revised, vdW-DF2 functional. While the vdW-DF2 approach was shown to perform much better for intermolecular interactions, its behavior at vdW distances is significantly deteriorated when compared to vdW-DF (Vydrov and Van Voorhis, 2010). Specifically, while the vdW C_6 coefficients in the vdW-DF method are accurate to 19%, the error increases to 60% when using vdW-DF2. These approaches illustrate the challenging problem of balancing between semilocal and nonlocal interactions in a meaningful manner.

Following the success of the vdW-DF approach, Vydrov and Van Voorhis (VV) provided a significantly simplified vdW functional derivation and revised the definition of local polarizability by employing a semiconductorlike dielectric function along with the Clausius-Mossotti relation between polarizability and dielectric function (Vydrov and Van Voorhis, 2009, 2012). The VV approach requires one parameter for the local polarizability and a second one for the coupling between the nonlocal vdW energy with the parent DFA approach. The VV functional was assessed with a wide range of semilocal and hybrid functionals, and by tuning these two parameters, it yielded remarkable performance for intermolecular interactions compared to benchmark data from high-level quantum-chemical calculations (Vydrov and Van Voorhis, 2012). Other approaches, such as the C09x functional of Cooper (2010) and the "opt" family by Klimeš, Bowler, and Michaelides (2010, 2011), rely on the same definition in Eq. (5); however, the coupling with the DFA is revised by adjusting one or more parameters in the semilocal functional. The opt functional parameters, in particular, were adjusted to a benchmark database of intermolecular interaction energies showing a good performance for cohesive properties of solids (Klimeš, Bowler, and Michaelides, 2011). There are indications, however, that the opt functionals overestimate the binding in larger and more complex molecular systems (Klimeš and Michaelides, 2012).

These recent developments have led to many novel insights into the nature of vdW interactions. However, the drastic approximations in $E_{\mathrm{nl}}^{\mathrm{vdW\text{-}DF}}$ in terms of the additive polarizability and the dependence on the electron density on two points only must be assessed carefully for realistic materials. The neglected nonadditive effects can play an important role in many systems (Dobson, White, and Rubio, 2006; Misquitta *et al.*, 2010, 2014; Ruzsinsky *et al.*, 2012; Gobre and Tkatchenko, 2013; Tao and Perdew, 2014; Tkatchenko, 2015; Ambrosetti *et al.*, 2016). Also, the neglected three-body Axilrod-Teller and higher-order terms may be quite prominent as well (Donchev, 2006; Shtogun and Woods, 2010; DiStasio, von Lilienfeld, and Tkatchenko, 2012; Tkatchenko, DiStasio *et al.*, 2012; Marom *et al.*, 2013; Ambrosetti, Alfe *et al.*, 2014; Kronik and Tkatchenko, 2014). At this point it is unclear how to incorporate higher-order terms in existing nonlocal vdW functionals without substantially increasing their cost. One possibility is going toward RPA-like approaches, but this would mean departing from a pure density-functional picture. Another possibility entails further coarse graining of the system to a fragment-based description, the progress of which is summarized next.

2. Fragment-based methods for van der Waals interactions

Fragment-based methods can be traced back to the original work of London (1930), in which case by utilizing second-order perturbation theory for the Coulomb interaction the dispersion energy between two spherical atoms A and B can be obtained. The London expression, often using just the dipolar term $C_{6,AB}/R_{AB}^6$, is the basis for calculating vdW dispersion energies in a wide range of atomistic methods, including Hartree-Fock calculations (Hepburn and Scoles, 1975; Ahlrichs, Penco, and Scoles, 1977), DFA calculations (Johnson and Becke, 2005; Grimme, 2006; Tkatchenko and Scheffler, 2009; Grimme *et al.*, 2010; Steinmann and Corminboeuf, 2011), and quantum chemistry methods (Tkatchenko *et al.*, 2009). $E_{\mathrm{vdW}}^{(2)}$ is valid only at large separations for which the overlap between orbitals of atoms A and B can be neglected. At shorter separations the overlap naturally reduces the interaction (Koide, 1976), which can be conveniently included by a *damping* function (Tang and Toennies, 1984; Johnson and Becke, 2005; Grimme, 2006; Tkatchenko and Scheffler, 2009; Grimme *et al.*, 2010)

$$E_{\mathrm{vdW}}^{(2)} = \sum_{n}^{6,8,10,\ldots} f_{\mathrm{d},n}(R_{AB},R_{c,AB}) \frac{C_{n,AB}}{R_{AB}^n}, \tag{6}$$

where $f_{\mathrm{d},n}(R_{AB},R_{c,AB})$ is the damping function that depends on a cutoff radius $R_{c,AB}$ [Fig. 2(d)]. This type of approach can be quite useful in DFA-GGA functionals, such as PBE (Perdew, Burke, and Ernzerhof, 1996), which perform very

well for chemical bonds. In this case, the dipolar approximation to Eq. (6) is sufficient (Elstner and Hobza, 2001; Wu *et al.*, 2001; Wu and Yang, 2002; Grimme, 2004; Zimmerli, Parrinello, and Koumotsakos, 2004). These "DFT-D" approaches have experienced tremendous developments. In particular, Grimme (2006) published a set of empirical parameters for a range of elements and demonstrated that the addition of dispersion energy to a wide range of functionals yields remarkably accurate results for intermolecular interactions. In the latest DFT-D3 method, Grimme extended his empirical set of parameters to cover elements from H to Pu (Grimme *et al.*, 2010).

Considerable efforts have been dedicated toward determining vdW parameters directly from electronic structure calculations also. (Johnson and Becke (2005) developed an approach based on the exchange-hole dipole moment to determine vdW coefficients, which can be computed by using Hartree-Fock orbitals. Later, Steinmann and Corminboeuf (2011) presented an alternative derivation based on electron density and its first and second derivatives. The alternative derivation of the fragment-based vdW-DF functional by Sato and Nakai (2009, 2010) demonstrated an interesting connection (and potential equivalence) between fragment-based methods and explicit nonlocal functionals. Tkatchenko and Scheffler (2009) (TS) developed a DFA based approach to determine both $C_{6,AB}$ coefficients and $R_{c,AB}$ radii as functionals of the electron density, which implies that the vdW parameters respond to changes due to hybridization, static charge transfer, and other electron redistribution processes. The TS approach demonstrated that by utilizing the electron density of a molecule and high-level reference data for the free atoms, it is possible to obtain asymptotic vdW coefficients with accuracy of 5.5%, improving by a factor of 4–5 on other existing approaches at the time. Bučko *et al.* (2013a, 2014) pointed out that an iterative Hirshfeld partitioning scheme for the electron density can significantly extend the applicability of the TS method to ionic materials.

This field is still developing at a rather quick pace; therefore revised and completely new fragment-based approaches are still being introduced.

3. Beyond pairwise additivity: Improved accuracy and efficiency via many-body van der Waals methods

In more complex and heterogeneous systems, it is necessary to go beyond the simple additive models and further efforts of atomistic vdW modeling must be directed toward the inclusion of many-body effects. In principle, RPA using DFA orbitals provides a good model; however, the dependence of χ_0 on the exchange-correlation functional and the high computational cost in the χ_0 computations may be limiting factors. The main challenge is to construct reliable approximations for the long-ranged vdW correlations, since the short-ranged correlation effects are well accounted for in DFA. Therefore, the full $\chi_0(\mathbf{r},\mathbf{r}',i\omega)$ is often unnecessary as is the case in nonmetallic or weakly metallic systems. In such situations, it is possible to describe χ_0 by a set of localized atomic response functions (ARFs), which can be constructed to accurately capture the electronic response beyond a certain cutoff distance.

Although the ARF concept has been employed in *model systems* starting 50 years ago (Bade, 1957; Donchev, 2006, Cole *et al.*, 2009; Shtogun and Woods, 2010; Liu, Angyan, and Dobson, 2011), only recently has this idea been extended to nonlocal vdW interactions in *realistic materials* (DiStasio, Gobre, and Tkatchenko, 2014). For this purpose, spatially extended ARFs that increase the applicability of the model to include close contact have been used within the so-called many-body dispersion (MBD) method, schematically illustrated in Fig. 2(b) (Tkatchenko, DiStasio *et al.*, 2012; Ambrosetti, Reilly *et al.*, 2014). Within this approach, each pth atom in the material is represented by a single dipole oscillator with a frequency-dependent polarizability

$$\alpha_p(i\omega)=\frac{\alpha_{p,0}\omega_{p,0}^2}{\omega_{p,0}^2+\omega^2},$$

where $\alpha_{p,0}$ is the static polarizability and $\omega_{p,0}$ is an effective excitation (or resonant) frequency. The bare ARF response then is written as

$$\chi_{0,p}(\mathbf{r},\mathbf{r}',i\omega) = -\alpha_p(i\omega)\nabla_{\mathbf{r}}\delta^3(\mathbf{r}-\mathbf{R}_p)\otimes\nabla_{\mathbf{r}'}\delta^3(\mathbf{r}'-\mathbf{R}_p), \quad (7)$$

where $\mathbf{R}_p$ is the location of the pth atom and $\otimes$ signifies a tensor product. The bare response function for a collection of atoms follows simply as the direct sum over the individual ARFs, $\chi_0(\mathbf{r},\mathbf{r}',i\omega)=\chi_{0,p}(\mathbf{r},\mathbf{r}',i\omega)\oplus\chi_{0,q}(\mathbf{r},\mathbf{r}',i\omega)\oplus\cdots$. The ARF response contains the infinite-order correlations from the start and it can be used in Eq. (1) to calculate the interaction energy. It has been demonstrated that the RPA correlation energy is equivalent to the exact diagonalization of the Hamiltonian corresponding to ARFs coupled by a long-range dipole potential (Tkatchenko, Ambrosetti, and DiStasio, 2013). Using second-order perturbation theory one also recovers the well-known pairwise-additive formula for the vdW energy (Tkatchenko, Ambrosetti, and DiStasio, 2013).

We note that the solution of Eq. (1) for a model system of ARFs yields an expression for the long-range correlation energy beyond what would simply be called "vdW dispersion energy" in the traditional London picture (London, 1930). Even for two atoms described by dipole-coupled ARFs, the correlation energy contains an infinite number of terms $C_{n,AB}/R_{AB}^n$. The polarizability of the combined AB system in general is not equal to the sum of polarizabilities of isolated atoms A and B, and higher-order correlation terms account precisely for this fact. It was found that the convergence of the perturbative series expansion in Eq. (6) can be extremely slow, especially for systems which have either high polarizability density or low dimensionality. This is clearly illustrated by the binding energy in supramolecular complexes or double-walled nanotubes, for which even 8-body terms make a non-negligible contribution to the correlation energy on the order of 2%–3% (Ambrosetti, Alfe *et al.*, 2014).

D. Applications of atomistic van der Waals methods to materials

Our previous discussions show that the developments of novel many-body methods and understanding of many-body

effects in the vdW energy are an area of significant current interest (Tkatchenko, DiStasio *et al.*, 2012; Otero-de-la Roza and Johnson, 2013; Silvestrelli, 2013; Ambrosetti, Reilly *et al.*, 2014; Modrzejewski, Chałasinski, and Szczesniak, 2014). This is highly motivated from an experimental point of view as well. Being able to describe vdW interactions in different systems is highly desirable in order to explain existing and predict new experimental findings. Figure 3 summarizes typical results from *ab initio* calculations, as described later, for cohesion energies and error ranges as compared to available reference data.

1. Finite and periodic molecular systems

For smaller molecules, high-level quantum-chemical benchmarks using coupled-cluster calculations are now widespread (Jurecka *et al.*, 2006; Takatani *et al.*, 2010; Rezac, Riley, and Hobza, 2011). In particular, the coupled-cluster method with single, double, and perturbative triple excitations [CCSD(T)] is currently considered as the "gold standard" of quantum chemistry. For yet larger molecules (up to 200 light atoms), it is possible to carry out diffusion quantum Monte Carlo (DQMC) calculations (Ambrosetti, Alfe *et al.*, 2014; Benali *et al.*, 2014) using massively parallel computer architectures. DQMC calculations in principle yield the exact solution (within statistical sampling accuracy) for the Schrödinger equation within the fixed-node approximation (Foulkes *et al.*, 2001). Examples of small molecules benchmark databases are those for the S22 (Jurecka *et al.*, 2006; Takatani *et al.*, 2010) and S66 (Rezac, Riley, and Hobza, 2011) dimers, containing 22 and 66 dimers, respectively. For supramolecular systems, the S12L database was recently introduced by Grimme (2012) and benchmark binding energies for 6 of these 12 complexes were calculated using DQMC (Ambrosetti, Alfe *et al.*, 2014). For extended periodic molecular crystals, one can rely on experimental lattice enthalpies, extrapolated to 0 K and with zero-point energy subtracted. Two databases, C21 (Otero-de-la Roza and Johnson, 2012) and X23 (Reilly and Tkatchenko, 2013a), were recently introduced for molecular crystals. Both of these databases include molecular crystals bound primarily by either hydrogen bonds or vdW dispersion, including a few crystals with mixed bonding nature. The X23 database extended the C21 one and improved the calculation of vibrational contributions required to convert between experimental sublimation enthalpies and lattice energies.

Initially, the development of atomistic methods for vdW interactions was largely driven by their performance for small molecules in the S22 and S66 databases. Currently, the best methods are able to achieve accuracies of 10–20 meV (better than 10%) in the binding energies compared to reference CCSD(T) values (Fig. 3). The errors are due to inaccuracy in the asymptotic vdW coefficients, empirical parameters in damping functions, and errors in the exchange-correlation functional.

Because of such rather uniform performance of different methods for small molecules, the focus has shifted to assessing the performance for larger systems. Here, in fact, the differences are more prominent, because the vdW energy makes a much larger relative contribution to cohesion. For example, for polarizable supramolecular systems, such as the "buckyball catcher" complex, pairwise dispersion corrections overestimate the binding energy by 0.4–0.6 eV (Tkatchenko, Alfè, and Kim, 2012) compared to reference DQMC values. Only upon accurately including many-body dispersion effects does one obtain results within 0.1 eV from the best available benchmark (Ambrosetti, Alfe *et al.*, 2014). So far, vdW-DF functionals have not been applied to study binding energetics in the S12L database.

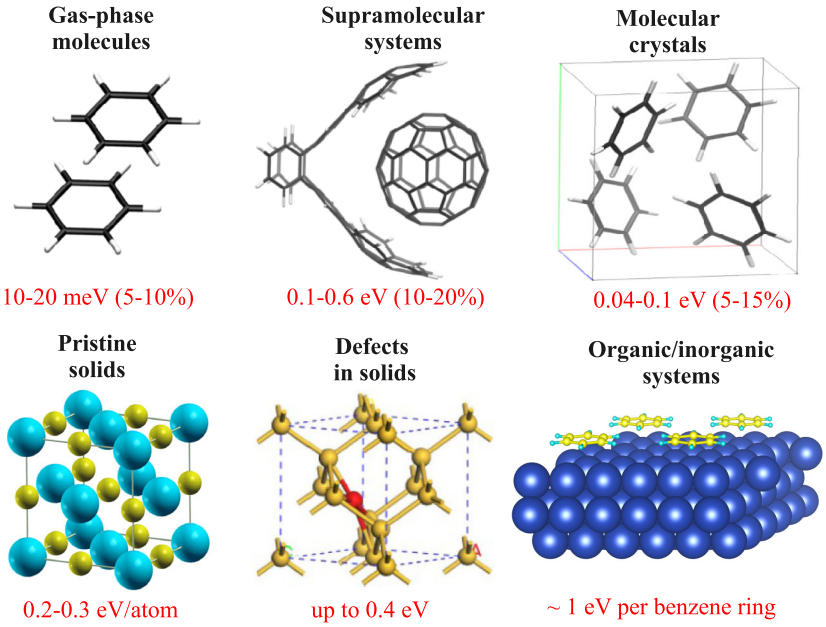

FIG. 3. Various types of materials with calculated cohesion energies and errors as compared to available reference data. The top row of values shows typical errors of atomistic vdW methods compared to benchmark bending energies, while the bottom row of values shows contributions of the vdW energy to the binding energy of the corresponding materials.

For periodic molecular crystals, some pairwise and many-body fragment-based methods are able to achieve remarkable accuracy of 40–50 meV per molecule (5% mean absolute relative error), compared to experimental results (Reilly and Tkatchenko, 2013a, 2013b; Brandenburg and Grimme, 2014). Since the difference in lattice energies between various available experiments is on the same order of magnitude, this highlights the mature state of vdW dispersion corrections to the DFA. The vdW-DF2 approach yields a somewhat larger error of ≈70 meV (7.5%) on the C21 database (Otero-de-la Roza and Johnson, 2012). Understanding the performance of different vdW-inclusive methods for large molecular systems is still a subject of ongoing research. Some of the pairwise correction approaches have been specifically fitted to periodic systems, trying to mimic many-body screening effects by changing the short-range damping function. This procedure seems to work well for certain molecular crystals with high symmetry, but this is obviously not a transferable approach.

Many-body vdW correlations become even more relevant for the *relative* energetics of molecular systems, which are essential to predict the correct polymorphic behavior of molecular crystals. Marom *et al.* (2013) demonstrated the fact that only upon including many-body effects is one able to correctly reproduce the structures and relative stabilities of glycine, oxalic acid, and tetrolic acid. Another interesting example is the aspirin crystal, for which a long-standing controversy has been about the relative stability of polymorphs forms I and II (Ouvrard and Price, 2004). Reilly and Tkatchenko (2014) recently demonstrated that the stability of the most abundant form I arises from an unexpected coupling between collective vibrational and electronic degrees of freedom (dynamic plasmon-phonon coupling). In this case, many-body vdW correlations renormalize phonon frequencies leading to low-frequency phonon modes that increase the entropy and ultimately determine the stability of this ubiquitous form of aspirin in comparison to the metastable form II. Furthermore, the bulk and shear moduli of both forms are substantially modified and become in better agreement with experiments when calculated with DFA + MBD. The aspirin example illustrates how the inclusion of many-body vdW effects may lead to novel qualitative predictions for the polymorphism and elastic response of molecular materials.

2. Condensed materials

For hard solids (ionic solids, semiconductors, and metals), the role of vdW interactions was considered to be negligible for a long time, as judged, for example, by classical condensed-matter textbooks (Ashcroft and Mermin, 1976; Kittel, 1986). The rather strong cohesion in hard solids stems from covalent and metallic bonds or from classical Coulomb interaction between localized charges (Fig. 3). Early estimates of vdW interactions in hard solids varied substantially from being negligible to being very important (Mayer, 1933; Rehr, Zaremba, and Kohn, 1975; Ashcroft and Mermin, 1976; Richardson and Mahanty, 1977; Tao, Perdew, and Ruzsinszky, 2010). Recently, this issue was systematically revisited by employing DFA with vdW interactions. Zhang *et al.* (2011) demonstrated that long-range vdW interactions account for ≈ 0.2 eV/atom in the cohesive energy for Si, Ge, GaAs, NaCl, and MgO, and 9–16 GPa in the bulk modulus. This amounts to a contribution of 10%–15% in the cohesive energy and bulk modulus—far from being negligible if one aims at an accurate description of these properties. Klimeš, Bowler, and Michaelides (2011) applied their opt functionals based on the vdW-DF approach to a large database of solids finding that vdW interactions play an important role for an accurate description of cohesive properties. Overall, their conclusion is that vdW interactions allow the improvement of the performance of many different *xc* functionals, achieving good performance for both small molecules and hard solids.

Because vdW interactions are important for absolute cohesive properties of solids, any property that depends on energy *differences* is also likely to be influenced by vdW effects. Therefore, vdW interactions often play an important role in the relative stabilities of different solid phases, phase transition pressures, and phase diagrams as demonstrated for polymorphs of TiO_2 (Moellmann *et al.*, 2012), ice (Santra *et al.*, 2011), different reconstructed phases of the oxidized Cu(110) surface (Bamidele *et al.*, 2013), and alkali borohydrides (Huan *et al.*, 2013).

The properties of many solids are substantially affected by the presence of simple and complex defects, such as neutral and charged interstitials and vacancies (Freysoldt *et al.*, 2014). The formation of defects entails a modification of polarization around defect sites and this can have a substantial effect on the contribution of vdW energy to the stability and mobility of defects. Gao and Tkatchenko (2013) demonstrated the fact that the inclusion of many-body vdW interactions in DFA improves the description of defect formation energies, significantly changes the barrier geometries for defect diffusion, and brings migration barrier heights into close agreement with experimental values. In the case of Si, the vdW energy substantially decreases the migration barriers of interstitials and impurities by up to 0.4 eV, qualitatively changing the diffusion mechanism (Gao and Tkatchenko, 2013). Recently, the proposed mechanism was confirmed by explicit RPA calculations (Kaltak, Klimeś, and Kresse, 2014).

3. Interfaces between molecules and solids

The predictive modeling and understanding of hybrid systems formed between molecules and solids are essential prerequisites for tuning their electronic properties and functions. The vdW interactions often make a substantial contribution to the stability of molecules on solids (Tkatchenko *et al.*, 2010). Indeed, until recent developments for efficiently incorporating the long-range vdW energy within state-of-the-art DFAs, it was not possible to study the structure and stability of realistic interfaces (Liu, Tkatchenko, and Scheffler, 2014). Exposed surfaces of solid materials are characterized by the formation of collective electronic states; thus the long-range screening effects should be treated at least in an effective way, as done, for example, in the DFT + vdW^{surf} method that accounts for the collective electronic response effects by a combination between an interatomic dispersion expression and the Lifshitz-Zaremba-Kohn theory (Ruiz *et al.*, 2012). This method was demonstrated to be reliable for the structure and stability of a broad class of organic molecules adsorbed on metal surfaces, including benzene, naphthalene, anthracene,

diindenoperylene, C_{60}, and sulfur and oxygen-containing molecules (thiophene, NTCDA, and PTCDA) on close-packed and stepped metal surfaces, leading to an overall accuracy of 0.1 Å in adsorption heights and 0.1–0.2 eV in binding energies with respect to state-of-the-art experiments (Liu, Tkatchenko, and Scheffler, 2014).

A particularly remarkable finding is that vdW interactions can contribute more to the binding of strongly bound molecules on transition-metal surfaces than they do for molecules physisorbed on coinage metals (Carrasco, Hodgson, and Michaelides, 2012; Liu *et al.*, 2012). The accurate inclusion of vdW interactions also significantly improves molecular tilting angles and adsorption heights and can qualitatively change the potential-energy surface for adsorbed molecules with flexible functional groups. Activation barriers for molecular switches (Liu *et al.*, 2013) and reaction precursors (Rodriguez-Reyes *et al.*, 2014) are modified as well. Ongoing work concentrates on understanding the interplay between many-body effects within the solid material and collective effects within the adsorbed molecular layers.

III. DIRAC MATERIALS BEYOND ATOMIC SCALE SEPARATIONS

Without a doubt, novel *ab initio* methods have advanced our understanding of vdW interactions between systems at atomic scale separations. When the objects are taken farther apart, however, other approaches become more appropriate. Dispersion interactions involving objects with macroscopic dimensions at distances for which the electronic distribution overlapping effects are not important are typically described by the Lifshitz formalism (Lifshitz, 1956; Dzyaloshinskii, Lifshitz, and Pitaevskii, 1961), which has been the mainstream theory for conventional metals and dielectrics for over several decades. New materials with Dirac spectra are emerging, however, and the Lifshitz approach is an excellent tool to capture the signatures of the Dirac carriers in the vdW and Casimir interactions.

A. Lifshitz formalism

A generalized Lifshitz formula can be obtained from the ACFDT expression in Eq. (1) for distance separations larger than several Å's, where the overlap of the electronic distribution residing on each object can be neglected. In this case, the response properties are independent of each other; thus they are described by the individual response functions $\chi_0^{(1,2)}$ (1, 2 denote the two objects) and the mutual Coulomb potential can be taken as a perturbation. Although $\chi_0^{(1,2)}$ do not include electronic correlations from the overlap, they contain the electronic correlations within each object. When $\chi_0^{(1,2)}$ are calculated via the RPA approach and the mutual Coulomb interaction is described by the RPA ring diagrams (Lifshitz, 1956; Dzyaloshinskii, Lifshitz, and Pitaevskii, 1961; Fetter and Walecka, 1971), the ACFDT expression [Eq. (1)] is transformed to the nonretarded Lifshitz formula given in the Fourier basis for planar homogeneous objects (Despoja, Sunjic, and Marusic, 2007; Dobson and Gould, 2012)

$$\frac{E^{(L)}}{A}=\hbar\int\frac{d\mathbf{k}_\parallel}{(2\pi)^2}\int_0^\infty\frac{d\omega}{2\pi}\log[1-\chi_0^{(1)}(\mathbf{k}_\parallel,i\omega)V_{12}(\mathbf{k}_\parallel,i\omega)\times\chi_0^{(2)}(\mathbf{k}_\parallel,i\omega)V_{21}(\mathbf{k}_\parallel,i\omega)], \tag{8}$$

where A is the area, $\mathbf{k}_\parallel$ is the 2D wave vector, and $V_{12}(\mathbf{k}_\parallel,i\omega)$ is the Coulomb interaction between the two objects.

Distance separations on the order of sub-μm and μm scales are characteristic for the Casimir regime, where retardation becomes prominent. For such separations one has to include all photon interactions being exchanged with the finite speed of light c. The Casimir energy can be derived using scattering methods by solving the boundary conditions arising from the electromagnetic Maxwell equations. The interaction energy can be written in the form (Lambrecht, Maia Neto, and Reynaud, 2006; Lambrecht and Marachevsky, 2008; Rahi *et al.*, 2009)

$$\frac{E^{(C)}}{A}=\hbar\int_0^\infty\frac{d\omega}{2\pi}\times\int\frac{d\mathbf{k}_\parallel}{2\pi^2}\log\det\left[\mathbb{I}-\mathbb{R}_1(i\omega)\mathbb{R}_2(i\omega)e^{-2d\sqrt{\omega^2/c^2+\mathbf{k}_\parallel^2}}\right], \tag{9}$$

where $\mathbb{R}_{1,2}$ are the reflection matrices of the individual objects evaluated at imaginary frequencies. The reflection matrices describe appropriate boundary conditions and they are expressed in terms of the macroscopic response properties of the objects. Equation (9) can be obtained equivalently via QED techniques relying on the evaluation of the Maxwell stress tensor whose components represent the vacuum expectation of the electromagnetic field and they are given in terms of the dyadic Green's function (more details on this approach are found in Sec. V) (Dzyaloshinskii, Lifshitz, and Pitaevskii, 1961; Buhmann and Welsch, 2007). Utilizing the fluctuation-dissipation theorem and standard complex contour integration techniques, Matsubara frequencies $i\omega_n=in2\pi k_BT/\hbar$ are introduced in the description. As a result, the Casimir interaction energy $E^{(C)}$ can be cast into a temperature-dependent form using

$$\hbar\int_0^\infty\frac{d\omega}{2\pi}\to k_BT{\sum_{n=0}^{\infty}}'$$

(the prime in the sum means that the $n=0$ term is multiplied by $1/2$). We further note that by setting $c=\infty$ in Eq. (9) the nonretarded Lifshitz expression [Eq. (8)] is recovered.

Being able to utilize independently calculated response properties with different models (including RPA or the Kubo formalism) or even use experimental data in Eqs. (8) and (9) has been especially useful for the versatility of the Lifshitz macroscopic approach. In addition, the Matsubara frequencies give the means to take into account temperature in the interaction unlike the *ab initio* methods (Sec. II), which calculate the vdW energy at zero temperature. Much of the progress in theoretical and experimental work concerning typical metals and dielectrics interactions, captured by the Lifshitz formalism, has been summarized in several books and

recent reviews (Lamoreaux, 2005; Parsegian, 2006; Buhmann and Welsch, 2007; Bordag, Klimchitskaya *et al.*, 2009; Klimchitskaya, Mohideen, and Mostepananko, 2009; Dalvit *et al.*, 2011).

It was revealed that the interplay between the Lifshitz approach and the Drude dielectric gives unexpected outcomes for the thermal interaction between typical metals (Boström and Sernelius, 2000), namely, that the low-frequency transverse electric contribution to the Casimir force is zero. Later on, the thermal Casimir force was calculated with the plasma model and critically compared with the results obtained using the Drude model (Bordag *et al.*, 2000). The main issue is that the particular description of the low-frequency optical response of the systems leads to different magnitudes, especially at larger separations where the difference can be as large as 100%. Sushkov *et al.* (2011) measured the Casimir force between metallic samples, and they interpreted their results in agreement with the Drude model, after subtracting a force systematics due to electrostatic patches that was modeled and fitted to the total observed force. Recent independent measurements of patch potential distributions on metallic samples used in Casimir force experiments report different strengths and scaling laws for the patch contribution to the total force (Behunin *et al.*, 2014; Garrett, Somers, and Munday, 2015). We should note, however, that Bezerra *et al.* 2011)) criticized the interpretation based on the Drude model done by Sushkov *et al.* (2011). In contrast, several other Casimir experiments (Decca *et al.*, 2005, 2007; Banishev, Chang, Klimchitskaya *et al.*, 2012; Chang *et al.*, 2012; Banishev *et al.*, 2013a, 2013b) are in agreement with the plasma model description, which is surprising given that this model neglects dissipation effects in metals. For separations on the submicron scales, however, the differences between the plasma versus the Drude model calculations are on the order of a few percent in the studied geometries and conditions. A proposal based on the isoelectronic technique, which eliminates the need for electrostatic corrections due to patches, was put forward that makes a significant step forward toward understanding this problem (Bimonte, 2014a, 2014b, 2015). With this setup, it becomes possible to strongly enhance the discrepancy between the predictions for the Casimir force based on either model for the dielectric response. Recent measurements are in favor of theoretical extrapolations to low frequency based on the plasma model (Bimonte, López, and Decca, 2016). This issue is currently under investigation in the context of typical materials and magnetodielectrics by tackling fundamental theoretical questions, such as the importance of thermal effects, the validity of the Nernst theorem, and the consistency with the Bohr–van Leeuwen theorem (Bezerra *et al.*, 2004; Geyer, Klimchitskaya, and Mostepanenko, 2005, 2010; Høye *et al.*, 2007; Pitaevskii, 2008, 2009; Bimonte, 2009; Dalvit and Lamoreaux, 2009; Klimchitskaya and Mostepanenko, 2015a).

The materials library is expanding, however. This is not only important for giving new light in the Drude versus plasma models problem, but also in identifying novel directions for fluctuation-induced interactions. A subset of systems, characterized by Dirac fermions in their low-energy spectra, has emerged recently (Welding, Black-Schaffer, and Balatsky, 2014). This distinct class of materials has properties markedly different from the ones of conventional metals and semiconductors whose fermions obey the Schrödinger's equation. Recent discoveries have shown that there are many types of systems with Dirac nodes in the band structure, including graphene, topological insulators (TIs), and Weyl semimetals. Research efforts on vdW and Casimir interactions involving graphene and related systems have shown that fluctuation-induced phenomena are strongly influenced by the Dirac nature of the carriers. As discussed previously, *ab initio* calculations have been indispensable for the demonstration of atomic registry-dependent effects, unusual scaling laws, farsightedness, and the many-body nature of their vdW interaction in graphitic systems (Lebegué *et al.*, 2010; Shtogun and Woods, 2010; Bučko *et al.*, 2013a, 2013b, 2014; Gobre and Tkatchenko, 2013). Nevertheless, it is very important from a fundamental point of view to consider regimes where the dispersion interactions are determined primarily by the low-energy Dirac carriers. Unlike *ab initio* methods which take into account the entire band structure of the interaction materials, the Lifshitz formalism relying on response functions calculated via low-energy models gives us an opportunity to study the emergent physics of the Dirac carriers in vdW and Casimir forces.

B. Basic properties of graphene nanostructures

After the discovery of graphene (Novoselov *et al.*, 2004), significant progress was made toward understanding its properties. For example, basic science in terms of the 2D Dirac-like nature (Neto *et al.*, 2009), electronic transport (Das Sarma *et al.*, 2011), collective effects due to electron-electron interactions (Kotov *et al.*, 2012), and spectroscopy (Basov *et al.*, 2014) has been studied. Quasi-1D allotropes, such as carbon nanotubes (CNTs) and graphene nanoribbons (GNRs), are also available (Saito, Dresselhaus, and Dresselhaus, 1998; Ma, Wang, and Ding, 2013), and key scientific breakthroughs have been summarized (Charlier, Blase, and Roche, 2007; Yaziev, 2010). In addition to the internal properties, understanding how chemically inert carbon nanostructures interact at larger length scale separations (more than several Å's) is of primary importance. Much progress in the past several years has been achieved toward learning how such dispersive forces are influenced by the graphitic internal properties and external factors, such as temperature, doping, and applied fields. This knowledge is relevant for a variety of phenomena including the formation and stability of materials and composites, adsorption, manipulation of atoms, and operation of devices, among others. Since the description of the interaction via the macroscopic Lifshitz formalism depends upon the low-energy electronic structure and optical properties, here we provide an overview of the relevant characteristics of graphene, CNTs, and GNRs.

Graphene is a 2D atomic layer composed of hexagonally oriented rings (Fig. 4). Many of its properties can be captured by a nearest-neighbor tight-binding model within the first Brillouin zone with two inequivalent K points at $\mathbf{K} = (\pm 4\pi/\sqrt{3}a, 0)$ (a is the graphene lattice constant), which describes a π valence bonding band with one electron and an empty π^* antibonding band with one hole. The linearization of the energy spectrum around the $\mathbf{K}$ centered

valleys yields the low-energy massless chiral Dirac-like Hamiltonian in 2D

$$H_{\rm gr} = \hbar v_F \sigma \cdot \mathbf{q} - \mu, \tag{10}$$

where μ is the chemical potential and σ is the 2D spinor. The nonzero spinor components σ_x, σ_y are the Pauli matrices, which refer to the graphene pseudospin rather than the real spin. The energy spectrum $E_{\rm gr}$ is linear with respect to the wave vector $\mathbf{q} = \mathbf{k} - \mathbf{K}$ according to $E_{\rm gr} = \hbar v_F q$ with the electronic group velocity being $v_F = \sqrt{3} t_0 a/2\hbar \sim 10^6$ m/s (t_0 is the nearest-neighbor tight-binding hopping integral). It is interesting to note that although graphene was synthesized not long ago, theoretical insight in terms of the low-energy massless Dirac-like $H_{\rm gr}$ was discussed much earlier by Semenoff (1984), who expanded upon the tight-binding description introduced by Wallace (1947).

The tight-binding model can be extended to CNTs as well. By imposing periodic boundary conditions around the cylindrical circumference, the corresponding wave functions are zone folded, meaning that the wave vector in the azimuthal direction takes a set of discrete values. The nomenclature of CNTs is described via a chirality vector $\mathbf{C}_h = n\mathbf{a}_1 + m\mathbf{a}_2$, where n and m are integers and $\mathbf{a}_{1,2}$ are defined in Fig. 4(a). As a result, single-walled CNTs are denoted via a chirality index (n, m) with the achiral nanotubes labeled as armchair (n, n) or zigzag $(n, 0)$, as shown in Fig. 4. The CNT energy bands can also be found (Mintmire, Dunlap, and White, 1992; Tasaki, Maekawa, and Yamabe, 1998) with zone-folding boundary conditions leading to a chirality dependent energy spectrum. The tight-binding energy band structure for GNRs, on the other hand, is obtained by requiring the wave function be periodic along the GNR axis and vanish at the edges, which introduces edge dependent (zigzag or armchair) phase factors in the energy spectra (Brey and Fertig, 2006; Akhmerov and Beenakker, 2008; Sasaki *et al.*, 2011).

The electronic structure of graphene systems determines their optical response properties—key components for the vdW and Casimir calculations. The Dirac-like carriers have profound effects on how electromagnetic excitations are handled by graphene. The chiral symmetry for the graphene quasiparticles in a given K valley is either parallel or antiparallel to the direction of motion of the electrons and holes. An immediate consequence is that in the $k_B T \ll \hbar\omega$ limit the optical conductivity for undoped graphene is independent of any materials properties $\sigma_0 = e^2/4\hbar$ (Kuzmenko *et al.*, 2008). Even at room temperature, it is found experimentally that the optical absorption is very small ~2.3% and it depends only on the fine structure constant $\alpha = e^2/\hbar c = 1/137$ (Nair *et al.*, 2008). Doping and gating influence the optical properties significantly leading to Pauli blocking for photons with energy less than $2\mu_F$ (μ_F is the Fermi level) and achieving carrier concentrations which can modify the transmission in the visible spectrum (Li *et al.*, 2008; M. Liu *et al.*, 2011). Graphene plasmonics is also quite interesting since graphene plasmons are tunable by gating and doping and they are temperature dependent (Gangadharaiah, Farid, and Mishchenko, 2008). In addition to longitudinal plasmons, graphene can support a transverse plasmon mode. It is also interesting to note that the longitudinal modes are gapless; however, the transverse ones exist in the window $1.7 < \hbar\omega/\mu_F < 2$ and can be tunable from radio to infrared frequency by doping and electric fields (Mikhailov and Ziegler, 2007).

Plasmons in GNRs can exist in the near-infrared to far-infrared range and further tunability via a gate voltage can be achieved (Freitag *et al.*, 2013). The optical properties of CNTs are also quite unique. The CNT optical activities, such as electron-energy-loss spectroscopy (EELS) spectra and circular dichroism, are chirality dependent (Wang *et al.*, 2005; Dresselhaus *et al.*, 2007). Competing effects due to Coulomb interactions and an attractive *e-h* coupling are strong in CNTs, which have led to the realization that strong excitonic effects need to be taken into account (especially in small diameter nanotubes) to achieve agreement with experimental optical data (Spataru *et al.*, 2001, 2004, 2005).

The optical response of graphene can be described by considering its 2D conductivity tensor calculated within the

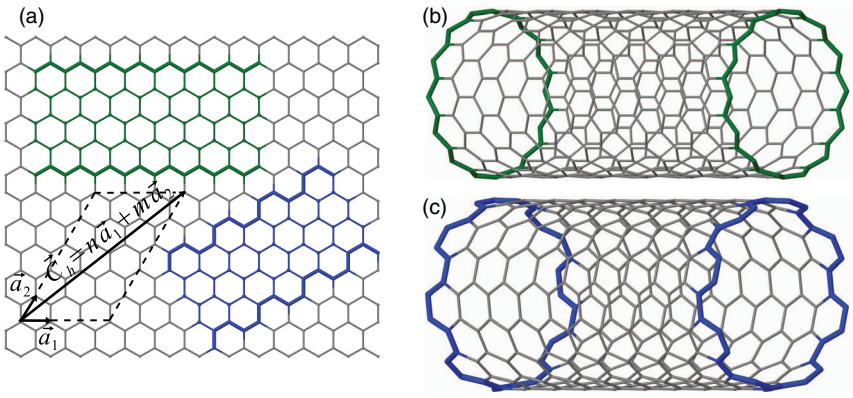

FIG. 4. (a) A graphene layer is an atomically thin sheet of honeycomb carbon atoms. Zigzag (green) and armchair (blue) graphene nanoribbons can be realized by cutting along the specified edges. Carbon nanotubes can be obtained by folding along the chirality vector $\vec{C}_h$, determined by the indices n and m and the lattice unit vectors $\vec{a}_{1,2}$. The chirality index (n, m) uniquely specifies each nanotube with two achiral examples shown: (b) zigzag $(m, 0)$ and (c) armchair (n, n). Alternatively, folding a zigzag nanoribbon along the axial direction results in an armchaired nanotube, while folding an armchair nanoribbon gives a zigzag nanotube.

Kubo formalism (Falkovsky and Varlamov, 2007). Evaluating this general expression for the lowest conduction and highest valence energy bands in the $\mathbf{q} \to 0$ approximation leads to the intraband (intra) and interband (inter) contributions

$$\sigma_{\text{intra}}(i\omega) = \frac{e^2 \ln 2}{\hbar^2 \pi\beta\omega} + \frac{e^2}{\hbar^2 \pi\beta\omega} \ln[\cosh(\beta\Delta) + \cosh(\mu\beta)] - \frac{e^2\Delta^2}{\pi\hbar^2\omega} \int_\Delta^\infty \frac{dE}{E^2} \frac{\sinh(\beta E)}{\cosh(\mu\beta) + \cosh(\beta E)}, \tag{11}$$

$$\sigma_{\text{inter}}(i\omega) = \frac{e^2\omega}{\pi} \int_\Delta^\infty dE \frac{\sinh(\beta E)}{\cosh(\mu\beta) + \cosh(\beta E)} \frac{1}{(\hbar\omega)^2 + 4E^2} + \frac{e^2\omega\Delta^2}{\pi} \int_\Delta^\infty \frac{dE}{E^2} \frac{\sinh(\beta E)}{\cosh(\mu\beta) + \cosh(\beta E)} \times \frac{1}{(\hbar\omega)^2 + 4E^2}, \tag{12}$$

where Δ is an energy gap in the graphene spectrum. When $\Delta = \mu = 0$ and $k_B T \ll \hbar\omega$, σ acquires the universal value $\sigma_0 = e^2/4\hbar$, also confirmed experimentally (Li *et al.*, 2008; Nair *et al.*, 2008). The graphene conductivity is isotropic when spatial dispersion is not taken into account and the difference between σ_{xx} and σ_{yy} (graphene is in the x-y plane) is mostly pronounced for larger q (Falkovsky and Varlamov, 2007; Drosdoff *et al.*, 2012).

The optical response properties can also be characterized by considering the longitudinal polarization function $\chi_l(q, i\omega)$, which corresponds to the longitudinal component of the conductivity

$$\sigma(q, i\omega) = \frac{ie^2\omega}{q^2} \chi_l(q, i\omega)$$

for $q \to 0$. Alternatively, the transverse electric (TE) and transverse magnetic (TM) excitations can be captured via the polarization tensor Π calculated by a $(2+1)$ Dirac model (Bordag, Fialkovsky *et al.*, 2009; Fialkovsky, Marachevsky, and Vassilevich, 2011; Klimchitskaya, Mostepanenko, and Sernelius, 2014; Sernelius, 2015). It is found that the longitudinal polarization function is related to the Π_{00} component

$$\chi_l = -\frac{1}{4\pi e^2 \hbar} \Pi_{00},$$

while the transverse polarization function is

$$\chi_{tr} = -\frac{c^2}{4\pi e^2 \hbar\omega^2} (k^2 \Pi_{tr} - q_l^2 \Pi_{00}).$$

The optical response of the quasi-1D structures, such as GNRs and CNTs, follows from the Kubo formalism for graphene. Taking into account the zone-folded wave functions and chirality dependent energies leads to the intraband and interband optical conductivity spectra of CNTs (Tasaki, Maekawa, and Yamabe, 1998). Similarly, incorporating the edge dependent wave functions with the appropriate tight-binding energies results in the intraband and interband conductivities of zigzag and armchair GNRs (Brey and Fertig, 2006; Sasaki *et al.*, 2011).

C. Casimir interactions and graphene nanostructures

1. Graphene

The vdW and Casimir interactions involving a graphene sheet and semi-infinite dielectric medium can be calculated using the fully retarded expression in Eq. (9) with response properties [Eqs. (11) and (12)] corresponding to its low-energy Dirac spectrum. The boundary conditions are contained in the matrices $\mathbb{R}_{1,2}$, whose nonzero diagonal components for a graphene or semi-infinite medium system with dielectric and magnetic response properties reflecting the TE (ss) and TM (pp) modes are

$$R_1^{(ss)} = -\frac{2\pi\omega\sigma\bar{q}c^2}{1 + 2\pi\omega\sigma\bar{q}c^2}, \qquad R_1^{(pp)} = \frac{2\pi\sigma\bar{q}/\omega}{1 + 2\pi\sigma\bar{q}/\omega}, \tag{13}$$

$$R_2^{(ss)} = \frac{\mu(i\omega)\bar{q} - \bar{k}}{\mu(i\omega)\bar{q} + \bar{k}}, \qquad R_2^{(pp)} = \frac{\epsilon(i\omega)q - \bar{k}}{\epsilon(i\omega)\bar{q} + \bar{k}}, \tag{14}$$

where $\bar{q} = \sqrt{k_\parallel^2 + (\omega/c)^2}$ and $\bar{k} = \sqrt{k_\parallel^2 + \mu(i\omega)\epsilon(i\omega)\omega^2/c^2}$. The dielectric and magnetic response functions for the semi-infinite medium are $\epsilon(i\omega)$ and $\mu(i\omega)$, respectively. The reflection coefficients here are expressed in terms of the graphene conductivity σ; however, these can be given equivalently via other response characteristics using the relations discussed previously. For a graphene-graphene system, the components of the $\mathbb{R}_2$ matrix are replaced by the components of the $\mathbb{R}_1$ matrix.

One of the first studies of Casimir interactions for graphene was reported by Bordag *et al.* (2006), where they considered graphene or perfect metallic semi-infinite mediums and atom and graphene systems. Graphene was modeled as a plasma sheet leading to results strongly dependent on the plasma frequency. A more suitable representation of the graphene sheet was later considered by taking into account the Dirac-like nature of the carriers explicitly. It was obtained that the Casimir force is quite weak compared to the one for perfect metals and that it is strongly dependent upon the Dirac mass parameter (Bordag, Fialkovsky *et al.*, 2009). Describing the graphene response via the 2D universal graphene conductivity σ_0 as valid in the $k_B T \ll \hbar\omega$ limit (Falkovsky and Varlamov, 2007; Nair *et al.*, 2008), others (Drosdoff and Woods, 2010) found a unique form of the graphene-graphene Casimir force per unit area A,

$$\frac{F_0}{A} = -\frac{3\hbar\sigma_0}{8\pi d^4} = -\frac{3e^2}{32\pi d^4}.$$

This result shows that the distance dependence is the same as the one for perfect metals whose Casimir force is

$$\frac{F_m}{A} = -\frac{\hbar c\pi^2}{240 d^4},$$

however the magnitude is much reduced $F_0/F_m \sim 0.00538$. It is interesting to note that retardation does not affect the

interaction and $\hbar$ is canceled after taking into account that $\sigma_0 = e^2/4\hbar$.

The graphene interaction has also been investigated via the nonretarded Lifshitz formalism in Eq. (8) (Dobson, White, and Rubio, 2006; Gómez-Santos, 2009; Sarabadani *et al.*, 2011; Sernelius, 2015), where the polarization and Coulomb interaction are calculated with the RPA approach. The RPA is a useful tool to study long-ranged dispersive interactions as it gives a natural way to take into account the electron correlation effects of each object and spatial dispersion (Fetter and Walecka, 1971; Dobson, 2011), as discussed earlier. It was found that for separations $d > 50$ nm the nonretarded Lifshitz approach results in a graphene-graphene force of the form $F_0/A = -B/d^4$, where the magnitude of the constant B agrees with the results from the retarded Casimir calculations (Drosdoff and Woods, 2010; Drosdoff *et al.*, 2012). It is thus concluded that the graphene-graphene interaction is determined by the nonretarded TM mode contribution (captured in the longitudinal polarization) even at distances corresponding to the Casimir regime. These results are truly remarkable since the interaction appears to be independent of all of the graphene properties in the low T and/or $d > 50$ nm regime. A further interpretation can be given by noting that the electromagnetic fluctuations exchange occurs at speed v_F [Eq. (10)] rather than the speed of light. This means that the typical thermal wavelength $\lambda_T = \hbar c/k_B T$, which sets the scale where quantum-mechanical ($d < \lambda_T$) or thermal ($d > \lambda_T$) fluctuations dominate the interaction, becomes $\tilde{\lambda}_T = \hbar v_F/k_B T$. The quantum-mechanical contributions determine the graphene interaction at separations $d < \tilde{\lambda}_T \sim 50$ nm as opposed to $d < \lambda_T \sim 7$ μm for typical metals and dielectrics at $T \sim 300$ K. The thermal fluctuations for graphene become relevant at much reduced distances, and for $d > \tilde{\lambda}_T$ the interaction is

$$\frac{F_T}{A} = -\frac{\zeta(3)}{8\pi}\frac{k_B T}{d^3},$$

where $\zeta(n)$ is the Riemann zeta function (Gómez-Santos, 2009). Essentially, v_F takes the role of the speed of light enhancing the importance of the zero Matsubara frequency at much lower T and smaller d as compared to conventional metals and dielectrics.

For closer separations ($d < 50$ nm), a more complete model for the graphene properties is needed. Deviations from the asymptotic behavior at low T are found (Drosdoff and Woods, 2010) by using the graphene optical conductivity taken into account by a Drude-Lorentz model that corresponds to higher frequency range $\pi \to \pi^*$ and $\sigma \to \sigma^*$ transitions. Recently, it was shown that the Casimir interaction in a stack of identical graphene layers exhibits a fractional distance dependence in the energy ($E \sim d^{-5/2}$) as a result of the Lorentz oscillators (Khusnutdinov, Kashparov, and Woods, 2015). Other researchers (Gould, Simpkins, and Dobson, 2008; Gould, Gray, and Dobson, 2009; Lebegué *et al.*, 2010; Gould, Dobson, and Lebegué, 2013; Gould, Lebegué, and Dobson, 2013) utilized the RPA approach combined with first-principles calculations for the electronic structure to investigate the nonretarded interaction at very short separations ($d < 10$ nm) for an infinite number of parallel graphene layers. Interestingly, the interaction energy is found to be $E \sim d^{-4}$. This insulatorlike behavior is attributed to the full energy band structure [beyond the two-band model in Eq. (10)] and the associated higher transitions in the response properties. Others (Sarabadani *et al.*, 2011) also considered the vdW interaction in a multilayered graphene configuration within the RPA; however, the reported unusual asymptotic distance dependences may be an artifact of the considered finite graphene thickness.

It was also shown that temperature together with other factors, such as doping or external fields, affects the graphene thermal and quantum-mechanical regimes in an intricate way. In particular, the classical Casimir-vdW interaction determined by the thermal fluctuations was examined by several authors in different situations. Fialkovsky, Marachevsky, and Vassilevich (2011) used the polarization tensor and corresponding reflection coefficients to express the dominating thermal regime [$k_B T d/\hbar c \gg \alpha \ln(\alpha^{-1})/2\zeta(3)$] in terms of the fine structure constant α. Sernelius (2011) utilized the longitudinal graphene response in Eq. (8) to show that doping plays an important role in the interaction at larger separations as the force can be increased by an order of magnitude for large degrees of doping. Bordag, Klimchitskaya, and Mostepanenko (2012) and Klimchitskaya and Mostepanenko (2013) used the fully relativistic Dirac model with the T-dependent polarization tensor to investigate how a finite mass gap Δ in the Dirac model affects these regimes in graphene-graphene and graphene and dielectrics. It is found that for $k_B T \ll \Delta$ thermal fluctuations are not important, while for $\Delta \leq k_B T$ the thermal effects become significant, as shown in Figs. 5(a) and 5(b). The thermal and quantum-mechanical regimes were also studied by Drosdoff *et al.* (2012) via the longitudinal thermal conductivity, which includes spatial dispersion, an energy gap, and chemical potential in the Dirac model. They showed that tuning Δ and μ can be effective ways to modulate the interaction; however, the spatial dispersion does not play a significant role except for the case of small Δ and low T, as shown in Figs. 5(d) and 5(e).

Recent studies (Klimchitskaya and Mostepanenko, 2014; Klimchitskaya, Mostepanenko, and Sernelius, 2014; Bordag *et al.*, 2015; Sernelius, 2015) provided a thorough analysis of the balance between the thermal and quantum-mechanical effects in the graphene Casimir interaction. It is shown that equivalent representations within the temperature-dependent longitudinal and transverse polarization and the temperature-dependent polarization tensor are possible. The comparison between results from the temperature-dependent polarization tensor and density-density correlation function shows that at low T both approaches give practically the same results proving that retardation and TE polarization are unimportant. For $T \neq 0$, deviations are found as shown in Fig. 5(c) for graphene-graphene and graphene-metal configurations.

Dobson, Gould, and Vignale (2014) revealed that the collective excitations beyond the RPA approximation may be quite important, qualitatively and quantitatively, for the

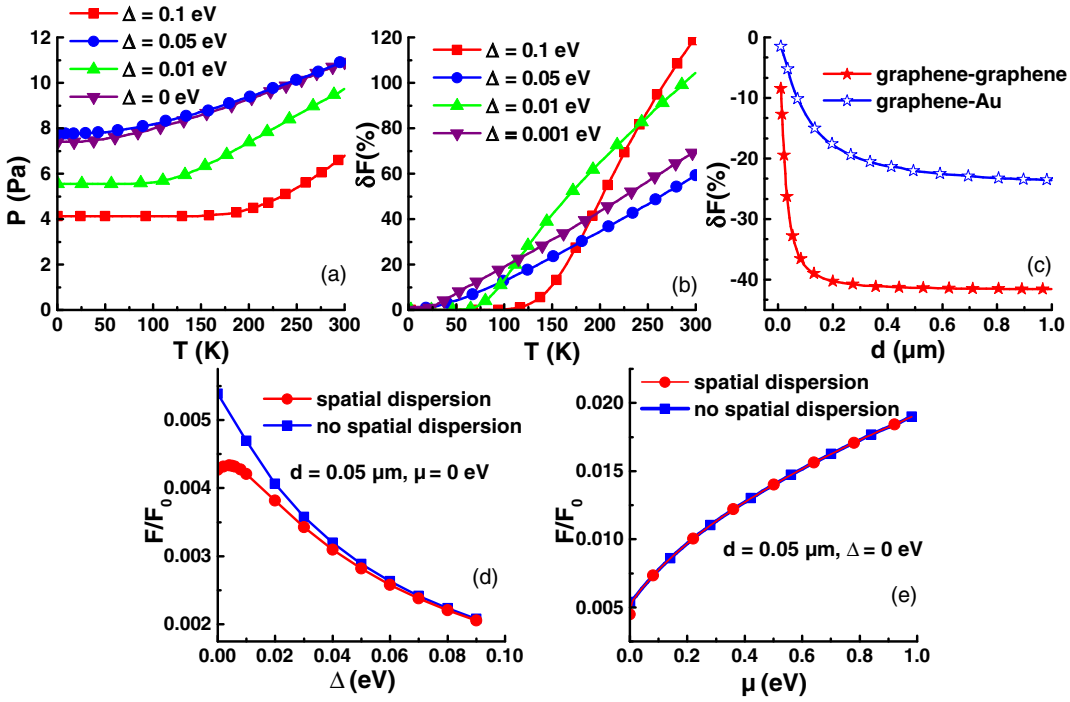

FIG. 5. (a) Casimir pressure between two graphene sheets at separation $d = 30$ nm as a function of temperature for different values of the gap Δ. Adapted from Klimchitskaya and Mostepanenko, 2013. (b) Relative thermal correction $\delta F(\%) = [F(T) - F(T = 0)]/F(T = 0)$ for the graphene-Si plate interaction at separation $d = 100$ nm. Adapted from Bordag, Klimchitskaya, and Mostepanenko, 2012. (c) Relative deviation $\delta F(\%) = [F_{dd}(T) - F_{pt}(T)]/F_{pt}(T)$ for graphene-graphene (red) and graphene-Au plate (blue) interactions, where $F_{dd}(T)$ is the Casimir force calculated via the density-density correlation function and $F_{pt}(T)$ is the Casimir force calculated via the polarization tensor. Adapted from Klimchitskaya, Mostepanenko, and Sernelius, 2014. Casimir graphene-graphene force normalized to $F_0 = -3e^2/(32\pi d^4)$ with and without spatial dispersion in the graphene conductivity at $T = 0$ K as a function of (d) the gap Δ and (e) the chemical potential μ. From Drosdoff *et al.*, 2012.

graphene nonretarded vdW interaction. In general, it is assumed that higher vertex corrections may change the magnitude of the force somewhat, but not the asymptotic distance dependence. However, this may not be the case for graphene as the type of renormalization yields very different results. The renormalization-group method (Kotov *et al.*, 2012; Sodemann and Fogler, 2012) results in a weak correction to the interaction energy as opposed to the two-loop level in the large-N limit approach (Das Sarma, Hwang, and Tse, 2007), where the characteristic distance dependence has a different power law (Dobson, Gould, and Vignale, 2014). These findings indicate that graphene may be the first type of material for which RPA is not enough to capture the vdW force in the quantum limit. Along the same lines, Sharma *et al.* (2014) showed that for strained graphenes, where electron-electron correlations beyond RPA are much more pronounced, corrections to the vdW interaction, consistent with the renormalization-group model, are found.

Besides the fundamental questions regarding basic properties of graphene Casimir and vdW interactions, other and more exotic applications of this phenomenon have been proposed. For example, Phan *et al.* (2012) proposed that a graphene flake suspended in a fluid, such as Teflon or bromobenzene, can serve as a prototype system for measuring thermal effects in Casimir interactions. The balance of gravity, buoyancy, and the Casimir force on the flake creates a harmoniclike potential, which causes the flake to be trapped. By measuring changes in the temperature-dependent frequency of oscillations, one can potentially relate these changes to the Casimir interaction. Alternative ways to tailor the graphene Casimir interaction have also been recognized. For example, Svetovoy *et al.* (2011) showed that the thermal effects can be enhanced or inhibited if one considers the force between graphene and different substrates. Sernelius (2012) found that retardation due to the finite speed of light can also be made prominent depending on the type of substrates graphene interacts with. Drosdoff and Woods (2011) proposed that metamaterials with magnetically active components can result in a repulsive Casimir force. Phan *et al.* (2013) showed a regime where repulsion can be achieved with a lipid membrane. Also, Dirac carriers with constant optical conductivity result in unusual Casimir effects behavior in nonplanar objects. For example, the interaction on a spherical shell with $\sigma = \text{const}$ has markedly different asymptotic behavior and sign when compared to the one for a plasma shell or for planar sheets with $\sigma = \text{const}$ (Bordag and Khusnutdinov, 2008; Khusnutdinov, Drosdoff, and Woods, 2014).

The Casimir-Polder force involving atoms and graphene sheets has also been of interest due to their relevance to several phenomena, including trapping or coherently manipulating ultracold atoms by laser light (Ito *et al.*, 1996; Bajcsy *et al.*, 2009; Goban *et al.*, 2012). The theoretical description follows from Eq. (9) by considering one of the substrates as a rarefied dielectric (Dzyaloshinskii, Lifshitz, and Pitaevskii, 1961;

Lifshitz and Pitaevskii, 1980; Milonni, 1993). In addition to atom and graphene (Judd *et al.*, 2011), configurations containing additional substrates have been studied (Chaichian *et al.*, 2012). Others have suggested that it may be possible to observe quantum reflection of He and Na atoms via the Casimir-Polder interaction as a means to discriminate between the Dirac and hydrodynamic model description for graphene (Churkin *et al.*, 2010). Casimir-Polder shifts of anisotropic atoms near multilayered graphene sheets in the presence of a Huttner-Barnett dielectric (a linearly polarizable medium, which is modeled by microscopic harmonic fields) have also been calculated (Eberlein *et al.*, 2012). Thermal fluctuation effects in atom and graphene configurations can also be much stronger due to the reduced thermal wavelength $\tilde{\lambda}_T$. Thermal Casimir-Polder effects become apparent for $d > 50$ nm at room temperature as the interaction is essentially due to the zero Matsubara frequency giving rise to $F_T = -3k_BT\alpha(0)/4d^4$ (Chaichian *et al.*, 2012; Drosdoff *et al.*, 2012; Kaur *et al.*, 2014; Bordag *et al.*, 2015). Interesting possibilities for temporal changes in the atomic spectrum affecting the graphene sheet by creating ripples have also been suggested (Ribeiro and Scheel, 2013a). The Casimir-Polder force has also been explored for shielding vacuum fluctuations using the framework of the Dirac model (Ribeiro and Scheel, 2013b).

2. Quasi-1D graphene nanostructures

Investigating atom and CNT interactions is of utmost importance for applications, such as trapping cold atoms near surfaces (Petrov *et al.*, 2009; Goodsell *et al.*, 2010), manipulating atoms near surfaces for quantum information processing (Schmiedmayer, Folman, and Calarco, 2002), and hydrogen storage (Dillon *et al.*, 1997). CNT-CNT interactions are relevant for the stability and growth processes of nanotube composites (Charlier, Blase, and Roche, 2007). To calculate the interaction, one must take into account the cylindrical boundary conditions. Researchers have utilized scattering techniques to study the distance dependence involving metallic wires with Dirichlet, Neumann, and perfect-metal boundary conditions (Emig *et al.*, 2006; Noruzifar, Emig, and Zandi, 2011). Inclined metallic wires have also been considered (Dobson, Gould, and Klich, 2009; Noruzifar *et al.*, 2012; Rodriguez-Lopez and Emig, 2012). Calculations for CNT interactions, however, are challenging as one has to take into account simultaneously the chirality dependent response properties and the cylindrical boundary conditions for the electromagnetic fields.

The Lifshitz approach was applied to CNTs via the proximity force approximation, which is typically appropriate at sufficiently close separations (Blocki *et al.*, 1977). The cylindrical surface is represented by an infinite number of plane strips of infinitesimal width, which are then summed up to recover the CNT surface. This method has been applied to atom and single-walled nanotubes and atom and multiwall nanotubes treated as a cylindrical shell of finite thickness (Blagov, Klimchitskaya, and Mostepanenko, 2005, 2007; Bordag *et al.*, 2006; Klimchitskaya, Blagov, and Mostepanenko, 2008; Churkin *et al.*, 2011). In these studies, the dielectric response of the nanotubes is not chirality dependent. Blagov, Klimchitskaya, and Mostepanenko (2005) used an extrapolated dielectric function for graphite, Bordag *et al.* (2006) used the response to be due to a surface density of the π electrons smeared over the surface, Blagov, Klimchitskaya, and Mostepanenko (2007) utilized a free-electron gas representation for the cylindrical CNT surfaces, while Churkin *et al.* (2011) took the graphene Dirac and hydrodynamic models. In these works, the interaction energy is always of the form $E = -C_3(d)/d^3$, where the coefficient $C_3(d)$ is also dependent on the cylindrical curvature and atomic polarizability.

Interactions between nanotubes in a double-wall configuration have been calculated using the QED approach suitable for dispersive and absorbing media as well (Buhmann and Welsch, 2007). Within this formalism the boundary conditions are taken into account by solving the Fourier domain operator Maxwell equations using a dyadic Green's function, which also allows the inclusion of the chirality dependent response properties of the individual nanotubes. The calculations utilize the fluctuation-dissipation theorem and the force per unit area is the electromagnetic pressure on each surface expressed in terms of the Maxwell stress tensor (Tomaš, 2002). For planar systems, the QED and the Lifshitz theory lead to the same expression [Eq. (9)], which has also been shown for systems involving graphene (Hanson, 2008; Drosdoff and Woods, 2010). The QED method, applied to the interaction in various double-walled CNTs, revealed that the chirality dependent low-energy surface plasmon excitations play a decisive role in the interaction (Popescu, Woods, and Bondarev, 2011; Woods *et al.*, 2013). The attractive force is actually dominated by low-energy interband plasmon excitations of both nanotubes. The key feature for the strongest attraction is for the CNTs to have overlapping strong plasmon peaks in the EELS. This is true for concentric (n, n) armchair CNTs, which exhibit the strongest interaction as compared to tubes with comparable radii, but having other chiralities, as shown in Fig. 6. The results are consistent with electron diffraction measurements showing that the most probable double-walled CNT is the one in which both tubes are of armchair type (Harihara *et al.*, 2006). This indicates that the mutual Casimir interaction influenced by the collective excitations may be a potential reason for this preferential formation.

The Casimir-Polder interaction involving CNTs has also been considered via the QED formalism. For this purpose, one utilizes a generalized atomic polarizability tensor containing dipolar and multipolar contributions and a scattering Green's function tensor expressed in cylindrical wave functions (Tai, 1994; Li *et al.*, 2000; Buhmann *et al.*, 2004). It has been shown that the chirality dependent CNT dielectric function plays an important role determining the strength of the atom and nanotube coupling (Fernari, Scheel, and Knight, 2007). The QED approach was also used initially by Bondarev and Lambin (2004, 2005), where the nonretarded interaction potential is equivalently given in terms of a photonic density of states. These studies also show that the interaction is sensitive to the CNT chirality (Rajter *et al.*, 2007, 2013). It was found that the stronger optical absorption by the metallic CNTs suppresses the vdW atomic attraction, which can be of importance to tailor atomic spontaneous decay near CNT surfaces.

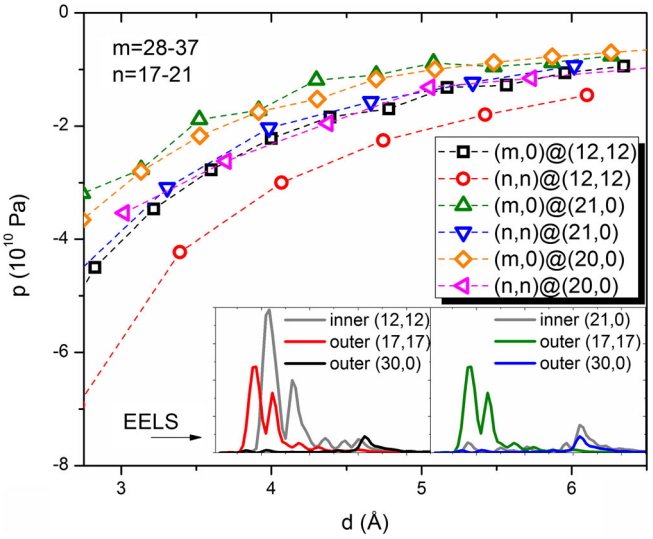

FIG. 6. Electromagnetic pressure on each nanotube in a double-wall CNT system as a function of separation. The inset shows calculated EELS for several armchair (n,n) and zigzag $(n,0)$ nanotubes as a function of frequency in eV. The attraction is strongest between two concentric armchair nanotubes due to the presence of strong overlapping low-frequency peaks in the spectra. The notation $(m,0)@(n,n)$ corresponds to $(m,0)$ as the inner tube and (n,n) as the outer tube.

For GNRs the situation is even more technically difficult as compared to nanotubes since analytical results for the boundary conditions for striplike systems are not available. Nevertheless, a perturbation series expansion of the Lifshitz formula in the dilute limit separates the geometrical and dielectric response property contributions into convenient factor terms, which can be quite useful to study the finite extensions of the nanoribbons in their vdW interaction (Stedman, Drosdoff, and Woods, 2014). A recent study also showed that a nonretarded Lifshitz-like formula for the vdW interaction between parallel quasi-1D systems having width $W \ll d$ can also be derived (Drosdoff and Woods, 2014). The force per unit length is written in terms of a TM-like "reflection coefficient" containing the GNR response properties, which makes the expression reminiscent of the Lifshitz vdW expression for planar objects in Eq. (9). This is quite appealing as it presents a general way to calculate vdW interactions in any type of 1D parallel systems.

Applying this theory to GNRs described by their specific response properties (Brey and Fertig, 2006) shows that the chemical potential is crucial in the interplay between quantum-mechanical and thermal effects in the interaction. A μ-dependent transition between these two regimes is reported correlating with the onset of intraband transitions (Drosdoff and Woods, 2014). While GNRs with $\mu = 0$ behave like typical dielectric materials with a vdW force $F \sim -1/d^6$, when $\mu \sim E_g$ (E_g is the energy gap in the GNR band structure), the interaction becomes completely thermal with a characteristic behavior

$$F = -\frac{\pi k_B T}{64 d[\ln(d/W)]^2}.$$

For semiconductors, such as GaAs wires, however, thermal fluctuations dominate the interaction completely. This is at complete odds with the dispersive interaction involving standard materials, where thermal effects are typically very small (Klimchitskaya, Mohideen, and Mostepananko, 2009). It turns out that for GaAs quantum wires the plasma frequency is much reduced as compared to 3D GaAs (Das Sarma, Hwang, and Zheng, 1996) resulting in the force being dominated by the $n = 0$ Matsubara term.

D. Materials with topologically nontrivial phases

In addition to graphene, there are other materials with Dirac spectra and TIs have a special place in this class of systems. TIs are a new phase of matter with nontrivial topological invariants in the bulk electronic wave function space. The topological invariants are quantities that do not change under continuous deformation, and they lead to a bulk insulating behavior and gapless surface Dirac states in the band structure (Qi, Hughes, and Zhang, 2008; Hasan and Kane, 2010; Qi and Zhang, 2011; Ando, 2013; Cayssol, 2013). The modern history of TIs started with the realization that a strong spin-orbit coupling can result in a TI phase with several materials being proposed as possible candidates, including Bi_xSb_{1-x}, Bi_2Se_3, Bi_2Te_3, and $TlBiSe_2$ among others (Chen *et al.*, 2009; Ando, 2013). In the low momentum limit the 2D states, which are topologically protected by symmetry invariance, are described by a helical version of the massless Dirac Hamiltonian (Zhang *et al.*, 2009; Liu *et al.*, 2010)

$$H_{\text{surf}} = \hat{\mathbf{z}} \cdot (\sigma \times \mathbf{k}), \tag{15}$$

where $\hat{\mathbf{z}}$ is the unit vector perpendicular to the surface (located in the x-y plane), $\sigma = (\sigma_x, \sigma_y, \sigma_z)$ are the Pauli matrices, and $\mathbf{k}$ is the 3D wave vector.

Topologically nontrivial materials can be classified via their symmetries and dimensions (Schnyder *et al.*, 2008; Kitaev, 2009; Hasan and Kane, 2010; Ryu and Takayanagi, 2010) or by dimensional reduction (Qi, Hughes, and Zhang, 2008). Three-dimensional systems are characterized by time reversal (TR) symmetry leading to each eigenstate of the Hamiltonian (15) being accompanied by its TR conjugate or Kramers partner (Schnyder *et al.*, 2008). Experimentally, however, one observes an odd number of Dirac states. This is understood by realizing that the Dirac cones of the Kramer's pairs appear on each side of the surface of the material and the cone in empty space cannot be detected. In addition, these surface states are protected from backscattering by the TR symmetry, which makes them insensitive to spin-independent scattering—a useful feature for quantum computation applications (Leek *et al.*, 2007). Chern insulators (CIs) are essentially two-dimensional TIs and their low-energy band structure, also described by Eq. (15), consists of an even number of helical edge states. CIs have strong enough interband exchange energy, responsible for the hybridization of the surface states from the Dirac cone doublets. CI states are further described by a topological integer Chern number $C \in \mathbb{Z}$ quantified as $C = \frac{1}{2}\sum_{i=1}^{N} \text{sign}(\Delta_i)$, where N denotes the (even) number of Dirac cones and Δ_i is the mass gap of each Dirac cone. The mass gap can be tailored by an applied

magnetic field or other means and it can be positive or negative.

The properties affecting the vdW and Casimir interactions in systems with topologically nontrivial phases are linked to the dimensionality and response characteristics of the involved Dirac materials. The optical conductivity components of TIs and CIs involving the low-energy Dirac carriers have been obtained within the standard Kubo approach or the quantum kinetics equation method (Tse and MacDonald, 2010; Rodriguez-Lopez and Grushin, 2014). Analytical representations for the longitudinal surface optical conductivity in the small temperature regime $k_B T \ll \min(|\mu_F|, |\Delta|)$ (here μ_F is the Fermi energy relative to the Dirac point) and small disorder have been found (Tse and MacDonald, 2010, 2011; Chen and Wan, 2011, 2012; Grushin *et al.*, 2012) with expressions similar to the ones for graphene [Eqs. (11) and (12)]. In addition, the topologically protected surface states lead to a strong quantum Hall effect without an external magnetic field whenever perturbations breaking the TR symmetry induce a gap in the band structure. For the low-energy carriers in Eq. (15) the associated surface Hall conductivity has the following expression at imaginary frequency:

$$\sigma_{xy}(i\omega) = -\frac{\alpha c \Delta}{2\pi\hbar\omega}\left[\tan^{-1}\left(\frac{\hbar\omega}{2\epsilon_c}\right) - \tan^{-1}\left(\frac{\hbar\omega}{2|\Delta|}\right)\right]. \quad (16)$$

Here ϵ_c is the energy cutoff of the Dirac Hamiltonian, which we associate with the separation between the Dirac point and the closest bulk band.

For the Casimir interaction involving CIs, it is important to note that these materials can exhibit a quantum anomalous Hall effect at zero frequency or in the absence of an external magnetic field. By tuning the mass gap (via doping or changing the magnetization of the involved material), one can make the zero-frequency 2D optical conductivity vanish $\sigma_{xx}(\omega = 0, |\mu_F| < |\Delta|) = 0$, while the Hall conductivity becomes $\sigma_{xy}(\omega = 0, |\mu_F| < |\Delta|) = (\alpha c/4\pi)\mathrm{sign}(\Delta)$. After summing up the contributions from all Dirac cones, one obtains a *quantized* Hall conductivity in terms of the Chern number $\sigma_{xy}(\omega = 0) = (\alpha c/2\pi)C$.

Inducing a mass gap has important consequences for the surface Hall response in 3D TIs as well. By applying an external magnetic field, it is possible to realize the fractional quantum Hall effect with a quantized conductivity

$$\sigma_{xy}(\omega = 0, |\Delta| > |\mu_F|) = \frac{\alpha c}{2\pi}(\tfrac{1}{2} + n),$$

where n is an integer (Zheng and Ando, 2002; Hasan and Kane, 2010). Nevertheless, one also needs to add the bulk dielectric response. Typically, a standard Drude-Lorentz model is sufficient, and it has been shown that specifically for the Casimir interaction a single oscillator for the dielectric function is enough to capture the characteristic behavior (Chen and Wan, 2011; Grushin, Rodriguez-Lopez, and Cortijo, 2011; Grushin and de Juan, 2012). Therefore, the bulk response can be considered as

$$\epsilon(i\omega) = \epsilon_0 + \frac{\omega_e^2}{\omega_R^2 + \omega^2},$$

where ω_e is the strength of the oscillator and ω_R is the location of the resonance.

The surface response properties dramatically affect the electrodynamics in topologically nontrivial materials in 3D. In fact, the electrodynamic interaction can be described via generalized Maxwell equations containing a magnetoelectric coupling due to the surface Hall conductivity. Equivalently, this generalized electrodynamics includes an *axion* field $\theta(\mathbf{r}, t)$ manifested in a Chern-Simmons term in the Lagrangian, $\mathcal{L}_\theta = [\alpha\theta(\mathbf{r}, t)/2\pi^2]\mathbf{E}\cdot\mathbf{B}$, whose role is to preserve the TR symmetry in the Maxwell equations (Wilczek, 1987). While $\theta(\mathbf{r}, t)$ depends on position and time in general, for topological insulators, this is a constant field, such that $\theta \neq 0$ in the bulk and $\theta = 0$ in the vacuum above the surface of the material. We further note that the quantization of the Hall effect in 3D TIs is inherited in the axion term according to $\theta = (2n+1)\pi$ (Qi, Hughes, and Zhang, 2008; Essin, Moore, and Vanderbilt, 2009).

The concept of axion electrodynamics was first proposed in high-energy physics as a possible means to explain dark matter (Peccei and Quinn, 1977; Wilczek, 1987), and now an axion type of electromagnetic interactions appears in the description of condensed-matter materials, such as TIs. The axion field originating from the topologically nontrivial surface states leads to many new properties, including induced magnetic monopoles, a quantized Faraday angle in multiple integers of the fine structure constant, and a large Kerr angle (Wilczek, 1987; Qi *et al.*, 2009; Tse and MacDonald, 2010, 2011). The modified electrodynamics due to the Chern-Simmons term with the associated boundary conditions is also of importance to the Casimir interaction as shown earlier from a high-energy physics perspective (Bordag and Vassilevich, 2000).

E. Possibility of Casimir repulsion in topological materials

The underlying electronic structure of the materials and their unconventional Hall response open up opportunities to explore the Casimir effect in new directions. Figure 7(a) depicts the low-energy Dirac band structure for an appropriate lattice model for a CI with the associated longitudinal (σ_{xx}) and Hall (σ_{xy}) conductivities (Grushin *et al.*, 2012; Rodriguez-Lopez and Grushin, 2014). The reflection matrices in the Lifshitz expression from Eq. (9) have been determined for two semi-infinite TI substrates with isotropic surface conductivity σ_{ij} and dielectric and magnetic bulk response properties taken as diagonal 3D matrices $\epsilon = \epsilon(\omega)\mathbb{I}$ and $\mu = \mu(\omega)\mathbb{I}$, respectively. Generalizations due to nonlocal effects and anisotropies in the response (Grushin, Rodriguez-Lopez, and Cortijo, 2011), as well as finite width substrates (Peterson and Ström, 1974), can also be included. The reflection coefficients for CIs follow from the ones for the 3D TIs simply by setting $\epsilon, \mu \to 1$ (Tse and MacDonald, 2012; Martinez and Jalil, 2013; Rodriguez-Lopez and Grushin, 2014). It turns out, however, that in all cases the surface Hall conductivity is a key component in

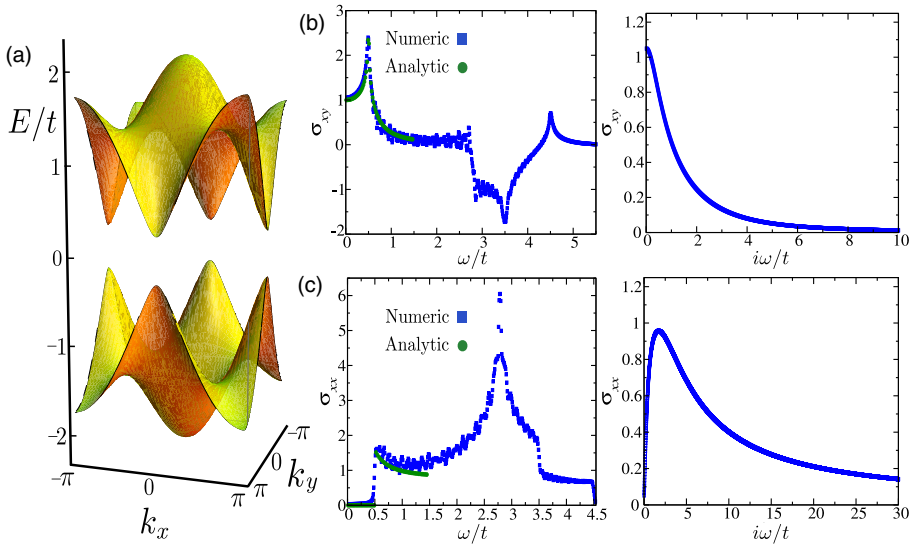

FIG. 7. (a) Energy band structure of a CI calculated via a generic two-band tight-binding model (Grushin *et al.*, 2012). The low momentum limit of the energy band structure is consistent with the Dirac Hamiltonian in Eq. (15). (b) Real part of $\sigma_{xy}(\omega)$ (left panel) and $\sigma_{xy}(i\omega)$ (right panel). (c) Real parts of $\sigma_{xx}(\omega)$ (left panel) and $\sigma_{xx}(i\omega)$ (right panel) correspond to the energy band structure from (a). The calculations are performed with $C = 1$, $\Delta = 0.25t$, and $\epsilon = 2.25t$ (t denotes the hopping integral for the employed lattice model; here it is taken to be equal to the frequency bandwidth). The conductivities are in units of $\alpha c/(2\pi)$. The analytically found $\sigma_{xx}(\omega)$ and $\sigma_{xy}(\omega)$ are in excellent agreement with numerically evaluated Kubo expressions. From Rodriguez-Lopez and Grushin, 2014.

understanding the asymptotic distance dependence, magnitude, and sign of the interaction.

Figure 8(a) summarizes results for calculated Casimir energies at the quantum-mechanical regime (low T and/or large d). The graph indicates that there is a change of distance dependence behavior when comparing the small and large d asymptotics for interacting CIs. The analytical expressions for the conductivity components, which agree very well with the numerical Kubo formalism calculations according to Figs. 7(b) and 7(c), are especially useful in better understanding the underlying physics of the Casimir energy. It was obtained that the energy at small d is determined by the longitudinal component of the conductivity and the interaction is always attractive (Rodriguez-Lopez and Grushin, 2014). For large d, however, it is possible to achieve repulsion if the two CIs have Chern numbers $C_1 C_2 < 0$ and the Hall conductivity is much larger than the longitudinal one. The interaction energy in this case is a nonmonotonic function of distance and it is quantized according to $E \sim C_1 C_2$, which also indicates that the strongest repulsion occurs for materials with large Chern numbers. It is concluded that if repulsion is desired, one must search for CI materials with vanishing diagonal conductivity components and strong Hall conductivity capable of sustaining much enhanced C numbers. Let us note that a quantized Casimir interaction may be typical for materials that can support a strong Hall effect. In fact, such a phenomenon was predicted to

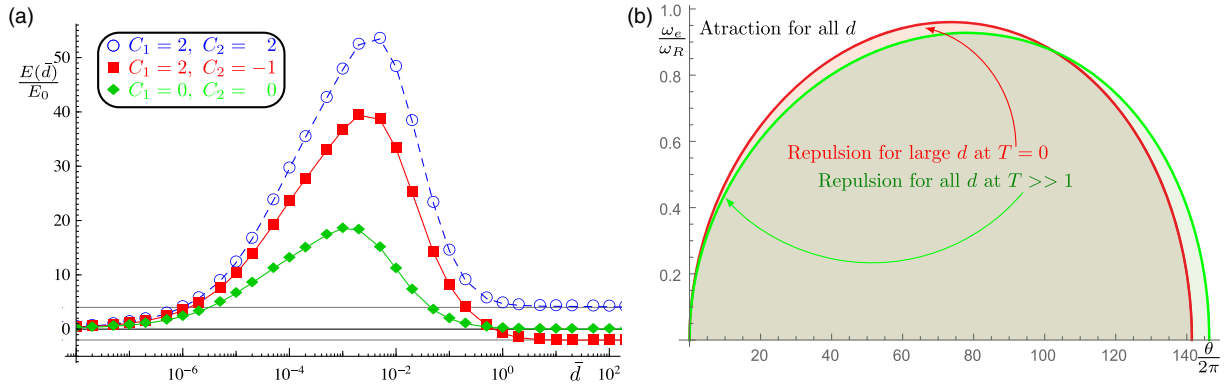

FIG. 8. (a) Casimir interaction energy $E(d)$ between two CIs in units of $E_0(d) = -\hbar c\alpha^2/(8\pi^2 d^3)$ as a function of $\bar{d} = td/\hbar c$ for different values of $C_{1,2}$ and $|\Delta| = t$. (b) Phase diagram $(\omega_e/\omega_R, \theta/2\pi)$ for the interaction energy between two semi-infinite TI substrates for all separation scales. The parameters ω_e and ω_R correspond to the strength and location of the Drude-Lorentz oscillator, respectively. The repulsion for large separations at $T = 0$ K is given by the red region (outlined by the red line), while the repulsion for all separations at high T is given by the green region (outlined by the green line). Here $\theta/2\pi = (n + 1/2)$ and $\theta_1 = -\theta_2 = \theta$ for the substrates. Repulsion is observed for a large range of Chern numbers. Adapted from Rodriguez-Lopez and Grushin, 2014.

exist in graphene-graphene systems at sufficiently large separations with an external magnetic field (Tse and MacDonald, 2012). The associated Landau-level filling factors in the Hall conductivity lead to a quantization condition in the force, and similar findings have been reported for atom and graphene configurations (Cysne *et al.*, 2014).

The Casimir interaction between TIs has also been studied, in which case the bulk dielectric response is included (Sec. III.D). Recent work (Grushin and Cortijo, 2011) has shown that the energy has unique characteristics due to the balance between the bulk and surface state contributions mediated by the axion term θ. Figure 8(b) summarizes numerical results for the interaction energy phase diagram showing repulsive and attractive regimes depending on the Drude-Lorentz parameters (ω_e/ω_R) and the surface contribution (θ). Reported analytical calculations enable a better understanding of the important factors determining the interaction in various limits. It is found that if the bulk response is treated as a single Lorentz oscillator, it is possible to obtain Casimir repulsion at larger separations (Rodriguez-Lopez, 2011), where the surface contributions through the Hall conductivity dominate the response provided $\theta_1\theta_2 < 0$. For shorter separations the bulk response becomes dominant, and the Casimir interaction is attractive. One also obtains attraction at all distance scales when $\theta_1\theta_2 > 0$ (Rodriguez-Lopez, 2011). Others have predicted that repulsion is also possible in the regime of short separations; however, this is considered to be an artifact of a frequency independent surface conductivity taken in the calculations (Chen and Wan, 2011; Grushin and Cortijo, 2011; Grushin, Rodriguez-Lopez, and Cortijo, 2011; Nie *et al.*, 2013). In addition, several recent works have shown that the behavior of the Casimir interaction and the existence of repulsion, in particular, depend strongly on the magnitude of the finite mass gap, the applied external magnetic field, and the thickness of the TI slabs (Chen and Wan, 2011; Nie *et al.*, 2013). The thermal Casimir interaction between TIs has also been studied (Grushin and Cortijo, 2011; Rodriguez-Lopez, 2011). The energy corresponding to the $n = 0$ Matsubara term depends strongly on the axion fields. The interaction is found to be attractive when $\theta_1\theta_2 > 0$. However, thermal Casimir repulsion is obtained at all distances for $\theta_1\theta_2 < 0$ as shown in Fig. 8(b). Similar considerations for repulsion may apply for CIs, since their thermal Casimir energy can be obtained analogously to be proportional to the surface Hall conductivities $\sigma_{xy}^{(1)}\sigma_{xy}^{(2)}$. These results indicate that topological Dirac materials, such as 2D CIs and 3D TIs, may be good candidates to search for a repulsive thermal Casimir interaction.

The long-ranged dispersive interactions involving systems with nontrivial topological texture are complex phenomena. Materials with Dirac carriers lend themselves as templates where concepts, typically utilized in high-energy physics, cross over to condensed-matter physics with vdW and Casimir interactions as a connecting link. Topologically nontrivial features in the electronic structure and optical response properties result in unusual asymptotic distance dependences, an enhanced role of thermal fluctuations at all distance scales, and new possibilities of Casimir repulsion. Ongoing work in the area of Dirac materials will certainly continue stimulating further progress in the field of vdW and Casimir physics and further widening the scope of fluctuation-induced phenomena.

IV. STRUCTURED MATERIALS

The geometry of the interacting objects and the interplay with the properties of the materials is also of interest for tailoring the Casimir force. Structured materials, including metamaterials, photonic crystals, and plasmonic nanostructures, allow the engineering of the optical density of states by proper design of their individual components. As a result, one is able to manipulate the interaction utilizing complex, nonplanar geometries. Recent experimental studies have begun the exploration of such geometry effects particularly with dielectric and metallic gratings (Chan *et al.*, 2008; Intravaia *et al.*, 2013). The theoretical description has been challenging due to the complex dependence of dispersive interactions upon nonplanar boundary conditions. One approach relies on effective medium approximations, where the emphasis is on models of the dielectric response of the composite medium as a whole. The second approach deals with particular boundary conditions via computational techniques. While the interaction of electromagnetic waves with metallic and dielectric structures of complex shapes is well established in classical photonics, the main challenge stems from the inherently broadband nature of Casimir interactions, where fluctuations at all frequencies and wave vectors have to be taken into account simultaneously.

A. Metamaterials

Electromagnetic metamaterials are composites consisting of conductors, semiconductors, and insulators that resonantly interact with light at designed frequencies. The individual components make up an ordered array with unit cell size much smaller than the wavelength of radiation. As a result, an electromagnetic wave impinging on the material responds to the overall combination of these individual scatterers as if it were an effectively homogeneous system. Metamaterials were speculated almost 50 years ago by Victor Veselago (1968), who was the first to explore materials with negative magnetic permeability in optical ranges. However, it was over 20 years ago that John Pendry proposed the workhorse metamaterials' structure, the split-ring resonator (SRR), that allowed an artificial magnetic response and was a key theoretical step in creating a negative index of refraction (Pendry *et al.*, 1999). David Smith and colleagues were the first to experimentally demonstrate composite metamaterials, using a combination of plasmonic-type metal wires and an SRR array to create a negative effective permittivity $\epsilon_{\text{eff}}(\omega)$ and a negative effective permeability $\mu_{\text{eff}}(\omega)$ in the microwave regime (Shelby, Smith, and Schultz, 2001). Many exotic phenomena have been discovered afterward, including negative index of refraction, reversal of Snell's law, perfect focusing with a flat lens, reversal of the Doppler effect and Cherenkov radiation, electromagnetic cloaking, and transformation optics.

Such materials are of great interest for Casimir force modifications. Casimir repulsion was predicted by Boyer (1974) between a perfectly conducting plate and a perfectly permeable one, but it may also occur between real plates as

long as one is mainly (or purely) nonmagnetic and the other mainly (or purely) magnetic (Kenneth *et al.*, 2002). The latter possibility was considered unphysical (Iannuzzi and Capasso, 2003), since naturally occurring materials do not show strong magnetic response at near-infrared or optical frequencies, corresponding to gaps $d = 0.1$–$10\ \mu$m. However, recent progress in nanofabrication has resulted in metamaterials with magnetic response in the visible range of the spectrum (Shalaev, 2007), fueling the hope for "quantum levitation."

The Casimir force for structured materials with unit cells much smaller than the wavelength of light can be calculated via Eq. (9) for magnetodielectric media with reflection coefficients for two identical substrates ($\mathbb{R}_1 = \mathbb{R}_2 = \mathbb{R}$) found as

$$R^{(ss)} = \frac{\mu_{\rm eff}(i\omega)\bar{q} - \bar{k}}{\mu_{\rm eff}(i\omega)\bar{q} - \bar{k}}, \qquad R^{(pp)} = \frac{\epsilon_{\rm eff}(i\omega)\bar{q} - \bar{k}}{\epsilon_{\rm eff}(i\omega_n)\bar{q} - \bar{k}}, \quad (17)$$

where $\bar{q} = \sqrt{k_\parallel^2 + (\omega/c)^2}$ and $\bar{k} = \sqrt{k^2 + \mu_{\rm eff}\epsilon_{\rm eff}\omega^2/c^2}$. Calculations based on this approach suggested that left-handed metamaterials might lead to repulsion (Henkel and Joulain, 2005; Leonhardt and Philbin, 2007). Metamaterials, however, typically have narrow-band magnetic response and are anisotropic. Thus questions naturally arise concerning the validity of such predictions for real systems. Given that the Lifshitz formula is dominated by low-frequency modes $\omega < c/d$, a repulsive force is in principle possible for a passive left-handed medium as long as $\mu_{\rm eff}(i\omega)$ is sufficiently larger than $\epsilon_{\rm eff}(i\omega)$ in that regime. Then the repulsion is a consequence of the low-frequency response behavior and not of the fact that the medium happens to be left handed in a narrow band about some real resonant frequency. Application of the Lifshitz formalism requires the knowledge of $\epsilon_{\rm eff}(i\omega)$ and $\mu_{\rm eff}(i\omega)$ for a large range, up to the order of $\omega = c/d$. Such functions can be evaluated via the Kramers-Kronig relations in terms of $\epsilon_{\rm eff}(\omega)$ and $\mu_{\rm eff}(\omega)$ at real frequencies. The point about the broadband nature of the response properties is very important, as it shows that knowledge of a metallic-based metamaterial near a resonance is not sufficient for the computation of Casimir forces: the main contribution to $\epsilon_{\rm eff}(i\omega)$ and $\mu_{\rm eff}(i\omega)$ typically comes from frequencies lower than the resonance frequency. This also implies that repulsive forces, if any, are in principle possible without the requirement that the metamaterial resonance should be near the frequency scale defined by the inverse of the gap of the Casimir cavity.

In typical metamaterial structures, the effective electric permittivity $\epsilon_{\rm eff}(\omega)$ and magnetic permeability $\mu_{\rm eff}(\omega)$ close to the metamaterial resonance are well described in terms of a Drude-Lorentz model,

$$\epsilon_{\rm eff}(\omega), \mu_{\rm eff}(\omega) = 1 - \frac{\Omega_{e,m}^2}{\omega^2 - \omega_{e,m}^2 + i\gamma_{e,m}\omega} \quad (18)$$

in which Ω_e (Ω_m) is the electric (magnetic) oscillator strength, ω_e (ω_m) is the metamaterial electric (magnetic) resonance frequency, and γ_e (γ_m) is a dissipation parameter. These parameters depend mainly on the subwavelength geometry of the unit cell, which can be modeled as a *LRC* circuit. For metamaterials that are partially metallic, such as SRRs (operating in the GHz–THz range) and fishnet arrays (operating in the near infrared or optical) away from resonance, it is reasonable to assume that the dielectric function also has a Drude background

$$\epsilon_D(\omega) = 1 - \frac{\Omega_D^2}{\omega(\omega + i\gamma_D)}$$

(here Ω_D is the plasma frequency and γ_D is the Drude dissipation rate). As the Drude background overwhelms the resonant contribution at low frequencies, it contributes substantially to the Casimir force between metallic metamaterial structures. Effects of anisotropy, typical in the optical response of 3D metamaterials and of 2D metasurfaces, can also be incorporated (Rosa, Dalvit, and Milonni, 2008a). Figure 9, which depicts the Casimir force between two identical planar 3D uniaxial metamaterials that have only electric anisotropy, shows that the interaction is always attractive.

A key issue here is the realization that it is incorrect to use these Drude-Lorentz expressions when computing dispersion interactions (Rosa, Dalvit, and Milonni, 2008b). Indeed, although Eq. (18) is valid close to a metamaterial resonance, it does not hold in a broadband frequency range. In particular, calculations based on Maxwell's equations in a long wavelength approximation for SRRs result in a slightly different form for the effective magnetic permeability (Pendry *et al.*, 1999)

$$\mu_{\rm SRR}(\omega) = 1 - \frac{f\omega^2}{\omega^2 - \omega_m^2 + i\gamma_m\omega}, \quad (19)$$

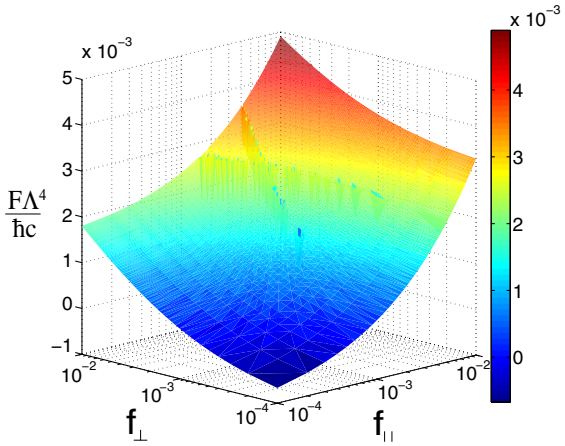

FIG. 9. Casimir force per unit area A between a metallic semispace and an anisotropic metallic-based planar magnetic metamaterial with a weak Drude background. The filling factors $f_\parallel$ and $f_\perp$, parallel and orthogonal to the vacuum-metamaterial interface, account for the fraction of metallic structure contained in the metamaterial. The SRR Drude parameters are $\Omega_D = 2\pi c/\Lambda = 1.37 \times 10^{16}$ rad/s and $\gamma_D = 0.006\Omega_D$ (corresponding to silver) and its Drude-Lorentz parameters are $\Omega_e/\Omega_D = 0.04$, $\Omega_m/\Omega_D = 0.1$, $\omega_e/\Omega_D = \omega_m/\Omega_D = 0.1$, and $\gamma_e/\Omega_D = \gamma_m/\Omega_D = 0.005$. The Drude parameters for the metallic semispace are $\Omega = 0.96\Omega_D$ and $\gamma = 0.004\Omega_D$. Temperature is set to zero, and the distance between the bodies is fixed at $d = \Lambda$. From Rosa, Dalvit, and Milonni, 2008a.

where the filling factor $f < 1$ is a geometry dependent parameter. The crucial difference between Eqs. (18) and (19) is the ω^2 factor in the numerator of the latter, a consequence of Faraday's law (Rosa, 2009). Although close to the resonance both expressions give almost identical behaviors, they differ in the low-frequency limit $\mu_{\rm eff}(i\omega) > 1$, while $\mu_{\rm SRR}(i\omega) < 1$. The fact that all passive materials have $\epsilon(i\omega) > 1$ implies that Casimir repulsion is impossible for any magnetic metamaterial made of metals and dielectrics (Rosa, Dalvit, and Milonni, 2008a). This conclusion is confirmed by scattering theory calculations that do not rely on any effective medium or homogenization approximations. For example, Yannopapas and Vitanov (2009) exactly computed the Casimir force for 2D metasurfaces made of a square close-packed array of nonmagnetic microspheres of $LiTaO_3$ (an ionic material) or of CuCl (a semiconductor). Although the systems are magnetically active in the infrared and optical regimes, the force between finite slabs of these materials and metallic slabs is attractive since the effective electric permittivity at imaginary frequencies is larger than the magnetic permeability. In Fig. 10 we show the Casimir force (normalized with respect to the ideal zero-temperature Casimir force F_C) between a gold plate and a 2D $LiTaO_3$ metasurface together with the effective permittivity and permeabilities of a close-packed $LiTaO_3$ crystal. The results confirm that the Casimir interaction is attractive in magnetic metamaterials made of nonmagnetic meta-atoms. In contrast, intrinsically magnetic meta-atoms could potentially lead to Casimir repulsion. Naturally occurring ferromagnets do not show magnetic response in the infrared and optical regimes, as needed by the Casimir effect, but small magnetic nanoparticles (e.g., a few nanometer-sized Ni spheres) become superparamagnetic in the infrared. A realization of the original idea for Casimir repulsion by Boyer was then proposed based on a metasurface made of such intrinsically magnetic nanoparticles (Yannopapas and Vitanov, 2009).

Chiral metamaterials made of metallic and dielectric meta-atoms were also proposed as candidates for Casimir repulsion (Zhao *et al.*, 2009). When described by an effective medium theory, such systems possess an effective magnetoelectric response that modifies the standard constitutive relations in Maxwell's equations as $\mathbf{D} = \epsilon_0\epsilon\mathbf{E} + i\kappa_m\mathbf{H}/c$ and $\mathbf{B} = \mu_0\mu\epsilon\mathbf{H} - i\kappa_m\mathbf{E}/c$. Close to a resonance, the magnetodielectric coefficient κ_m can be modeled as

$$\kappa_m(\omega) = \frac{\omega_{\kappa_m}\omega}{\omega^2 - \omega_{\kappa_m r}^2 + i\gamma_{\kappa_m}\omega}.$$

For such materials the reflection matrix is no longer diagonal and there is polarization mixing. Repulsive Casimir forces and stable nanolevitation was predicted for strong chirality (large values of $\omega_{\kappa_m}/\omega_{\kappa_m r}$) (Zhao *et al.*, 2009). However, these results were shown to be incompatible with the passivity and causal response of the materials (Silveirinha and Maslovski, 2010), which implies that the condition $\mathrm{Im}[\epsilon(\omega)]\mathrm{Im}[\mu(\omega)] - (\mathrm{Im}[\kappa_m(\omega)])^2 > 0$ must be satisfied. This relation imposes a limit of the strength of the imaginary part of κ_m and results in an attractive Casimir force between chiral metamaterials made of metallic or dielectric meta-atoms for any physical values of the magnetoelectric coupling (Silveirinha, 2010). These theoretical arguments were also confirmed by full-wave simulations of chiral metamaterial structures (McCauley, Zhao *et al.*, 2010), and it was shown that microstructure effects (i.e., proximity forces and anisotropy) dominate the Casimir force for separations where chirality was predicted to have a strong influence. Still, chiral metamaterials may offer a way to strongly reduce the Casimir force (Zhao *et al.*, 2010).

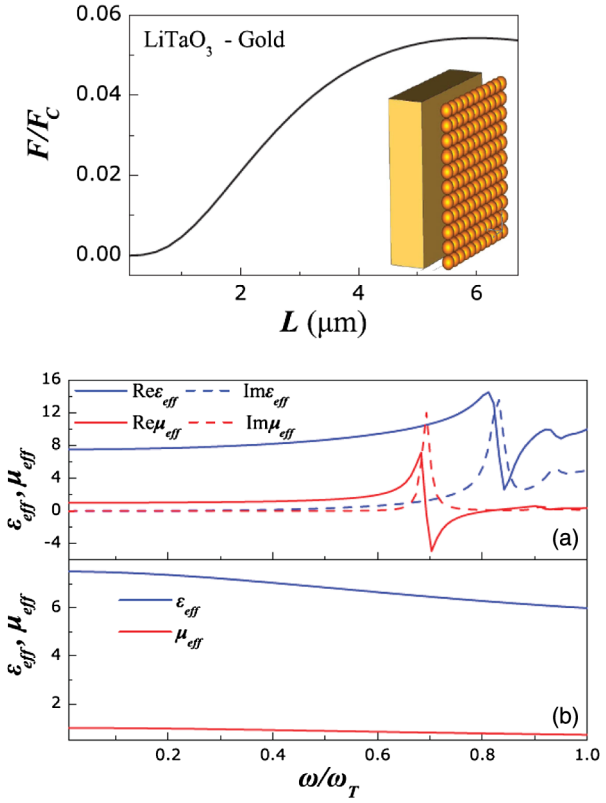

FIG. 10. Top: Normalized Casimir force as a function of separation between a gold semispace and a 2D metasurface made of close-packed (lattice constant $a = 11.24$ μm) $LiTaO_3$ spheres of radius $r = 5.62$ μm, calculated via scattering theory. The optical response of $LiTaO_3$ is described by a single-resonance Drude-Lorentz model $\epsilon(\omega) = \epsilon_\infty[1 + (\omega_L^2 - \omega_T^2)/(\omega_T^2 - \omega^2 - i\omega\gamma)]$, where $\epsilon_\infty = 13.4$, the transverse and longitudinal optical phonon frequencies are $\omega_T = 26.7 \times 10^{12}$ and $\omega_L = 46.9 \times 10^{12}$ rad/s, and the dissipation parameter is $\gamma = 0.94 \times 10^{12}$ rad/s. The gold Drude parameters are taken as $\hbar\Omega_D = 3.71$ eV and $\Omega_D\gamma_D^{-1} = 20$. Bottom: Effective permittivity and permeability of the close-packed $LiTaO_3$ spheres as a function of (a) real and (b) imaginary frequencies as calculated by the Maxwell-Garnett effective medium theory. From Yannopapas and Vitanov, 2009.

B. Photonic crystals

Photonic crystals are man-made electromagnetic structures that, unlike metamaterials, have unit cell sizes on the order of the wavelength of light. The most important property of photonic crystals made of low-loss dielectric periodic

structures occurs when the wavelength is about twice their period (Joannopoulos *et al.*, 2008). Many exotic phenomena are found, including the appearance of photonic band gaps preventing light from propagating in certain directions with specified frequencies, the localization of electromagnetic modes at defects, and the existence of surface states that bound light to the surface for modes below the light line. Photonic crystals were codiscovered by Yablonovitch (1987), who proved that spontaneous emission is forbidden when a three-dimensional periodic structure has an electromagnetic band gap which overlaps with an electronic band edge, and John (1987), who showed that strong localization of photons could take place in disordered dielectric superlattices. The simplest possible photonic crystal, a 1D multilayered stack made of materials of alternating dielectric constants, had been already investigated more than a century ago by Lord Rayleigh. Today photonic crystals come in different fashions, including complex 3D structures [e.g., the Yablonovite (Yablonovitch, Gmitter, and Leung, 1991)], periodic dielectric waveguides, and photonic-crystal slabs and fibers.

Photonic crystals offer great flexibility in designing atomic traps close to surfaces at submicrometer distances allowing the integration of nanophotonics and atomic physics with a host of exciting quantum technologies. Trapping atoms near surfaces is determined by the Casimir-Polder force. However, in analogy to Earnshaw's theorem of electrostatics, there are no stable Casimir-Polder (or Casimir) equilibria positions for any arrangements of nonmagnetic systems, provided the electric permittivities of all objects are higher or lower than that of the medium in between them (Rahi, Kardar, and Emig, 2010). For example, there is no stable equilibrium position for a ground-state atom above a metallic or dielectric structure.[1] Fortunately, no such constraints exist for excited state atoms or when the trapping potential energy is the superposition of the Casimir-Polder interaction and an external optical trapping field.

The Casimir-Polder interaction can be calculated for an atom in state l with polarizability $\alpha_l(\omega)$ considering Eq. (9) for a rare-field dielectric, as shown in Dzyaloshinskii, Lifshitz, and Pitaevskii (1961), Lifshitz and Pitaevskii (1980), and Milonni (1993). Typically, the arising Green's function is solved via computational finite-difference time-domain (FDTD) techniques (to be reviewed in Sec. V). It has been shown that the Casimir-Polder force between a ground-state atom and a 1D dielectric grating can trap atoms along the lateral directions of the dielectric surface (Contreras-Reyes *et al.*, 2010). However, there is no trapping along the directions parallel to the grating's grooves. Fully stable traps in 3D can be obtained utilizing photonic crystals, such as 1D periodic dielectric waveguides (Hung *et al.*, 2013). These proposed structures support a guided mode suitable for atom trapping within a unit cell, as well as a second probe mode with strong atom-photon interactions. The combination of the light shifts from a laser beam together with the Casimir-Polder force from the dielectric nanostructure results in a fully stable, 3D atomic trap. Aligning the photonic band gap edges with selected atomic transitions substantially enhances the atom-photon interactions, since the electromagnetic density of state diverges due to a van Hove singularity. These ideas were recently implemented experimentally with a Cs atom trapped within a 1D photonic-crystal waveguide consisting of two parallel SiN nanobeams with sinusoidal corrugation (Goban *et al.*, 2014). The measured rate of emission into the guided mode along the 1D waveguide was $\Gamma_{1D} = 0.32\Gamma'$, where Γ' is the decay rate into all other channels. Such a high coupling rate is unprecedented in all current atom-photon interfaces and paves the way for studying novel quantum transport and many-body phenomena in optics. Other works involving atom-surface dispersive interactions in close proximity to photonic crystals include resonant dipole-dipole energy transfer (Bay, Lambropoulos, and Mølmer, 1997) and enhanced resonant forces (Incardone *et al.*, 2014) between atoms with transition frequencies near the edge of the photonic band gap, and strong localization of matter waves mediated by quantum vacuum fluctuations in disordered dielectric media (Moreno *et al.*, 2010).

C. Plasmonic nanostructures

Metallic nanostructures can support collective electromagnetic modes, such as surface plasmons (also known as surface plasmon polaritons), which can propagate along the surface, decay exponentially away from it, and have a characteristic frequency of the order of the plasma frequency (Maier, 2007). Surface plasmons affect the Casimir interaction in a nontrivial manner (Intravaia and Lambrecht, 2005), and this point was also discussed for Dirac materials in Sec. III. When written in terms of real frequencies, the Lifshitz formula, Eq. (9), for planar systems has a term arising from the propagative modes, which gives an attractive force at all distances. There is a second term associated with the evanescent hybrid plasmonic modes, which results in an attractive force at short distances (shorter than the plasma wavelength) and a repulsive one at longer distances. There is a subtle cancellation between the attractive and repulsive terms at large separations, resulting in an always attractive force between planar metallic surfaces for all separations. This observation suggests that metallic nanostructures at scales below the plasma wavelength can potentially enhance the repulsive contribution due to plasmons and lead to a suppression of the Casimir force. Nanostructured metallic surfaces with tailored plasmonic dispersions have already impacted classical nanophotonics, with applications ranging from extraordinary light transmission (Ebbesen *et al.*, 1998) to surface-enhanced Raman scattering (Nie and Emory, 1997). Metallic structures with strong deviations from the planar geometry and possessing geometrical features on very small scales are also likely to give significant new insights into potential Casimir devices.

In addition to plasmons associated with the metallic nature of the plates, there is another type of plasmonic excitation, the

[1]A corollary of this theorem is that there is no Casimir repulsion for any metallic- or dielectric-based metamaterial treated in the effective medium approximation. Hence, when applied to dispersive interactions, effective medium is a good approach only at separations larger than the unit cell dimensions of the metamaterial. At short distances, displacements of structured Casimir plates might lead to repulsion that, however, must be compatible with the absence of stable equilibria.

so-called spoof plasmons, that arise from geometry and exist even for perfectly reflecting surfaces. Pendry and co-workers (Pendry, Martin-Moreno, and Garcia-Vidal, 2004; Garcia-Vidal, Martín-Moreno, and Pendry, 2005) proposed engineered dispersion by periodically nanostructuring surfaces by perforating perfect electrical conductors. The resulting surfaces support surface modes that have dispersion similar to real surface plasmons in metals, but with the effective plasma frequency determined by the geometric parameters of the perforation. Spoof plasmons are also present in nanostructures made of real metals, enhance the modal density of states, and modify the Casimir interaction in nanostructured metallic cavities (Davids, Intravaia, and Dalvit, 2014).

Besides computations of the interaction in complex systems, including nanostructured surfaces (Büscher and Emig, 2004; Lambrecht and Marachevsky, 2008; Davids *et al.*, 2010; Intravaia *et al.*, 2012; Guérout *et al.*, 2013; Noto *et al.*, 2014), advances in Casimir force measurements have also been reported. However, the experimental progress has been limited due to difficulties associated with the reliable fabrication and the measurement of the force. Using an *in situ* imprinting technique, whereby the corrugation of a diffraction grating was imprinted onto a metallic sphere by mechanical pressure, the lateral Casimir force between two axis-aligned corrugated surfaces was measured as a function of their phase shift (Chen *et al.*, 2002; Chiu *et al.*, 2009, 2010), and the normal Casimir force between them was also measured as a function of the angle between their corrugation axes (Banishev, Wagner *et al.*, 2013). Nanostructured lamellar gratings made of highly doped Si have been used to measure the Casimir interaction with a metallic sphere (Chan *et al.*, 2008), with conclusive evidence of the strong geometry dependency and nonadditivity of the force. More recently, a strong Casimir force reduction through metallic surface nanostructuring was reported (Intravaia *et al.*, 2013). In Fig. 11 the experimental setup is shown, consisting of a plasmonic nanostructure in front of a metallic sphere attached to a microelectromechanical system (MEMS) oscillator. A deep metallic lamellar grating with sub-100 nm features strongly suppressed the Casimir force, and for large intersurface separations reduced it beyond what would be expected by any existing theoretical prediction. Existing state-of-the-art theoretical modeling, based on the proximity force approximation for treating the curvature of the large-radius sphere ($R = 151.7$ μm, much larger than any geometrical length scale in the system), and an exact *ab initio* scattering analysis of the resulting effective plane-grating geometry, did not reproduce the experimental findings. The development of a full numerical analysis of the sphere-grating problem, capable of dealing with the disparate length scales present in the experiment (Intravaia *et al.*, 2013) with plasmonic nanostructures, remains an open problem. A step in this direction was recently reported by Messina *et al.* (2015), where the exact Casimir interaction between a gold sphere and a fused silica 1D grating was numerically evaluated.

Nanostructured surfaces have also been used in studies of atom-surface dispersion interactions. Casimir-Polder forces between a single atom or a Bose-Einstein condensate (BEC) above a grating have been measured using different methods (Grisenti *et al.*, 1999; Oberst *et al.*, 2005; Perreault and Cronin, 2005; Pasquini *et al.*, 2006; Zhao *et al.*, 2008), and the

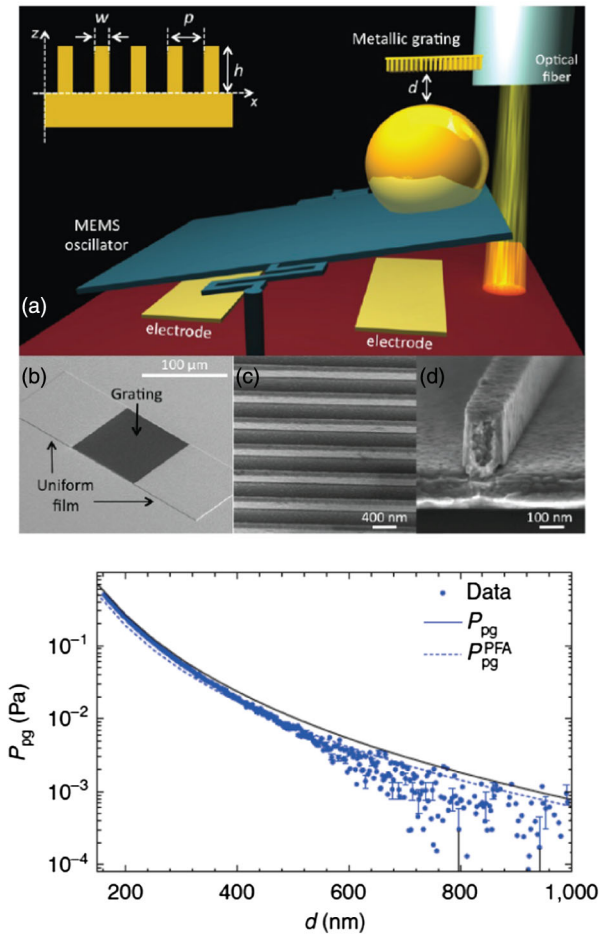

FIG. 11. Top: (a) Schematic of the experimental configuration used to measure the Casimir force between a gold-coated sphere and a gold nanostructured grating. One of the many nanostructures used in the experiment is shown [scanning electron microscopy images in (b)–(d)]. The radius of the Au sphere is $R = 151.7$ μm. Bottom: Plane-grating pressure as a function of sphere-grating separation for a lamellar grating with period $p = 250$ nm, tooth width $w = 90$ nm, and height $h = 216$ nm. Experimental measurements of sphere-grating force gradient divided by $2\pi R$ (dots with error bars), and plane-grating pressure computed with the proximity force approximation (dashed lines), exactly using scattering theory (solid line). From Intravaia *et al.*, 2013.

near- and field-field scaling laws of the Casimir-Polder potential were verified. Theoretical proposals have also been put forward to measure the Casimir-Polder potential at corrugated surfaces with Bose-Einstein condensates (Messina *et al.*, 2009; Moreno, Dalvit, and Calzetta, 2010). In a series of recent experiments, ultracold atoms were utilized to survey the potential landscape of plasmonically tailored nanostructures. Stehle *et al.* (2011) accelerated a Rb Bose-Einstein condensate toward Au plasmonic microstructures whose plasmons were excited by external laser fields in a Kretschmann configuration (Fig. 12). A blue-detuned laser beam generates an evanescent optical field that repels the atoms from the surface, while the atom-grating Casimir-Polder interaction produces an attractive potential. This combination results in a potential barrier that can be mapped by classical or quantum reflection measurements. Diffraction

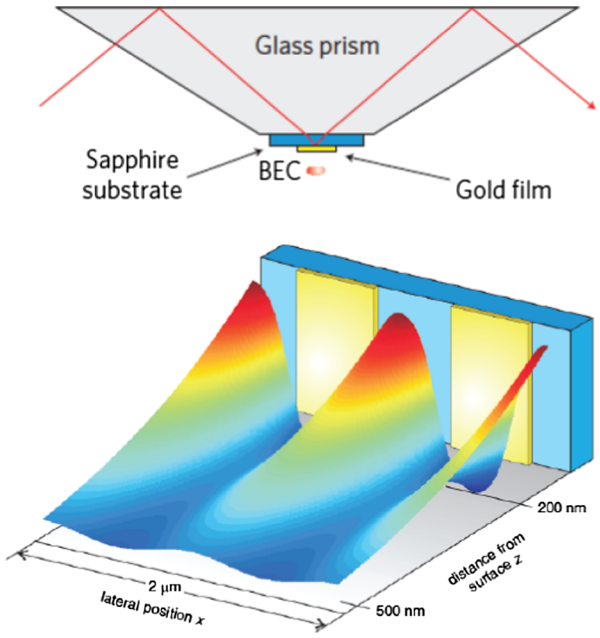

FIG. 12. Top: Schematic configuration to measure the Casimir-Polder potential probed by a BEC diffracted from a plasmonic nanostructured being excited by an external laser field in the Kretschmann configuration. Bottom: Atom-grating potential landscape arising from the combination of a repulsive evanescent-wave potential and the Casimir-Polder attraction. The external laser field has a power of $P = 211$ mW. The evanescent field from the grating modulates the repulsion, and the attractive Casimir-Polder potential is the strongest on top of the gold stripes. At a distance of 200 nm, the potential is laterally modulated with an amplitude of $\Delta E/k_B = 14$ μK. From Stehle *et al.*, 2011, and Bender *et al.*, 2014.

measurements of Bose-Einstein condensates from metallic nanogratings have allowed one to locally probe the Casimir-Polder potential (Bender *et al.*, 2014), revealing information about its landscape (Fig. 12) in agreement with theoretical calculations based on the scattering approach to atom-grating Casimir interactions.

V. NONTRIVIAL BOUNDARY CONDITIONS

In this section, we further delineate some of the ways in which Casimir interactions are fundamentally changed by the shapes of boundaries and interfaces of macroscopic bodies, leading for instance to complex and highly nonadditive effects (Dalvit *et al.*, 2011; Rodriguez, Capasso, and Johnson, 2011; Buhmann, 2012b; Reid, Rodriguez, and Johnson, 2013; Rodriguez *et al.*, 2015). Understanding the ways in which nontrivial shapes and boundary conditions affect the force has not only shed light on various ways to design forces used to combat unwanted Casimir effects in nanoelectromechanical system (NEMS) and MEMS, but continues to reveal regimes and situations where the often-employed PFA and pairwise summation (PWS) approximation fail dramatically. Such structures can also lead to forces that differ significantly from the attractive, monotonically decaying force laws associated with planar bodies and/or dilute, atomic media. Underlying the study of nontrivial boundary conditions are novel theoretical techniques (reviewed below) that, while intimately related, bear little semblance to the original and decades-old formulas used to compute Casimir interactions.

Early studies of Casimir forces focused on simple geometries, e.g., planar bodies and generalizations thereof, by employing sum-over-mode formulations where the zero-point energy of electromagnetic fields (field fluctuations) rather than dipolar interactions (charge fluctuations) were summed (Casimir, 1948; Milonni, 1993). The equivalence of these two perspectives comes from the fluctuation-dissipation theorem, relating the properties (amplitude and correlations) of current fluctuations in bodies to the thermodynamic and dissipative properties of the underlying media (Lifshitz, 1956; Lifshitz and Pitaevskii, 1980; Eckhardt, 1984). Ultimately, the connection between current and field fluctuations arises from the well-known dyadic electromagnetic Green's function (Jackson, 1998):

$$G_{ij}(\mathbf{r},\mathbf{r}';\omega) = \{[\nabla\times\nabla\times -\varepsilon(\mathbf{r},\omega)\omega^2]^{-1}\hat{\mathbf{e}}_j\delta(\mathbf{r}-\mathbf{r}')\}_i, \quad (20)$$

where $\hat{\mathbf{e}}_j$ is the unit vector. The connection to sum-over-mode formulas arises from the trace of the Green's function being related to the electromagnetic density of states

$$\rho(\omega) = \frac{1}{\pi}\frac{d(\omega^2\varepsilon)}{d\omega}\mathrm{Tr}\mathrm{Im}G_{ij}(\mathbf{r},\mathbf{r},\omega),$$

which when integrated $\sum_\omega \rho(\omega) = \int d\omega\rho(\omega)$ leads to the famous $\mathcal{E} = \sum_\omega(\hbar\omega/2)$ formula (van Kampen, Nijober, and Schram, 1968; Gerlach, 1971; Rodriguez, Ibanescu, Iannuzzi, Joannopoulos, and Johnson, 2007). Although this formulation was originally developed in special geometries involving perfectly metallic conductors, where Hermiticity leads to well-defined modes, it has also been extended to handle other situations of interest such as open structures and lossy dielectrics (van Enk, 1995a; Genet, Lambrecht, and Reynaud, 2003; Mochan and Villarreal, 2006; Graham, Quandt, and Weigel, 2009; Davids *et al.*, 2010; Milton, Wagner *et al.*, 2010; Intravaia and Behunin, 2012). Despite these generalizations, the sum-over-mode approach poses practical challenges for computations in general structures due to the cumbersome task of having to compute all of the modes of the system (Ford, 1993; van Enk, 1995b; Rodriguez, Ibanescu, Iannuzzi, Joannopoulos, and Johnson, 2007).

Instead, more powerful applications of the fluctuation-dissipation theorem exist in which Green's functions are directly employed to compute energy densities and stress tensors (momentum transport) rather than modal contributions to the energy, reducing the problem to a series of classical scattering calculations: scattered fields due to known incident fields and sources. This latter viewpoint was originally employed by Lifshitz and others to calculate forces between planar dielectrics bodies (Dzyaloshinskii, Lifshitz, and Pitaevskii, 1961; Lifshitz and Pitaevskii, 1980), and it turns out to be much more useful when dealing with complex geometries. The advantage comes from the fact that the Green's function does not need to be obtained analytically as was done for planar bodies, but it can be routinely and efficiently computed numerically via classical electromagnetism. These ideas lie at the center of recently developed

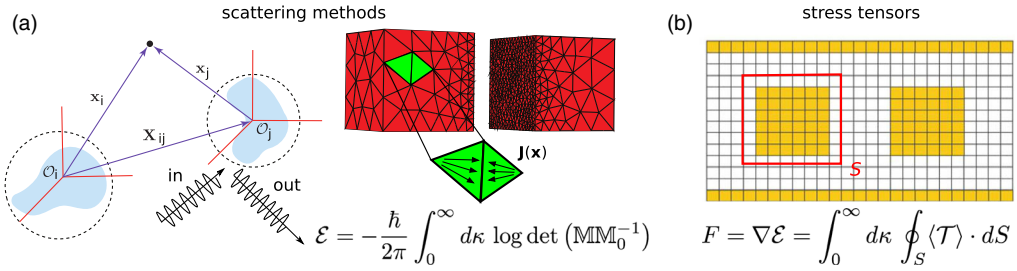

FIG. 13. Schematic illustration of numerical methods recently employed to compute Casimir interactions in complex geometries: (a) scattering methods where the field unknowns are either incident or outgoing propagating waves (left) or vector currents $\mathbf{J}(\mathbf{x})$ defined on the surfaces of the bodies (right), and the resulting energies are given by Eq. (21); (b) stress-tensor methods in which the force is obtained by integrating the thermodynamic Maxwell stress tensor over a surface surrounding one of the bodies utilizing the fluctuation-dissipation theorem.

general-purpose techniques, schematically shown in Fig. 13, for computing forces in complex structures which boil down to a series of classical scattering calculations of Green's functions (Rodriguez, Ibanescu, Iannuzzi, Joannopoulos, and Johnson, 2007; Pasquali and Maggs, 2008, 2009; Rodriguez *et al.*, 2009; Xiong and Chew, 2009; McCauley, Rodriguez *et al.*, 2010; Xiong *et al.*, 2010) or related quantities such as scattering matrices (Emig, 2003; Gies, Langfeld, and Moyaerts, 2003; Büscher and Emig, 2004; Gies and Klingmuller, 2006b; Lambrecht, Maia Neto, and Reynaud, 2006; Emig *et al.*, 2007; Kenneth and Klich, 2008; Rahi *et al.*, 2009; Reid *et al.*, 2009; Milton, Parashar *et al.*, 2010; Reid, White, and Johnson, 2011, 2013; Atkins *et al.*, 2013).

Despite their relative infancy, these methods have already led to a number of interesting predictions of unusual Casimir forces in a wide range of structures, including spheres (Gies and Klingmuller, 2006a; Emig, 2008; Maia Neto, Lambrecht, and Reynaud, 2008), cylinders (Emig *et al.*, 2006), cones (Maghrebi *et al.*, 2011), waveguides (Rodriguez, Ibanescu, Iannuzzi, Capasso *et al.*, 2007; Zaheer *et al.*, 2007; Rahi *et al.*, 2008; Rodriguez-Lopez, Rahi, and Emig, 2009; Pernice *et al.*, 2010), and patterned surfaces (Emig *et al.*, 2003; Büscher and Emig, 2004; Rodrigues *et al.*, 2006; Lambrecht and Marachevsky, 2008; Rodriguez, Joannopoulos, and Johnson, 2008; Chiu *et al.*, 2009, 2010; Davids *et al.*, 2010; Guérout *et al.*, 2013), among others (Rodriguez *et al.*, 2008; Rodriguez, McCauley *et al.*, 2010; Rodriguez, Woolf *et al.*, 2010; Broer *et al.*, 2012). Here we provide a concise but inclusive exposition of the main techniques employed in state-of-the-art calculations along with discussions of their suitability to different kinds of problems, all the while focusing on representative results that reveal the highly nonadditive character of Casimir forces.

A. Scattering methods

A sophisticated and powerful set of techniques for calculating Casimir forces are scattering methods [Fig. 13(a)]. While these approaches come in a variety of flavors, they often rely on formulations that exploit connections between the electromagnetic density of states (Emig, 2003; Gies, Langfeld, and Moyaerts, 2003; Emig *et al.*, 2006; Kenneth and Klich, 2008) or path-integral representations of the electromagnetic energy (Kardar and Golestanian, 1999; Lambrecht, Maia Neto, and Reynaud, 2006; Emig *et al.*, 2007; Kenneth and Klich, 2008; Rahi *et al.*, 2009; Reid *et al.*, 2009; Milton, Parashar *et al.*, 2010; Reid, White, and Johnson, 2011), and classical scattering matrices (Dalvit *et al.*, 2011). Regardless of the chosen starting point, the Casimir energy is often written in the following form:

$$\mathcal{E} = -\frac{\hbar}{2\pi}\int_0^\infty d\omega \log\det(\mathbb{M}\mathbb{M}_0^{-1}), \tag{21}$$

where the matrix $\mathbb{M}$ is

$$\mathbb{M} = \begin{pmatrix} \mathbb{M}^{(11)} & \mathbb{M}^{(12)} & \cdots \\ \mathbb{M}^{21} & \mathbb{M}^{(22)} & \cdots \\ \vdots & \vdots & \ddots \end{pmatrix}$$

whose diagonal blocks $\mathbb{M}^{(\alpha\alpha)}$ are precisely the scattering matrices of isolated bodies and whose off-diagonal blocks $\mathbb{M}^{(\alpha\beta)}$ encapsulate interactions and scattering among the bodies (Lambrecht, Maia Neto, and Reynaud, 2006; Rahi *et al.*, 2009). Multiplication by the inverse matrix $\mathbb{M}_0^{-1}$ ensures that the divergent, self-interaction energy of the bodies in isolation (separations $d \to \infty$) is subtracted, leaving behind a finite quantity (Rahi *et al.*, 2009).

Although Eq. (21) may appear largely unrelated to the Lifshitz formula [Eq. (9)], the connection between the two becomes apparent when considering extended structures. Specifically, given two semi-infinite, periodic bodies the formula can be written in the more familiar form $\mathcal{E} = \int_0^\infty d\omega \log\det\left(1 - \mathbb{R}^{(1)}\mathbb{M}^{(12)}\mathbb{R}^{(2)}\mathbb{M}^{(21)}\right)$, where $\mathbb{R}^{(\alpha)}$ are the reflection matrices of each individual half-space and $\mathbb{M}^{(\alpha\beta)}$ are translation matrices that describe wave propagation between them (Lambrecht, Maia Neto, and Reynaud, 2006; Lambrecht and Marachevsky, 2008; Rahi *et al.*, 2009). For planar bodies, as discussed in Sec. III.A, the scattering matrices can be expressed in a Fourier basis and the above expression reduces to the Lifshitz formula (Lifshitz, 1956), originally obtained via direct evaluation of the Maxwell stress tensor.

It is also possible to derive a slightly different scattering formula, known as the TGTG formula (Kenneth and Klich, 2008; Klich and Kenneth, 2009), in which the energy between two arbitrary bodies is expressed as

$$\mathcal{E} = \int_0^\infty d\kappa \log\det(1 - \mathbb{T}^{(1)}\mathbb{G}_0^{(12)}\mathbb{T}^{(2)}\mathbb{G}_0^{(21)}), \tag{22}$$

where $\mathbb{T}^{(\alpha)}$ are the T operators appearing in the Lippmann-Schwinger equation (related to the scattering matrices of individual bodies), and $\mathbb{G}_0^{(\alpha\beta)}$ are the homogeneous Green's functions of the intervening medium, describing the wave propagation. Note that even though these formulations may appear to be completely divorced from the original picture of dipole fluctuations, the fact that the energy is described by the scattering properties of the bodies is not surprising. In particular, as discussed later, at equilibrium it is possible to describe the statistics of field fluctuations independently of the corresponding current sources of the fluctuations (Lifshitz and Pitaevskii, 1980; Eckhardt, 1984). Intuitively, one can consider Casimir interactions as arising from the scattering and momentum exchange of vacuum electromagnetic fields originating from radiating sources infinitely far away (rather than within the bodies) and that ultimately end up equilibrating as they get scattered, absorbed, and reemitted by the bodies.

Equation (21) was originally exploited to study forces between highly symmetric structures, e.g., spheres and cylinders, where the corresponding propagators, scattering, and translation matrices can be expanded in terms of convenient, delocalized free-wave solutions of the Helmholtz equation (Kenneth and Klich, 2008; Lambrecht and Marachevsky, 2008; Rahi *et al.*, 2009; Milton, Parashar *et al.*, 2010; Maghrebi *et al.*, 2011), as illustrated in Fig. 13(a). The resulting spectral methods (Balian and Duplantier, 1978; Dalvit *et al.*, 2006; Lambrecht, Maia Neto, and Reynaud, 2006; Mazzitelli, Dalvit, and Lombardo, 2006; Emig *et al.*, 2007; Kenneth and Klich, 2008; Lambrecht and Marachevsky, 2008; Milton, Parashar, and Wagner, 2008; Rahi *et al.*, 2009) are advantageous in a number of ways: First, they yield analytical results that offer insight into the properties of the Casimir force at asymptotically large separations (Rahi *et al.*, 2009) or under assumptions of dilute media (Milton, Parashar, and Wagner, 2008; Milton and Wagner, 2008; Golestanian, 2009; Bitbol *et al.*, 2013). Second, the trace operations for smooth and high-symmetry structures can be efficiently implemented due to the very high-order and possibly even exponential convergence of the basis expansions (Boyd, 2001; Dalvit *et al.*, 2011). Finally, since the energy expressions involve simple products of scattering matrices having well-studied properties, this formulation is well suited for establishing general constraints on the signs and magnitudes of forces under various circumstances. Of particular importance is the recent demonstration that the force between any two mirror-symmetric bodies must always be attractive (Kenneth *et al.*, 2002; Kenneth and Klich, 2006), resolving a long-standing question about the sign of the internal pressure or self-force on a perfectly metallic, isolated sphere (the limit of two opposing hemispheres) (Boyer, 1968; Milton, DeRaad, and Schwinger, 1978; Brevick and Einevoll, 1988; Bordag, Mohideen, and Mostepanenko, 2001). Similarly, recent works have shown that stable suspensions (local equilibria) between vacuum-separated, nonmagnetic bodies are generally impossible (Lambrecht, Jaekel, and Reynaud, 1997; Rahi, Kardar, and Emig, 2010).

For more complicated bodies lacking special symmetries, involving sharp corners, or where nonuniform spatial resolution is desired, it is advantageous to employ localized basis functions. More commonly, the unknowns are defined on a generic mesh or grid and the resulting equations are solved numerically, examples of which are the finite-difference (Taflove and Hagness, 2000), finite element (Jin, 2002), and boundary element (Bonnet, 1999; Chew *et al.*, 2001) methods. The latter category is closely related to scattering methods (Rodriguez, Ibanescu, Iannuzzi, Joannopoulos, and Johnson, 2007; Reid *et al.*, 2009; Xiong *et al.*, 2010; Reid, White, and Johnson, 2011); in the surface-integral equation formulation of electromagnetic scattering, the scattering unknowns are fictitious electric and magnetic currents defined on the surfaces of the bodies, illustrated in Fig. 13(a), and expanded in terms of an arbitrary basis of surface vector fields (Chew *et al.*, 2001). The connection to scattering problems comes from the fact that incident and scattered fields are related to the current unknowns via homogeneous Green's functions (analytically known); not surprisingly, this formulation leads to a similar trace expression for the Casimir energy given in Eq. (21), except that the elements of $\mathbb{M}$ consist of overlap integrals among the various surface basis functions. A powerful implementation of this approach is the boundary element method (BEM), where the current unknowns are expanded in terms of localized basis functions (typically, low-degree polynomials) defined on the elements of some discretized surface, as illustrated in Fig. 13(a). As a result the $\mathbb{M}$ matrices turn out to be none other than the well-studied BEM matrices that arise in classical scattering calculations (Chew *et al.*, 2001). Such a formulation allows straightforward adaptations of sophisticated BEM codes, including recently published, free, and widely available software packages (Reid, 2012). Like most numerical methods, the BEM method can handle a wide range of structures, including interleaved bodies with corners, and enables nonuniform resolutions to be employed as needed.

B. Stress-tensor methods

Although originally conceived as a semianalytical method for computing forces in planar bodies (Jaekel and Reynaud, 1991; Zhou and Spruch, 1995; Klimchitskaya, Mohideen, and Mostepanenko, 2000; Tomaš, 2002), leading to the famous Lifshitz formula (Sec. III.A), the stress-tensor approach can also be straightforwardly adapted for numerical computations (Rodriguez, Ibanescu, Iannuzzi, Joannopoulos, and Johnson, 2007; Rodriguez, Joannopoulos, and Johnson, 2008; Rodriguez *et al.*, 2008, 2009; Xiong and Chew, 2009; McCauley, Rodriguez *et al.*, 2010) since it relies on repeated calculations of Green's functions. In this formulation [schematically shown in Fig. 13(b)], the Casimir force on an object is expressed as an integral of the thermodynamic, Maxwell stress tensor $\langle T_{ij}\rangle = \varepsilon(\langle E_i E_j\rangle - \frac{1}{2}\sum_k \langle E_k E_k\rangle) + (\langle H_i H_j\rangle - \frac{1}{2}\sum_k \langle H_k H_k\rangle)$ over an arbitrary surface S surrounding the object,

$$\mathbf{F} = \int_0^\infty d\kappa \iint_S \langle \mathbf{T}\rangle \cdot d\mathbf{S}. \tag{23}$$

Similar to scattering methods, here the picture of fluctuating dipoles is masked by an equivalent scattering problem involving fields rather than fluctuating volume currents,

whereby the correlation functions $\langle E_i E_j \rangle, \langle H_i H_j \rangle \sim G_{ij}$, a consequence of the fact that at equilibrium, currents and field fluctuations become thermodynamically equivalent (Eckhardt, 1984).

Beyond special-symmetry structures where the Green's functions can be expanded in a convenient spectral basis (Jaekel and Reynaud, 1991; Zhou and Spruch, 1995; Klimchitskaya, Mohideen, and Mostepanenko, 2000; Tomaš, 2002), recent implementations of the stress-tensor method for arbitrary geometries exploit general-purpose techniques, such as the finite-difference method illustrated in Fig. 13(b), where space is divided into a uniform grid of finite resolution, and the resulting matrix equations for the Green's functions are solved numerically (Strikwerda, 1989; Anderson *et al.*, 1999; Taflove and Hagness, 2000). Early implementations include both finite-difference frequency-domain (Rodriguez, Ibanescu, Iannuzzi, Joannopoulos, and Johnson, 2007; Xiong and Chew, 2009) and time-domain (Rodriguez *et al.*, 2009; McCauley, Rodriguez *et al.*, 2010) methods.

Because Casimir forces involve broad bandwidth fluctuations time-domain methods are advantageous in that $G_{ij}(\mathbf{r}, \mathbf{r}', \omega)$ at all frequencies can be computed at once via Fourier transforms (Taflove and Hagness, 2000). While the finite-difference stress-tensor method does not offer the efficiency and sophistication of other formulations and discretization schemes, such as the BEM fluctuating-surface current method (Reid, White, and Johnson, 2011), they are compensated by their flexibility and generality. For instance, they are extremely simple to implement [leading to many free and easy-to-use numerical packages (Oskooi *et al.*, 2010)], can handle many different kinds of boundary conditions and materials (including anisotropic and even nonlinear dielectrics), and are well understood. A BEM implementation of the stress-tensor method was also first suggested by Rodriguez, Ibanescu, Iannuzzi, Joannopoulos, and Johnson (2007) and subsequently implemented by Xiong and Chew (2009), although for small problems the trace formulas provide a simpler and more efficient alternative since they do not require repeated integration over surfaces and involve only products of BEM matrices. On the other hand, the stress-tensor method offers computational advantages for large problems since it involves repeated evaluation of Green's functions, or matrix-vector products, making it an ideal candidate for applications of fast-solver (iterative) techniques (Chew *et al.*, 1997).

C. Casimir interactions in complex geometries

While PFA and PWS approximations provide simple, quickly solvable, and intuitive expressions for forces in arbitrary geometries, they are uncontrolled when pushed beyond their limits of validity and have been shown to fail (even qualitatively) in the simplest of structures (Bordag, 2006; Gies and Klingmuller, 2006a; Dalvit *et al.*, 2011; Rodriguez, Capasso, and Johnson, 2011; Bitbol *et al.*, 2013). Increased demand for experimental guidance has stimulated recent efforts in quantifying the validity and accuracy of PFA (Chiu *et al.*, 2009, 2010).

Although PFA is technically only applicable in geometries with smooth, large-curvature objects and small separations, it has nevertheless been heuristically applied in the past to study a wide range of other situations (Lambrecht, Maia Neto, and Reynaud, 2008; Rodriguez *et al.*, 2015). For instance, a number of recent works have employed scattering methods to investigate extensions of PFA in the sphere-plate geometry at large separations in the idealized limit of perfect conductors (Bimonte *et al.*, 2012; Fosco, Lombardo, and Mazzitelli, 2012), where the PFA energy takes on the closed-form expression $\mathcal{E}_{\mathrm{PFA}} = \pi^3 \hbar c R / 1440 d^2$, where R denotes the sphere radius. The plotted ratio of energies in Fig. 14(a) shows that PFA increasingly overestimates the energy as

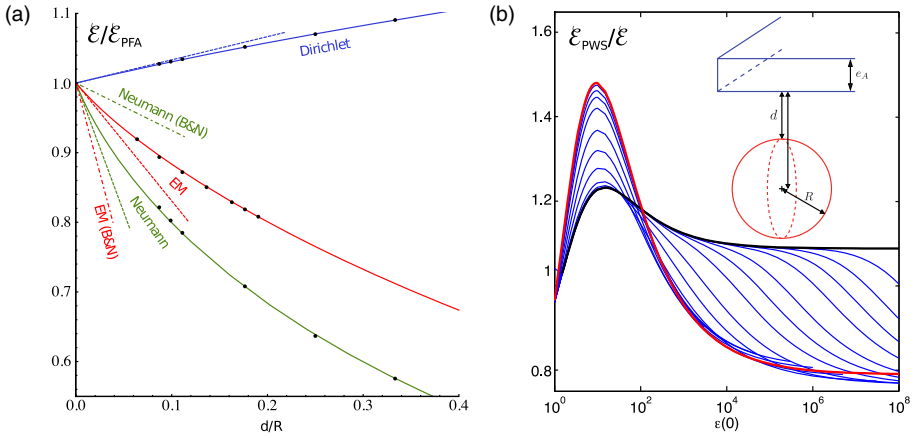

FIG. 14. Results illustrating the range of validity of PFA and PWS approximations in the sphere-plate geometry, involving a sphere of radius R separated from a semi-infinite plate by a surface-surface distance d. The exact Casimir energy is computed by application of the scattering method. (a) Ratio of the exact and PFA energies as a function of d/R for perfectly metallic conductors. Numerical data (dots) are compared to the first correction of the PFA (dashed lines), described in the text, and also to a fit performed via Padé approximants (solid curves), in which the energy ratio is given by $\mathcal{E}/\mathcal{E}_{\mathrm{PFA}} = 1 + (1/3)(1 - 60/\pi^2) d/R + (8/100)(d/R)^2 \log(d/R)$. From Bimonte *et al.*, 2012. (b) Ratio of the PWS and exact Casimir energies as a function of the static permittivities of the sphere and plate, for various ratios d/R (blue curves). The red (steepest) and black (least steep) curves represent equivalent results for the plate-plate and sphere-plate geometries in the limit of infinite separations. From Bitbol *et al.*, 2013.

$d \to \infty$, which is to be expected since at $d/R \gg 1$, the interaction approaches that of a dipole above a plate exhibiting a significantly faster decay $\sim 1/d^6$ (Buhmann and Welsch, 2007). Higher-order perturbative PFA corrections for large curvatures $d/R \ll 1$ have also been obtained (Bordag, 2006; Lambrecht, Maia Neto, and Reynaud, 2008; Bimonte *et al.*, 2012; Fosco, Lombardo, and Mazzitelli, 2012) [Fig. 14(a)]. Techniques based on Padé approximants, which constrain the force at short and large separations using gradient and multipole expansions [Fig. 14(a)], have also culminated in analytical expressions (Bimonte *et al.*, 2012), leading to the hope that similar methods can be applied to more complex geometries. The situation is more complicated in cases involving realistic metals and finite temperatures, as illustrated by recent predictions of *geothermal effects* involving nontrivial interplay between geometry, materials, and temperature in the sphere-plate geometry (Maia Neto, Lambrecht, and Reynaud, 2008; Canaguier-Durand *et al.*, 2010; Weber and Gies, 2010a, 2010b).

The PWS approximation, applicable in the limit of large separations and dilute media, relies on dividing the object into small elements ("atoms") and summing the corresponding vdW and Casimir-Polder interactions (Bergstrom, 1997; Veble and Podgornik, 2007; Milton, Parashar, and Wagner, 2008; Golestanian, 2009). The presence of multiple scattering, otherwise absent in the limit of weak coupling or dilute media (Milton, Parashar, and Wagner, 2008), has long been known to significantly modify the underlying two-body force laws (Axilrod and Teller, 1943). Despite these shortcomings, PWS approximations have been recently applied to numerically approximate interactions in complex geometries (Tajmar, 2004; Sedmik, Vasiljevich, and Tajmar, 2007), especially in the field of microfluidics (Stone and Kim, 2001; Parsegian, 2006). While PWS approximations are strictly applicable in the limit of dilute media, recently they were shown to lead to larger errors in the experimentally relevant case of dielectric materials (Bitbol *et al.*, 2013). This situation is illustrated in Fig. 14(b), which shows that PWS underestimates the energy in the perfect-metal limit ($\varepsilon \to -\infty$) by $\approx 20\%$, is exact in the dilute limit of $\varepsilon \to 1$, and is (surprisingly) most inaccurate at intermediate $\varepsilon \sim 10$ where it overestimates the energy by roughly 60%. Such counterintuitive results shed light on the complexities associated with dilute approximations, since a heuristic argument based on the screening of fields in materials with large dielectric contrasts would predict strictly monotonically increasing deviations. By examining interactions between compact objects at asymptotically large separations, it is also possible to obtain perturbative corrections to Casimir-Polder forces (Balian and Duplantier, 1977; Golestanian, 2000, 2009; Emig *et al.*, 2006; Emig, 2008; Milton and Wagner, 2008; Rahi *et al.*, 2009; Stedman, Drosdoff, and Woods, 2014). Formal derivations of PWS approximations in the limit of dilute media as well as perturbative corrections applicable in systems with larger index contrasts have also been developed (Milton, Parashar, and Wagner, 2008; Golestanian, 2009; Rodriguez-Lopez, 2009).

At intermediate separations that are on the order of the sizes of the objects and for realistic materials, neither PFA nor PWS, nor perturbative corrections thereof can accurately predict the behavior of the Casimir force. However, it is precisely this regime that is most easily tackled by numerical methods. Application of scattering methods to the study of compact bodies interacting with planar objects have led to a number of interesting predictions, a select number of which are illustrated in Fig. 15. In geometries involving perfect-conductor bodies with special symmetries such as spheres, cones, wedges, or cylinders, scattering-matrix methods have been employed to obtain both numerical and semianalytical results (Emig *et al.*, 2006, 2009; Mazzitelli, Dalvit, and Lombardo, 2006; Maia Neto, Lambrecht, and Reynaud, 2008; Rahi *et al.*, 2009; Dalvit *et al.*, 2011). Other, more complicated shapes such as waveguides, disks, cubes, tetrahedral particles, and capsules are less amenable to spectral methods, but have nevertheless been studied using brute-force techniques (Rodriguez, Ibanescu, Iannuzzi, Capasso *et al.*, 2007; Reid *et al.*, 2009; Atkins *et al.*, 2013; Reid, White, and Johnson, 2013). Figure 15 shows that the energy of a cone with a semiopening angle θ_0 and a substrate vanishes logarithmically $\mathcal{E} \sim -(\hbar c/d)(1/\log\theta_0)$ as $\theta_0 \to 0$, a type of divergence that is characteristic of lines and other scale-invariant objects (Maghrebi *et al.*, 2011). In contrast, the PFA energy is predicted to vanish linearly as $\theta_0 \to 0$. For a tilted wedge, the PFA energy remains constant until the back surface of the wedge becomes visible to the plate, while exact results indicate smoothly varying angle dependence despite the screening effects (Maghrebi *et al.*, 2011). Earlier calculations of forces between cylinders, spheres, and ellipsoidal bodies and plates have also demonstrated unexpectedly weak decay rates and other interesting nonadditive modifications (Dalvit *et al.*, 2006; Emig *et al.*, 2006, 2007, 2009; Mazzitelli, Dalvit, and Lombardo, 2006; Maia Neto, Lambrecht, and Reynaud, 2008). For more complicated structures, such as the pair of cubes shown in Fig. 15, it is more convenient to employ brute-force techniques like the BEM method (Reid, White, and Johnson, 2013).

Unusual Casimir interactions in multibody geometries have also recently been studied (Dalvit *et al.*, 2011; Rodriguez, Capasso, and Johnson, 2011). For instance, application of numerical methods [first employing stress tensors (Rodriguez, Ibanescu, Iannuzzi, Capasso *et al.*, 2007) and subsequently scattering matrices (Rahi *et al.*, 2008)] in a structure composed of two metallic coplanar waveguides suspended above adjacent metal sidewalls [Fig. 16(a)] reveal that the attractive Casimir force per unit length between the waveguides varies nonmonotonically as a function of their separation from the sidewalls h. Large deviations from PFA can be explained from the fact that PFA is unable to accurately capture the competing effects of TE and TM fields at small and large h (Hertzberg *et al.*, 2007; Zaheer *et al.*, 2007; Rahi *et al.*, 2008). Extensions of this geometry to situations involving finite rods, such as the cylindrically symmetric geometry of Fig. 16(a), where the sidewalls are joined to form a cylindrical tube and described by either perfect-electric or perfect-magnetic boundary conditions (McCauley, Rodriguez *et al.*, 2010), demonstrate the importance of dimensionality and boundary conditions on the behavior of the force. Along similar lines, structures involving periodic arrays of finite cylinders on slabs [Fig. 16(b)] reveal strong variations in the force depending on whether the arrays

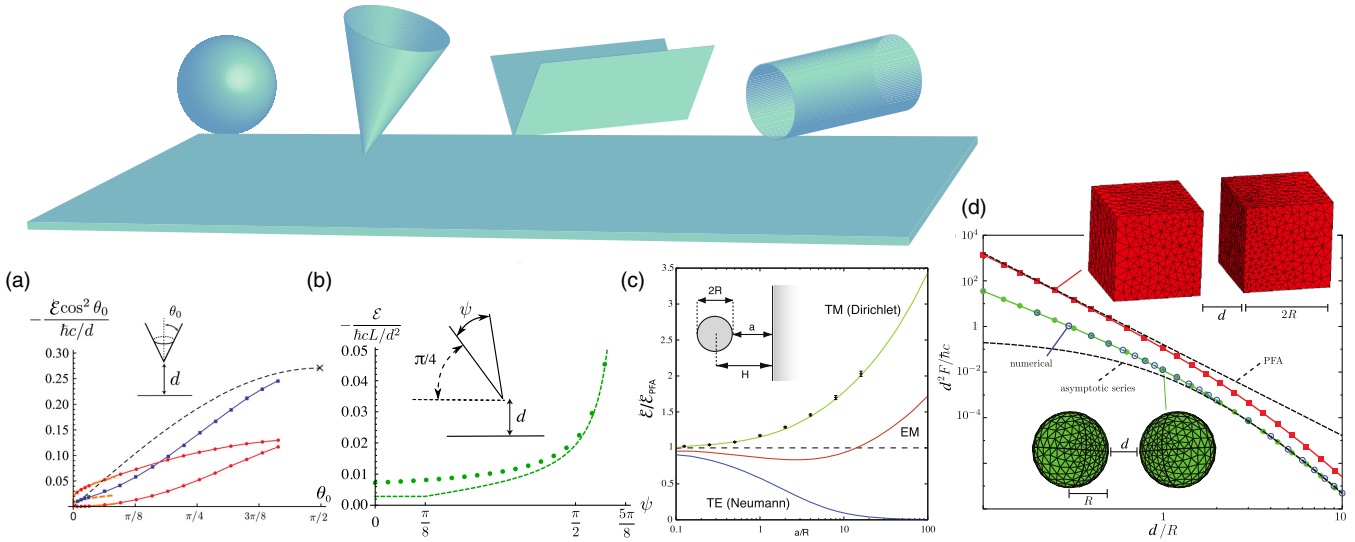

FIG. 15. Selected results of Casimir interactions involving compact bodies suspended above planar objects or interacting with other compact bodies, calculated via scattering-matrix techniques in combination with spectral methods. (a) Casimir energy of a perfectly conducting vertically oriented cone, suspended above a perfectly conducting plate by a fixed distance d, as a function of the semiopening angle θ_0 of the cone. From Maghrebi *et al.*, 2011. The PFA approximation is shown as the dashed line. (b) Casimir energy of a perfectly conducting wedge and plate of length L and tilt angle $\pi/4$ as a function of the opening angle ψ. The system is suspended above a semi-infinite perfectly conducting plate by a surface-surface distance d. From Maghrebi *et al.*, 2011. The PFA prediction, dashed lines, is compared to the exact calculation, solid circles. (c) Ratio of the exact Casimir and PFA energies of the perfectly conducting cylinder-plate structure shown in the inset, as a function of a/R, decomposed into TE and TM contributions. From Emig *et al.*, 2006. (d) Distance dependence of the Casimir force between perfectly conducting metallic cubes (red squares) or spheres (green circles), as computed by the BEM method of Reid, White, and Johnson (2013), divided by the corresponding PFA forces. Results for spheres are compared to computations performed using scattering-matrix methods (blue circles) which yield fast-converging semianalytical formulas, in contrast to situations involving realistic materials with dispersion such as gold, which require brute-force methods.

are aligned or crossed, even leading to changes in its sign at close separations when the system is immersed in a fluid (Rodriguez *et al.*, 2009; McCauley, Rodriguez *et al.*, 2010; McCauley, Rosa *et al.*, 2011). Exact calculations are also compared to predictions based on PFA, showing significant, qualitative deviations. An effective medium theory description of the problem, in which the slabs are treated as homogeneous, anisotropic dielectrics, gives surprisingly accurate predictions down to separations of the order of the period.

Objects with nontrivial geometry can also be utilized to obtain repulsive Casimir interactions in vacuum (Rodriguez *et al.*, 2015). A proof of principle of the feasibility of repulsion in vacuum was recently demonstrated using BEM and FDTD numerics in a structure involving a small, elongated particle above a plate with a hole (Levin *et al.*, 2010), shown schematically in Fig. 16(c). Because of constraints on the size of the particles and hole as well as on the length scales needed to observe these effects, the force in that geometry turns out to be too small (atto-Newtons) for current experimental detection (Levin *et al.*, 2010). However, extensions to multiple particles (attached to a substrate) have demonstrated a thousandfold force enhancements without the need to change hole radii or length scales (McCauley, Rodriguez *et al.*, 2011), as illustrated in Fig. 16(c). Interestingly, the enhancement can be understood as arising not only from the presence of additional bodies, but from increased repulsion due to the larger polarizability of the particles as they interact with fringing fields near the edge of the plate (Eberlein *et al.*, 2011; Milton *et al.*, 2011, 2012). One can also show that the interaction between a polarizable particle and a perfect-metal wedge or half plate is repulsive (Milton *et al.*, 2012), provided that the wedge is sufficiently sharp and that the particle is sufficiently anisotropic. Similar results should extend to vdW interactions on molecules and atoms near structured surfaces, but the main challenge in these systems is the need to attain a large degree of particle anisotropy. Recent calculations show that Rydberg atoms cannot achieve a high enough anisotropy (Ellingsen, Buhmann, and Scheel, 2010). Regardless of their current experimental observability and practical considerations, these recent theoretical predictions demonstrate the fact that geometry can prove to be a powerful resource for shaping Casimir forces.

VI. SOFT AND BIOLOGICAL MATERIALS

Besides the prominent role of fluctuation-induced interactions in inorganic materials systems, vdW forces have many other interesting manifestations. The adhesion of the gecko, with no help from glues, suction, or interlocking, is perhaps the most popular example for vdW interactions in biological and biorelated matter. Researchers have shown experimentally that vdW interactions between the gecko spatular toes and hydrophobic surfaces in air are responsible for the gecko clinging to substrates (Autumn and Peattie, 2002; Autumn *et al.*, 2002; Lee, 2014). Other experiments suggest that while geckos indeed use no glue, they do leave

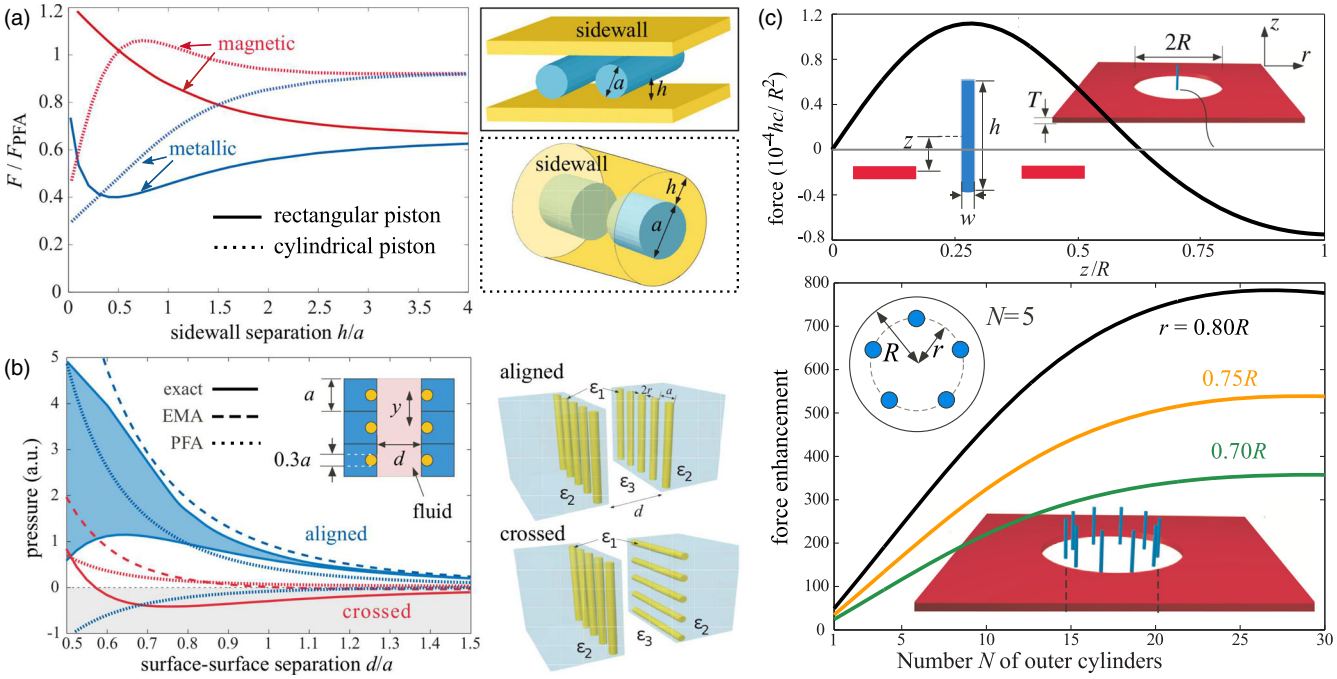

FIG. 16. Selected results illustrating unusual Casimir effects from nonadditive interactions in complex structures. (a) Casimir force between either translationally invariant waveguides (solid lines) or cylindrically symmetric rods (dotted lines), normalized by the corresponding PFA force, as a function of their separation from adjacent sidewalls a distance h apart (Rodriguez, Ibanescu, Iannuzzi, Capasso *et al.*, 2007; McCauley, Rodriguez *et al.*, 2010). Configurations of either perfect-electric (blue) or perfect-magnetic (red) conductors are considered. (b) Casimir pressure between two patterned structures involving periodic arrays of gold cylinders (ϵ_1) embedded in a semi-infinite silica substrate (ϵ_2) surrounded by ethanol (ϵ_3), as a function of their surface-surface separation d, computed by application of both scattering and FDTD methods (Rodriguez *et al.*, 2009; McCauley, Rodriguez *et al.*, 2010; McCauley, Rosa *et al.*, 2011). Exact calculations (solid lines), PFA (dotted lines), and effective medium theory (dashed lines) are also shown. (c) Casimir force between a small, anisotropic gold particle (top panel) or a circular array of N gold particles (bottom panel) and a gold plate with a hole (Levin *et al.*, 2010; McCauley, Rodriguez *et al.*, 2011), demonstrating repulsion for vacuum-separated metallic bodies.

"footprints" of residue identified as phospholipids with phosphocholine head groups (Hsu *et al.*, 2011). On the other hand, the contact surface between the gecko's toes and the substrate is saturated with methylene moieties of the phospholipids and contains no water. This is furthermore consistent with predominantly hydrophobic surface of gecko setae (Stark *et al.*, 2013), landing additional support to the mostly vdW origin of the adhesion force. Currently there is much gecko-inspired interest in constructing materials with similar adhesion properties (Jeonga and Suh, 2009). Single strand vertical arrays of cylindrical pillars produced by electron-beam lithography and etched into an array of vertical round shaped pillars are expected to show behavior similar to gecko toes. Dry adhesives for robotic applications based upon the characteristics of vertical and angled flaps from polydimethylsiloxane are also being considered for applications (Yu *et al.*, 2011).

A. The importance of aqueous solvent

The most important defining characteristics of vdW interactions in soft and biomatter comes from the presence of a solvent, i.e., water (Israelachvili, 1991). The interaction between two substrates with dielectric function $\varepsilon(\omega)$ separated by a water layer with $\varepsilon_w(\omega)$ can be described by the standard Lifshitz formula [Eq. (9)] (Bordag, Klimchitskaya *et al.*, 2009). The fact that typically $\varepsilon(0) \ll \varepsilon_w(0)$ makes the $n=0$ Matsubara term quite important and can account for about 50% or more of the total value of the Hamaker coefficient (Ninham and Parsegian, 1970). For lipid-water systems (Kollmitzer *et al.*, 2015) retardation effects are not important even at very large distances (Parsegian and Ninham, 1970; Parsegian, 2006). The significant thermal effects from the $n=0$ term show that results for vdW interactions in standard condensed media cannot be simply transcribed into the soft matter context. Also, apart from its large static dielectric constant, the full dielectric spectrum of water leads to non-monotonic features in the vdW interaction between ice and water vapor (Elbaum and Schick, 1991) or hydrocarbon films (Bar-Ziv and Safran, 1993) across a liquid water layer in the retardation regime (Wilen *et al.*, 1995).

Solvent effects are also important when their dispersion properties are in a certain relation with those of interacting materials. Recent work by Munday and Capasso (2007) and Munday, Capasso, and Parsegian (2009), as well as previous work by various others (Milling, Mulvaney, and Larson, 1996; Meurk, Luckham, and Bergstrom, 1997; Lee and Sigmund, 2001, 2002; Feiler, Bergstrom, and Rutland, 2008), made it clear that for specific asymmetric interaction geometries a solvent whose dielectric permittivity $\varepsilon_m(\omega)$ is between those of the interacting bodies 1 and 2, $\varepsilon_1(\omega) > \varepsilon_m(\omega) > \varepsilon_2(\omega)$, can create repulsive vdW interactions. Although in principle this

solvent-mediated Casimir-Lifshitz levitation has been known since the appearance of the Lifshitz theory (Dzyaloshinskii, Lifshitz, and Pitaevskii, 1961), it has not been used to effectively control the sign of the vdW interaction. Solvent mixtures with low molecular weight solutes such as glucose and sucrose also affect the dielectric properties of the solution and can thus modify the vdW interactions (Neveau *et al.*, 1977). Solventlike effects could be important also for two graphene sheets separated by atomic hydrogen gas, with one sheet adsorbed on a SiO_2 substrate, while the other is freestanding (Boström and Sernelius, 2012), as discussed in Sec. III.C.

Electrolyte screening is also a defining feature for biomatter in aqueous environments. The presence of salt ions screens the $n = 0$ Matsubara frequency in the Hamaker coefficient. The existence of this screening is connected to the fact that the $n = 0$ Matsubara term actually corresponds to the classical partition function of the system, and for confined Coulomb fluids, such as inhomogeneous electrolytes, can lead to a thoroughly different form of the $n = 0$ term in the full Matsubara sum of the Lifshitz theory (Podgornik and Zeks, 1988; Naji *et al.*, 2013), as discussed later. The screening of vdW interactions in electrolyte solutions can be derived in a variety of ways, most simply by replacing the Laplace equation with the linearized Debye-Huckel equation (Israelachvili, 1991; Parsegian, 2006). In this approach, the free ions present in the aqueous solution are taken into account just as in the case of bad conductors (Pitaevskii, 2008), where the number of charge carriers is small and obeys the Boltzmann statistics. The zero-frequency Matsubara term in Eq. (9) then leads to an approximate $n = 0$ Hamaker coefficient $\mathcal{H}_0(d) = (3/4)k_BT(1 + 2\kappa_0 d)e^{-2\kappa_0 d}$ (Parsegian, 2006). This expression is screened with half the Debye screening length $\kappa_0^{-1} = 8\pi\ell_B n_0$, where $\ell_B \simeq 0.7$ nm is the Bjerrum thermal length and n_0 is the bulk salt concentration.

In many biosystems, the vdW free energy is typically cast into the form of the Hamaker-type approximation $\mathcal{F}(d,T) = -\mathcal{H}(d)/12\pi d^2$, with the separation-dependent Hamaker coefficient that can be calculated exactly via the Lifshitz formalism, when accurate experimental data for the dielectric properties are available. For example, the Hamaker coefficients for lignin and glucomannan interacting with cellulose, titania, and calcium carbonate in vacuum, water, and hexane are found within a relatively narrow range of ~35–58 zJ for intervening vacuum and ≃8–17 zJ for an intervening aqueous medium (Hollertz *et al.*, 2013), with the dielectric response properties extracted via spectroscopic ellipsometry (Bergstrom *et al.*, 1999). The Hamaker coefficients for the interactions of the wood components with common additives in paper such as TiO_2 and $CaCO_3$ in water were obtained as ≃3–19 zJ (Hollertz *et al.*, 2013) and can explain important adhesion, swelling, and wetting phenomena ubiquitous in paper processing.

The long-range interaction between proteins is also of vdW nature (Leckband and Sivasankar, 1999; Leckband and Israelachvili, 2001). Estimates for protein-protein interactions across water or dilute salt solutions report Hamaker coefficients mostly within the range ≃10–20 zJ (Farnum and Zukoski, 1999). $\mathcal{H}$ for interacting proteins, such as bovine serum album, has been found to be ≃12 zJ by considering a Drude-Lorentz model for the dielectric function and the zero Matsubara frequency term included (Roth *et al.*, 1996; Neal, Asthagiri, and Lenhoff, 1998). Using the anisotropic coarse-grained model of a protein on the level of amino acid residues, one can calculate effective polarizabilities of bovine pancreatic trypsin inhibitor, ribonuclease inhibitor, and lysozyme in an aqueous solution (Song, 2002). These results have to be approached with caution, however. Accurate frequency-dependent polarizabilities are rarely available from either theoretical or experimental studies (Nandi, Bhattacharyya, and Bagchi, 2000); thus one has to rely on plausible but probably unrealistic model approximations (Song and Zhao, 2004). The same is true for the static dielectric constant that shows pronounced variation from the inside to the periphery of the protein (Li *et al.*, 2013). The anisotropic optical spectrum of collagen, a fibrous protein, has been calculated by *ab initio* methods (Poudel *et al.*, 2014) and used to estimate the corresponding nonisotropic Hamaker coefficients (Dryden *et al.*, 2015). The vdW interactions between collagen fibers show a substantial angle-independent component of the Hamaker coefficient ≃9.3 zJ. The origin of the angular dependence of vdW interactions is in fact twofold: the morphological anisotropy, given by the shape, and the material anisotropy, given by the dielectric response tensor. Both contribute to the general angular dependence and consequently torques between biological macromolecules (Hopkins *et al.*, 2015), see later discussion.

B. Lipid membranes

In general, the vdW interaction is of fundamental importance for the stability of biological matter (Nel *et al.*, 2009) and for membrane arrays, in particular (Petrache *et al.*, 2006; Pasichnyk, Everaers, and Maggs, 2008). The essential component of a membrane is the lipid bilayer, a planar layer of finite thickness composed of a hydrocarbon core with hydrophyllic boundaries facing the aqueous solution (Tristram-Nagle and Nagle, 2004). vdW interactions between lipid membranes were in fact the first example of using full Lifshitz theory in condensed media (Parsegian and Ninham, 1969). Calculated nonretarded Hamaker coefficients were found to be in the range 1–10 zJ. The importance of the ionic screening of the zero-frequency Hamaker term in electrolyte solutions for membranes has also been carefully quantified (Ninham and Parsegian, 1970; Petrache *et al.*, 2006). As stated in Sec. VI.A, the very high static dielectric constant of water (Parsegian, 2006) leads to an anomalously large contribution to the entropy of vdW interactions, which remains unretarded for all separations as it corresponds mostly to the $n = 0$ Matsubara term. However, taking into account electrolyte screening at sufficiently large salt concentrations reverses the anomalous effect of the water dielectric constant, so that retardation effects emerge from a combination of electrolyte screening and standard retardation screening (Ninham and Parsegian, 1970).

Most experiments yielding the strength of the nonretarded Hamaker coefficients are actually based on multilamellar interaction geometries that allow for detailed osmotic stress small-angle x-ray scattering (SAXS) studies (Tristram-Nagle

and Nagle, 2004; Kollmitzer *et al.*, 2015) (see Fig. 17). One also needs to consider the nonpairwise additive vdW effects in multilamellar geometries that can be significant (Narayanaswamy and Zheng, 2013). The interaction of a pair of two lipid membranes with thickness a at a separation d in a multilamellar stack yields for the interaction surface free energy density $\mathcal{F}(a,d)$:

$$\mathcal{F}(a,d) \simeq -\frac{k_B T}{4\pi(a+d)^2}\left\{\frac{1}{2}\left[\zeta\left(2,\frac{d}{a+d}\right)-2\zeta(2,1)+\zeta\left(2,\frac{d+2a}{a+d}\right)\right]\bar{\Delta}^2(0)+\sum_{n=1}^{\infty}\left[\mathcal{Z}\left(2+y,\frac{d}{a+d}\right)-2\mathcal{Z}(2+y,1)+\mathcal{Z}\left(2+y,\frac{d+2a}{a+d}\right)\right]\bar{\Delta}^2(\iota\omega_n)\right\}, \tag{24}$$

where $\zeta(m,n)$ is the zeta function and $y = 2(\omega_n/c)\sqrt{\epsilon_B(\iota\omega_n)}(a+d)$. The function $\mathcal{Z}(2+y,x)$ is exponentially screened with y according to Podgornik, French, and Parsegian (2006) and $\bar{\Delta}(\omega) = (\rho_A\epsilon_B - \rho_B\epsilon_A)/(\rho_A\epsilon_B + \rho_B\epsilon_A)$, where $\epsilon_A(\omega)$ and $\epsilon_B(\omega)$ are the permittivities of lipid and water, respectively. Also, $\rho^2_{A,B} = Q^2 - \epsilon_{A,B}\omega^2/c^2$, where Q is the magnitude of the transverse wave vector [for details see Podgornik, French, and Parsegian (2006)].

The nonadditive effects in $\mathcal{F}(a,d)$ vanish at $d \ll a$, where the interaction is obviously reduced to that of two semi-infinite lipid regions across water. Approximating the water response function by one Debye and 12 Lorentz oscillators (Roth and Lenhoff, 1996; Dagastine, Prieve, and White, 2000), and the lipid response function by four Lorentz oscillators in the ultraviolet regime (Parsegian, 2006) yields $\mathcal{H}(a = 4\text{ nm},\ d \sim a) = 4.3$ zJ. The usually quoted theoretical result with no retardation effects (Parsegian, 2006) is $\mathcal{H}(a, d \sim a) = 3.6$ zJ, while experimentally determined $\mathcal{H}$ is typically in the range 2.87–9.19 zJ for dimyristoyl phosphatidylcholine and dipalmitoyl phosphatidylcholine lipid multilayers (Petrache *et al.*, 1998). The lipid bilayer thickness dependence is clearly seen in recent experiments with dioleoyl phosphocholine/distearoyl-phosphocholine/cholestrol (DOPC/DSPC/Chol) mixtures that phase separate into liquid-ordered (Lo) and liquid-disordered (Ld) domains with $\mathcal{H} = 4.08$ zJ for Ld and $\mathcal{H} = 4.15$ zJ for Lo domains (Kollmitzer *et al.*, 2015).

Other fluctuation-induced Casimir-like interactions (Kardar and Golestanian, 1999) are also of relevance in the context of lipid membranes. Among these, the Helfrich interactions due to steric repulsion between fluctuating membranes have received very detailed attention; see Freund (2013) and Lu and Podgornik (2015). However, more directly related to the Casimir effect are the thermal height fluctuations of membranes, constrained on average to be planar, that can couple in various manners to the local membrane composition. For example, embedded macromolecules, such as proteins (Phillips, Kondev, and Theriot, 2008), cause modifications of the height fluctuations due to the spatial variation of the effective membrane rigidity at the position of the inclusion. Thus, there is an elastic Hamiltonian (Deserno, 2015) in terms of the membrane height function $h(\mathbf{x})$ (Lipowsky, 1991)

$$H[h(\mathbf{x})] = \int d^2\mathbf{x}\left\{\frac{1}{2}\kappa_r(\mathbf{x})[\nabla^2 h(\mathbf{x})]^2 + \bar{\kappa}_r(\mathbf{x})\left[\frac{\partial^2 h(\mathbf{x})}{\partial x^2}\frac{\partial^2 h(\mathbf{x})}{\partial y^2} - \left(\frac{\partial^2 h(\mathbf{x})}{\partial x \partial y}\right)^2\right]\right\}, \tag{25}$$

where the local bending rigidity $\kappa_r(\mathbf{x})$ and the local Gaussian rigidity $\bar{\kappa}_r(\mathbf{x})$ are position dependent upon $\mathbf{x} = (x,y)$ denoting the in-plane coordinates for the membrane projected area (Dean, Parsegian, and Podgornik, 2015). In single component membranes, where κ_r and $\bar{\kappa}_r$ are constant, the $\bar{\kappa}_r$ term is zero when the membrane is a free-floating sheet, since by virtue of the Gauss-Bonnet theorem it depends only on the boundary and topology of the membrane (David, 2004). The height correlator can be found analytically in this case (Deserno, 2015). In the presence of elastic inclusions, both moduli contain an unperturbed constant part $\kappa_{0,r}$ and $\bar{\kappa}_{0,r}$ as well as the

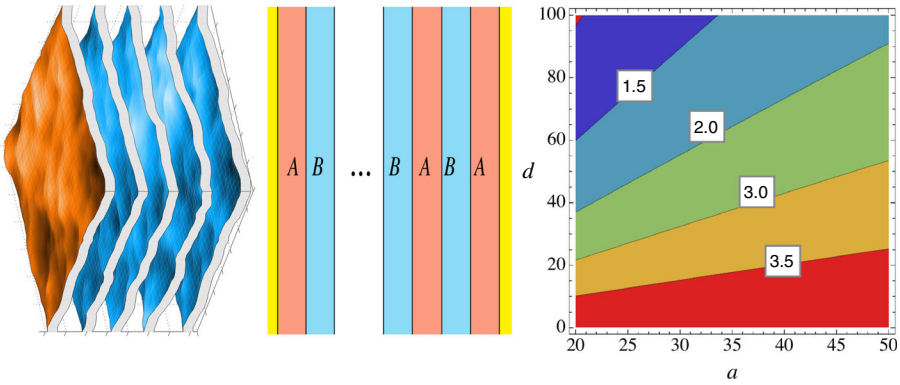

FIG. 17. Multilamellar array of lipid membranes immersed in water, each composed of a hydrocarbon core with two surface hydrophillic headgroup layers. Left: A realistic presentation with fluctuating positions of the membranes [for details see Kollmitzer *et al.* (2015b)]. Middle: A model system with a rigid array of alternating solvent (B) membrane (A) solvent (B) regions. Right: The Hamaker coefficient, $H(a,d)$ in [zJ], as a function of the separation between membranes d and the thickness of the lipid bilayers a in nm. The Hamaker coefficient is calculated based on the full dispersion spectra of water and lipids (hydrocarbons). From Podgornik, French, and Parsegian, 2006.

position dependent parts $\Delta\bar{\kappa}_r(\mathbf{x})$ and $\Delta\kappa_r(\mathbf{x}')$ that vanish outside of the inclusions. Other parametrizations of the effect of inclusions are also possible and have been considered (Netz, 1997). Alternatively, membrane inclusions can also be considered as curvature sources (Dommersnes and Fournier, 1999a). To the above energy one can also add surface energy and an external potential energy when appropriate (Noruzifar, Wagner, and Zandi, 2013). Apart from the order of derivatives in the fluctuating field, second for membranes and first for electrostatic field, and the local bending rigidity taking the role of the local dielectric permittivity, $H[h(\mathbf{x})]$ is completely analogous to the electrostatic field Hamiltonian (Naji *et al.*, 2013) or indeed to the Hamiltonian of critical mixtures (Trondle *et al.*, 2010). Thus one can expect that thermal fluctuation effects will also be present.

Indeed, inclusions in the membrane, which modify its local mechanical properties, can experience fluctuation-induced forces between them (Goulian, Bruinsma, and Pincus, 1993; Golestanian, Goulian, and Kardar, 1996a, 1996b; Park and Lubensky, 1996; Bartolo and Fournier, 2003; Lin *et al.*, 2011; Yolcu, Rothstein, and Deserno, 2011). The interactions are energetically of the order of k_BT and can in certain circumstances, in particular, for tensionless membranes, be long ranged and therefore potentially exhibit an important effect on the organization of the membrane (Machta, Veatch, and Sethna, 2012). Several studies have considered the coupling of membrane inclusions to the membrane curvature via the elastic stress (Bitbol, Dommersnes, and Fournier, 2010; Lin *et al.*, 2011; Yolcu, Rothstein, and Deserno, 2011) or to topological defects in orientational disorder (Golestanian, Goulian, and Kardar, 1996a; Korolev and Nelson, 2008). Assuming that $\kappa_r(\mathbf{x})$ and $\bar{\kappa}_r(\mathbf{x})$ are small, one can calculate the cumulant expansion of the partition function (Goulian, Bruinsma, and Pincus, 1993). The effective two-body interaction between regions deviating from the background rigidity $\kappa_{0,r}$ is then obtained in the simple form

$$H_2 = \frac{k_BT}{4\pi^2\kappa_{0,r}^2}\int d^2\mathbf{x}d^2\mathbf{x}'\frac{\Delta\bar{\kappa}_r(\mathbf{x})\Delta\kappa_r(\mathbf{x}')}{|\mathbf{x}-\mathbf{x}'|^4}+\cdots \tag{26}$$

after expanding to the lowest order in the deviation from the constant values of the rigidities $\Delta\bar{\kappa}_r(\mathbf{r})$ and $\Delta\kappa_r(\mathbf{r}')$ that vanish outside of the inclusion. When the separation between local regions (inclusions) characterized by change in rigidities is much larger than the size of the regions, the first-order term in a multipole expansion of the energy between the two regions therefore decays as the fourth power of separation. Notably, both $\kappa_r(\mathbf{x})$ and $\bar{\kappa}_r(\mathbf{x})$ have to be present in order to have a fluctuation interaction. On the other hand, considering membrane inclusions as curvature sources one can bypass these constraints, at the same time also strongly enhancing and increasing the range of the interactions (Dommersnes and Fournier, 1999a). These Casimir-like forces are dominated by fluctuations and their variance also shows a characteristic dependence on the separation (Bitbol, Dommersnes, and Fournier, 2010) as well as pronounced many-body aspects (Dommersnes and Fournier, 1999b), as expected for Casimir-like interactions.

Scattering methods developed for the electromagnetic Casimir effect (Rahi, Emig, and Jaffe, 2011) and discussed in Sec. V have been employed for the interaction between two membrane embedded disks of radius R to all orders, leading to an asymptotic result for large separations (Lin *et al.*, 2011). The effective field theory formalism also affords an efficient framework for the computation of membrane fluctuation-mediated interactions (Yolcu, Rothstein, and Deserno, 2011; Yolcu and Deserno, 2012). In the case of broken cylindrical symmetry of the inclusions, the fluctuation interaction retains the same separation dependence, but its strength depends on the two orientation angles as $\cos 2\theta_1 \cos 2\theta_2$ and $\cos 4(\theta_1+\theta_2)$ (Golestanian, Goulian, and Kardar, 1996b; Park and Lubensky, 1996). This of course implies the existence of fluctuation or vdW torques; see Sec. VI.C.

Experimentally, fluctuation-mediated interactions between membrane inclusions might be difficult to measure directly, if at all feasible. More promising seems to be the detection of their consequences, such as fluctuation-induced aggregation of rigid membrane inclusions (Dommersnes and Fournier, 1999b; Weikel, 2001) or through their effect on the miscibility of lipid mixtures in multicomponent membranes (Machta, Veatch, and Sethna, 2012; Dean, Parsegian, and Podgornik, 2015).

C. van der Waals torques

Biological materials are typically anisotropic in terms of shapes as well as response properties (Hopkins *et al.*, 2015). Such anisotropy leads to vdW torques, which were first studied by Kats (1978) for the special case of isotropic boundaries with anisotropic intervening material, and independently by Parsegian and Weiss (1972) who studied the inverse case of bodies with anisotropic dielectric response interacting across an isotropic medium in the nonretarded limit (Kornilovitch, 2013). The full retarded Lifshitz result was obtained only much later in a veritable *tour de force* by Barash (1978), following previous partial attempts (Barash, 1973), leading to a series of recent developments (van Enk, 1995b; Munday *et al.*, 2005; Shao, Tong, and Luo, 2005). The general Lifshitz formulas for the interaction between two anisotropic half-spaces or even an array of finite size slabs (Veble and Podgornik, 2009) are algebraically very complicated and untransparent, with little hope of a fundamental simplification (Philbin and Leonhardt, 2008). Morphological anisotropy effects are seen either between anisotropic bodies (Emig *et al.*, 2009; Rahi, Emig, and Jaffe, 2011) or between surfaces with anisotropic decorations such as corrugations (Banishev, Wagner *et al.*, 2013; Banishev *et al.*, 2014). vdW-like torques have also been predicted between anisotropic inclusions within fluctuating membranes (Golestanian, Goulian, and Kardar, 1996b; Park and Lubensky, 1996).

The first attempt to evaluate the vdW interaction between two cylinders comes from Barash and Kyasov (1989). Results for two infinitely long anisotropic cylinders can be obtained in a dilution process (Parsegian, 2006), such that the presence of dielectric cylinders can be considered as a small change of the dielectric permittivity of two semi-infinite regions (Pitaevskii, 2008). This approach leads to interactions between infinite cylinders of radius R at minimum separation d at any angle of

inclination θ in nonretarded (Rajter *et al.*, 2007) as well as retarded limits (Siber *et al.*, 2009), but also between cylinders and anisotropic semi-infinite layers (Saville *et al.*, 2006; Hopkins *et al.*, 2015). The vdW interaction free energy for inclined cylinders is

$$\mathcal{F}(d,\theta) = -\frac{(\pi R^2)^2}{2\pi d^4 \sin\theta}[\mathcal{A}^{(0)}(d) + \mathcal{A}^{(2)}(d)\cos 2\theta], \quad (27)$$

where $1/\sin\theta$ stems from the shape anisotropy and the $\cos 2\theta$ dependence associated with the material anisotropy; see Fig. 18. The Hamaker coefficients $\mathcal{A}^{(0)}(d)$ and $\mathcal{A}^{(2)}(d)$ are functions of separation and the relative anisotropy measures, but do not depend explicitly on the angle of inclination θ. They also depend on the material types and Matsubara sampling frequencies (Siber *et al.*, 2009; Stark *et al.*, 2015). In the symmetric interaction case (Hopkins *et al.*, 2015) both $\mathcal{A}^{(0)}(d)$ and $\mathcal{A}^{(2)}(d)$ decompose into a square and thus cannot be negative or change sign. In the asymmetric case, however, the signs of the interactions as well as the signs of the torques are more complicated, as they depend on the perpendicular and parallel dielectric responses of the interacting bodies. They do not follow the general rule for interacting planar bodies 1 and 2 across a medium m, with a change of sign implied by the sequence $\varepsilon_1(\omega) > \varepsilon_m(\omega) > \varepsilon_2(\omega)$; see Sec. VI.A.

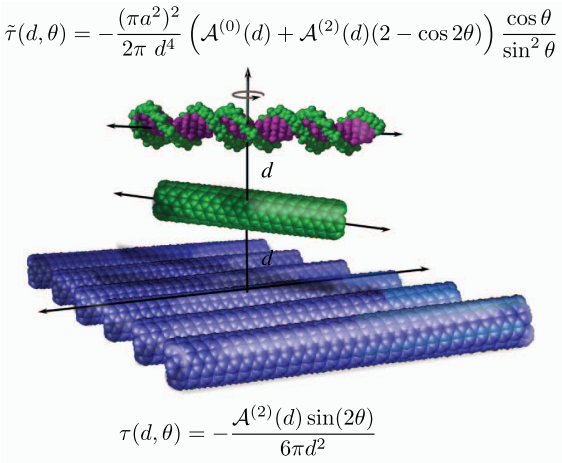

FIG. 18. Forces and torques between anisotropic molecules and molecular aggregates. Top: $\tilde{\tau}(d,\theta)$, torque between two inclined long cylindrical molecules (above DNA, below single-walled CNTs) as a function of the closest separation d and angle of inclination θ, calculated within the Lifshitz theory. The angle of inclination is between the axes of the two cylindrical systems. The two Hamaker coefficients $\mathcal{A}^{(0)}(d)$ and $\mathcal{A}^{(2)}(d)$ depend on the dielectric anisotropy of the interacting materials as well as on the separation due to retardation effects, but they do not depend on mutual orientation. Bottom: $\tau(d,\theta)$, torque per unit surface area between two planar semi-infinite slabs composed of arrays of cylindrical molecules at separation d with angle of inclination θ between their anisotropic uniaxial tensors. Only the surface layer of the bottom slab and one molecule of the upper slab are shown. Again, the Hamaker coefficient $\mathcal{A}^{(2)}(d)$ depends on the dielectric anisotropy of the interacting materials as well as on the separation due to retardation effects, but not on the orientation of the dielectric tensors. Adapted from Dryden *et al.*, 2015.

vdW torques between semi-infinite anisotropic materials also imply torques between anisotropic cylindrical molecules, such as filamentous graphitic systems of metallic and semiconducting single-walled CNTs (Rajter *et al.*, 2007, 2013; Siber *et al.*, 2009), multiple composites of DNA (Zheng *et al.*, 2009; Sontz, Muren, and Barton, 2012; Young *et al.*, 2014), type I collagen (Cheng *et al.*, 2008), and polystyrene (Jin *et al.*, 2005). DNA optical properties (Pinchuk, 2004) have been converted into the corresponding separation dependence vdW free energy in the case of pairs of nucleotides (Pinchuk and Vysotskii, 1999, 2001). A static dielectric constant of 8 for DNA, that enters the $n = 0$ Matsubara term, was recently measured inside single T7 bacteriophage particles by electrostatic force spectroscopy (Cuervo *et al.*, 2014). Optical dispersion data are also available for single nucleotides, nucleosides and their derivatives, synthetic polynucleotides (polyuridylic acid, polyadenylic acid, poly-AU), various nucleic acids, such as RNA and native bacterial DNAs in aqueous solutions (Voet *et al.*, 1963), or wet and dry polymerized oligonucleotides and mononucleotides (Silaghi *et al.*, 2005; Zalar *et al.*, 2007) as well as dry DNA thin films (Sonmezoglu and Sonmezoglu, 2011). Optical properties of DNA oligonucleotides (AT)10, (AT)5(GC)5, and (AT-GC)5 using *ab initio* methods and ultraviolet-visual decadic molar absorbance measurements show a strong dependence of the position and intensity of UV absorbance features on oligonucleotide composition and stacking sequence (Schimelman *et al.*, 2015). The calculated Hamaker coefficients for various types of DNA molecules are overall small but depend on the base-pair sequence details and could control the finer details of the equilibrium assembly structure (Bishop *et al.*, 2009). In fact, the stacking sequence dependence of the optical properties has important repercussions for the molecular recognition between two approaching DNA molecules that depends on vdW interactions (Lu, Naji, and Podgornik, 2015). The angle-independent part of the Hamaker coefficient is $\simeq$5 zJ, while the angular part is effectively zero when the zero-frequency Matsubara component is fully screened by the electrolyte solution. At least for DNA molecules, it then appears that the anisotropy effects stem purely from the shape anisotropy, whereas this is not the case for CNTs. Among the fibrous proteins collagen also shows strong vdW interactions with silica resulting in a Hamaker coefficient that is 39% larger than that of the silica-(GC)10 DNA interaction at 5 nm separation (Dryden *et al.*, 2015).

Although the vdW torque, defined as $\tau(d,\theta) = -\partial\mathcal{F}(d,\theta)/\partial\theta$, is eminently measurable, it has however not been measured directly yet (Iannuzzi *et al.*, 2005; Capasso *et al.*, 2007; Chen and Spence, 2011). The anisotropy that engenders the vdW torque can be of different origins: it can result either from anisotropy of the dielectric response of the interacting bodies or from their asymmetric shape (Hopkins *et al.*, 2015). Both give effective Hamaker coefficients that depend on the mutual orientation of the dielectric or shape axes (Dryden *et al.*, 2015). The material anisotropy can also be either intrinsic or a consequence of arrays of nanoparticles embedded in an isotropic background (Esquivel-Sirvent and Schatz, 2013), and/or a consequence of the action of external

fields (Esquivel-Sirvent, Cocoletzi, and Palomino-Ovando, 2010). It remains unclear which anisotropic effects would be best suited for accurate experiments or whether two-body or many-body configurations would be optimal (Lu and Podgornik, 2016).

D. Electrostatic fluctuations

The $n = 0$ ("static") Matsubara term corresponds to the classical partition function of the Coulomb system and can have a form very different from the one derived from the Lifshitz theory. For an interacting Coulomb fluid such as a confined electrolyte or plasma, a counterion only system, or a system of dipoles or polarizable particles in an inhomogeneous dielectric background, the $n = 0$ Matsubara term corresponds to the free energy of fluctuations around the mean field in the range of parameter space where the mean-field (Poisson-Boltzmann or weak coupling) approximation holds [for details, see Naji *et al.* (2013)]. This leads to effects such as screening of the Hamaker coefficient, universal value for the Hamaker coefficient, or its anomalous separation dependence. In effect, the $n = 0$ Matsubara term actually corresponds to Gaussian or one-loop electrostatic potential fluctuations around the mean field for a fully coupled system (Podgornik and Zeks, 1988; Netz, 2001b) and thus presents a first-order correction to the description of Coulomb fluids on the mean-field level (Holm, Kekicheff, and Podgornik, 2001). Formally this follows from an effective non-Gaussian "field action" $S[\phi]$ that one can derive from an exact field-theoretic representation of the confined Coulomb fluid partition function in terms of the fluctuating local electrostatic potential (Edwards and Lenard, 1962; Podgornik, 1990). The mean-field theory is then defined as the saddle point of this field action (Naji *et al.*, 2013).

Thermal fluctuations around the saddle point at the first-order loop expansion representing the contribution from correlated Gaussian fluctuations around the mean field or saddle-point solution (Dean *et al.*, 2014) lead to a thermal fluctuation-induced vdW-like attraction in the form of the trace log of the field-action Hessian

$$\mathcal{F} = -k_B T \mathrm{Tr}\, \log\left(\left.\frac{\delta^2 S[\phi]}{\delta\phi(\mathbf{r})\delta\phi(\mathbf{r}')}\right|_{\phi(\mathbf{r})=-i\psi_{\mathrm{PB}}(\mathbf{r})}\right) + \mathcal{O}(\phi^3), \tag{28}$$

where $\phi(\mathbf{r}) = -i\psi_{\mathrm{PB}}(\mathbf{r})$ is the saddle-point (Poisson-Boltzmann) electrostatic potential configuration. This second-order correction universally lowers the interaction pressure between surfaces and thus leads to an attractive contribution to the total interaction pressure. It also includes a term that exactly cancels the zero-frequency contribution in the Lifshitz theory (Podgornik, 1990) so it should be viewed as a substitute for the $n = 0$ Lifshitz term. As a rule, this fluctuation attraction is weaker than the repulsive leading-order saddle-point contribution; thus the total interaction remains repulsive (Netz and Orland, 2000; Netz, 2001a). In certain models that either assume charge asymmetry (Kanduc *et al.*, 2008), surface condensation, or adsorption of counterions on (fixed) charged boundaries, the repulsive mean-field effects are strongly suppressed and the total interaction is then mostly due to thermal fluctuations (Lau *et al.*, 2001, 2002; Lau and Pincus, 2002). This can happen in the case of oppositely charged surfaces where the thermal fluctuation interactions can become dominant (Lau and Pincus, 1999; Ben-Yaakov *et al.*, 2007; Kanduc *et al.*, 2008).

A related problem of thermal electrostatic fluctuations is presented by the Kirkwood-Shumaker (KS) interactions that exist between macroions with dissociable charges, such as proteins (Lund and Jonsson, 2013). Originally this interaction was obtained from a perturbation theory around an uncharged state (Kirkwood and Shumaker, 1952; Lund and Jonsson, 2013). The KS interaction is similar to the thermal vdW interaction but it corresponds to monopolar charge fluctuations (Adzic and Podgornik, 2014) and is thus in principle much longer ranged. Monopolar fluctuations cannot arise for fixed charges on interacting bodies and some surface charging mechanism or charge regulation, where the macroion surfaces respond to the local electrostatic potential with a variable effective charge, is needed (Borkovec, Jonsson, and Koper, 2001). Formally charge regulation can be described by another, nonlinear source term in the field action $f_S(\phi(\mathbf{r}))$ that involves the fluctuating potential at the surface (S) (Adzic and Podgornik, 2015). Nonlinearity of this field action is essential as a linear dependence on the fluctuating potential, in fact, corresponds to a fixed charge that cannot exhibit monopolar charge fluctuations. These are given by the surface capacitance determined by the second derivative of $f_S(\phi)$ with respect to the surface potential, and the KS interactions depend quadratically on this capacitance. The KS interaction between two macroions in the asymptotic regime between particles 1 and 2 then assumes the form $\mathcal{F} \sim -\mathcal{C}_1\mathcal{C}_2/R^2$. The exact form of f_S and thus the capacitance $\mathcal{C}$ is not universal as it depends on the surface-ion interaction (Fleck and Netz, 2007; Markovich, Andelman, and Podgornik, 2014; Adzic and Podgornik, 2015). Although calculating the KS interaction is challenging, exact solutions are available in 1D, demonstrating a rich variety of behaviors due to charge regulation and the ensuing correlated fluctuations (Maggs and Podgornik, 2014). Some of these 1D properties transfer also to the more realistic 3D models between globular proteins with dissociable surface charge groups (Adzic and Podgornik, 2015). Similar anomalously long-range monopolar fluctuations and concurrent Casimir or vdW-like interactions can also result from a different mechanism where monopolar charge fluctuations result not from charge regulation but rather from nanocircuits with capacitor components, where fluctuating charges are transferred through the wire connection in a capacitor system (Drosdoff *et al.*, 2016).

The link between Coulomb interactions and thermal Casimir and vdW interactions has been implicated also in some theoretical approaches to the Hofmeister or specific ion effects (Salis and Ninham, 2014). These works motivated numerous investigations of nonelectrostatic ion-specific interactions between ions and surfaces and their role in modifying surface tension of electrolyte solutions or indeed the solution behavior of proteins. In fact, the standard Onsager-Samaras result was only recently realized to be fluctuational in nature (Markovich, Andelman, and Podgornik, 2014). Ninham and

co-workers as well as others (Edwards and Williams, 2004) made attempts to include vdW interactions into a complete theory of ion interactions in confined aqueous solutions (Boström *et al.*, 2005, 2006; Boström and Ninham, 2006). The major problem in including vdW interactions into the description of inhomogeneous electrolytes is that the contributions of fixed charges and ion polarizability are in general not additive (Demery, Dean, and Podgornik, 2012). However, they sometimes can be approximated by an additive contribution on the strong coupling level, provided that the polarizability of the ions is large enough. A popular ansatz that simply adds a vdW ion-polarizability dependent contribution to the electrostatic potential of mean force has thus a very limited range of validity.

VII. EXPERIMENTS PROBING MATERIALS ASPECTS OF VAN DER WAALS AND CASIMIR INTERACTIONS

The small magnitude of the Casimir force has motivated many experimental efforts to measure this interaction with ever increasing precision. Such investigations have been invaluable in understanding the applicability of the Lifshitz formalism and its variations for standard metals (Au, Al, Cr), semiconductors (Si, Ge), and dielectrics (silica) in the plane-plane, sphere-plane, cylinder-plane, and atom-plane geometries (Lamoreaux, 1997; Mohideen and Roy, 1998; Roy, Lin, and Mohideen, 1999; Chan *et al.*, 2001; Bressi *et al.*, 2002; Decca *et al.*, 2003; Brown-Hayes *et al.*, 2005; Chen *et al.*, 2005; Obrecht *et al.*, 2007; Kim *et al.*, 2009). Several studies have shown that the interaction can be manipulated by utilizing specific materials characteristics. For example, using indium tin oxide (ITO) has proven a powerful way to reduce the Casimir force when compared to bodies made of noble metals (de Man *et al.*, 2009; de Man, Heeck, and Iannuzzi, 2010; Chang *et al.*, 2011; Banishev, Chang, Castillo-Garza *et al.*, 2012). Furthermore, according to Chang *et al.* (2011) and Banishev, Chang, Castillo-Garza *et al.* (2012), the UV illumination of an ITO plate transforms it into the dielectric state. As a result, the agreement with the predictions of the Lifshitz theory can be achieved only after one neglects the contribution of free charge carriers in the dielectric permittivity. Interesting possibilities from phase changing materials have also been found. Compositions characterized by amorphous to crystalline phase transitions can experience large changes in the response properties, which affect the Casimir interaction significantly (Torricelli *et al.*, 2010, 2012). The role of the magnetic response of ferromagnetic materials has also been probed experimentally (Banishev, Chang, Klimchitskaya *et al.*, 2012; Banishev *et al.*, 2013a, 2013b) using either a Ni or Au coated sphere and a Ni coated plate. They found the data to be in agreement with the plasma model and excluded the Drude model for the free-electron scattering in metals. They noted that the results of these measurements taken together with the measurement results for two Au test bodies cannot be reconciled with the Drude model even with the introduction of any background force (such as those arising from electrostatic patches), either attractive or repulsive.

Experimental research continues its advances in utilizing other materials and structured systems to probe this subtle force at various length scales. AFM techniques have been employed in vdW measurements giving unprecedented insight into smaller and heterogeneous systems. Pulling single molecules with an AFM tip from metallic surfaces (Wagner *et al.*, 2014) confirms the asymptotic d^{-3} force law and quantifies the nonadditive part of the vdW interaction. Nonadditive effects have also been demonstrated in adhesion measurements in various tribological environments as well (Loskill, Hahl *et al.*, 2012, Loskill, Puthoff *et al.*, 2012). Another recent report gives clear evidence of the vdW screening capabilities in graphene and MoS_2 heterostructures giving insight into adhesion properties of graphene and other layered materials (Tsoi *et al.*, 2014). These nonadditive and screening effects are particularly challenging for theory, which has motivated developments in first-principles calculations methods, as discussed in Sec. II.

The first experimental measurement of the Casimir force involving graphene was reported by Banishev, Wen *et al.* (2013). Subsequent investigations show good agreement between experimental data and calculations, taking into account the Dirac spectrum (Klimchitskaya, Mohideen, and Mostepanenko, 2014; Klimchitskaya and Mostepanenko, 2015b). However, many issues need to be investigated further. For example, more precise comparison with theory is needed, which requires measurements of freestanding graphene interactions. Schemes to determine the asymptotic distance dependence and temperature effects are absent. Experiments in this direction are extremely desirable as they can serve to validate the numerous theoretical predictions. Reliable experiments for stacks of graphene are also much desired in order to directly determine the binding energy of graphite and settle the wide range of values reported through indirect measurements (Benedict *et al.*, 1998; Zacharia, Ulbricht, and Hertel, 2004). It would also be interesting to seek experimental knowledge of vdW and Casimir interactions involving other systems with a Dirac spectrum. Probing novel topological phases in such dispersive interactions using topological and Chern insulators can be very beneficial.

Experimental measurements in structured materials continue to shed light on many aspects of the Casimir force, from nonadditive effects in grating and related geometries (Chan *et al.*, 2008; Banishev, Wagner *et al.*, 2013; Intravaia *et al.*, 2013) to repulsive interactions in interleaved structures (Rodriguez, Joannopoulos, and Johnson, 2008; Tang *et al.*, 2015), to strong temperature corrections arising at large separations (Sushkov *et al.*, 2011) or in situations involving structured magnetic media (Bimonte, 2015). Experiments at nanometric scales, involving objects with nontrivial surface topology due to roughness or patch charges, are also beginning to push the boundaries of theoretical techniques (Kim *et al.*, 2010; Dalvit *et al.*, 2011). For instance, recent AFM characterizations of the surface morphology of planar objects (van Zwol, Palasantzas, and De Hosson, 2008) coupled with predictions based on the above-mentioned state-of-the-art simulation techniques (Broer *et al.*, 2012) reveal that the presence of roughness on the scale of their separations manifests as strong deviations in the power-law scaling of the force (Broer *et al.*, 2013). Challenges that continue to be addressed in current-generation experiments include the need to control and calibrate materials properties. Specifically, accurate comparison between theory and experiments requires

accurate knowledge of the dielectric response over a broad spectral region, spurring recent efforts to characterize numerous material properties from dc to ultraviolet wavelengths (van Zwol, Palasantzas, and De Hosson, 2009; Sedighi *et al.*, 2014). Finally, a number of experiments employing novel fabrication techniques have begun to explore Casimir forces in on-chip, integrated systems (Yamarty and McNamara, 2009; Zho *et al.*, 2013) where parallelism is no longer a key impediment, removing the need for external instrumentation needed to bring objects closer together and paving the way for applications where the force is exploited in conjunction with other effects (e.g., mechanical or optical actuation) to enable new functionalities (Yamarty and McNamara, 2009; Pernice *et al.*, 2010; Rodriguez *et al.*, 2011).

On the other hand, small-angle x-ray scattering techniques are useful for measuring vdW potentials in soft matter and biomatter systems. Their contribution to the elucidation of the details of long-range interactions in multilamellar membrane array context is crucial and continuing (Kollmitzer *et al.*, 2015). It remains to be seen whether SAXS coupled to osmotic stress could provide also a vdW component to the interaction potential between filamentous biomolecules (Yasar *et al.*, 2015), allowing also a determination of the Hamaker coefficient that could be compared with calculations (Poudel *et al.*, 2014; Schimelman *et al.*, 2015). While the Hamaker coefficients for general proteins could be approaching solid predictions (Eifler *et al.*, 2014), their experimental determination is marred by the limitations inherent in the second virial coefficient determination of the global characteristics of the interaction potential (Prausnitz, 2015). Novel methodologies such as colloid-probe AFM could be a new potential source of valuable data on intermolecular potential (Borkovec *et al.*, 2012), including protein-protein interactions at all values of separation (Singh *et al.*, 2015).

VIII. FUTURE OUTLOOK

Casimir or vdW forces have manifestations in many parts of physics as discussed at length in this review. The quest for a fundamental understanding of these ubiquitous and subtle forces bridges concepts from condensed-matter and high-energy physics, which has become much more apparent with recent discoveries of novel materials. This field has also stimulated the development of computational methods at the atomistic level as well as larger scale with the goal of taking into account the collective and nonadditive nature of the same dispersive interaction. This particular direction has also been stimulated due to materials science expansion and better design of devices. Nevertheless, the field can become even broader with several eminent problems awaiting solutions.

Materials with Dirac spectrum hold much promise to discover new science about the vdW or Casimir interaction. Unusual behavior of the Casimir force in terms of sign, magnitude, distance dependence, and other factors has been found in graphene, TIs and CIs, as discussed in this review. But there are many new entering players with emergent properties. 2D TIs, such as HgTe/Cd/Te, Bi bilayers, and InAs/GaSb; 3D TIs, such as $Bi_{1-x}Sb_x$, Bi_2Te_3, Heusler alloys, and topological crystalline insulators, such as SnTe, $Pb_{1-x}Sn_xSe$, have prominent spin-orbit interaction, which coupled with the Dirac spectrum can lead to diverse optical response (Welding, Black-Schaffer, and Balatsky, 2014). 3D Weyl and Dirac semimetals such as Cd_3Al_2 and Na_3Bi can also be put in this category. Recent reports show that the quantum electrodynamics in Weyl semimetals results in a nontrivial response due to the associated axion field, which can lead to a repulsive Casimir interaction (Grushin, 2012; Wilson, Allocca, and Galistki, 2015). However, external electric and magnetic fields together with temperature and doping can modulate the electronic structure and optical properties by creating new topological phases, such as valley polarized materials, for example. These are yet to be studied in the context of the vdW and Casimir interactions (Rodriguez-Lopez *et al.*, 2016).

Another interesting direction to explore originates from nonlocality, especially at very small separations. For instance, at nanometric scales, the combination of structured materials, thermal as well as dielectric inhomogeneities, and nonlocal effects associated with atomic scale physics, can potentially conspire to affect fluctuation phenomena. Preliminary works studying nonlocal material effects have begun to shed light on these issues (Esquivel-Sirvent *et al.*, 2006; Despoja, Sunjic, and Marusic, 2011; Luo, Zhao, and Pendry, 2014). One promising set of scattering techniques that could be used to tackle these emerging regimes are volume-integral equation methods, related to surface-integral equations but involving volume rather than surface currents inside the bodies (Polimeridis *et al.*, 2015). Another set of techniques that are beginning to pave the way for fundamentally new designs in nanophotonics but which have yet to be exploited in Casimir computations are large-scale optimization methods (Bendsoe and Sigmund, 2003). While such brute-force explorations require careful and efficient formulations due to the large number of required calculations, the above-mentioned numerical developments offer hope that such an approach to design is within reach. Finally, although many of the interesting, nonadditive Casimir effects predicted thus far still remain out of reach of current experiments, perhaps related physical principles can be employed to discover other structures where nonmonotonicity and/or repulsion is larger and more experimentally accessible.

Transformation optics, a powerful method for solving Maxwell's equations in curvilinear coordinates (Leonhardt, 2006; Pendry, Schurig, and Smith, 2006), may offer a different perspective to the vdW and Casimir effects, especially for systems that have sizes comparable to their separation. It can be an efficient numerical approach for vdW calculations by taking into account nonlocal effects for absorption and scattering spectra, electromagnetic modes, and field enhancement. Transformation optics has been a powerful tool for optics design with applications, such as perfect lensing and cloaking (Pendry, Schurig, and Smith, 2006). Recent reports have shown interesting physical insight for vdW interactions in 3D objects with nonlocal dielectric properties (Pendry, Fernandez-Dominguez, and Zhao, 2013; Luo, Zhao, and Pendry, 2014). An exciting future direction can be to examine many of such predictions and applications in the context of vdW and Casimir interactions for new directions of control and manipulations.

We further note that fluctuation-induced phenomena go beyond the dipolar fluctuations that give rise to the vdW and Casimir forces. Charge and potential fluctuations, beyond the

situations discussed in biomaterials, may be very interesting in solid state devices. Dispersive forces of charged objects are much less studied. Systems with reduced dimensionality may be used to investigate much longer ranged monopolar fluctuation forces which can exist on their own or be entangled with the "traditional" dipolar fluctuations (Bimonte, 2007; Drosdoff *et al.*, 2016). This practically unexplored direction holds promise to expand fluctuation-induced interactions beyond dipolar excitations and further broaden the perspective of Casimir-like phenomena.

We conclude with the puzzle about the relaxation properties of conduction carriers and their role in the Lifshitz theory. As discussed in Sec. III.A, depending on the dielectric model used different magnitudes of the thermal Casimir force between metallic or magnetic systems are predicted. Some measurements show that the Drude model is in agreement with the experimental data (Sushkov *et al.*, 2011), while other reports are in favor of the plasma model (Decca *et al.*, 2005, 2007; Banishev, Chang, Klimchitskaya *et al.*, 2012; Chang *et al.*, 2012; Banishev *et al.*, 2013a, 2013b; Bimonte, López, and Decca, 2016). To date, a basic understanding of this fundamental problem in Casimir physics is still missing. More work is needed in precise measurements and calculations involving standard materials with various geometries and distance ranges by taking into account simultaneously dispersion, electrostatic effects, defects, and imperfections in the interacting objects. Another potential way to resolve this issue is to consider materials with reduced dimensions and novel phases. For example, the thermal fluctuation effects are much more prominent for graphene, which can be a possible direction to explore in this context. A different pathway could be that more sophisticated models for the response properties are needed. Nevertheless, a possible resolution to this open problem may be found by improving our understanding of materials properties.

IX. CONCLUSIONS

A broad perspective in materials and their properties was given to the field of van der Waals and Casimir interactions. This comprehensive review shows that this is a broad area where materials have played an important role in motivating the development of new theoretical models and computational approaches as well as advances in experimental techniques. Materials may hold the answers to several open problems in fluctuation-induced phenomena, which are of fundamental and applications relevance.

ACKNOWLEDGMENTS

L. M. W. acknowledges financial support from the U.S. Department of Energy under Award No. DE-FG02-06ER46297. D. A. R. D. was supported by the LANL LDRD program. A. T. thanks the European Research Council (ERC StG VDW-CMAT) for funding. P. R.-L. acknowledges financial support from People Programme (Marie Curie Actions) of the European Union's Seventh Framework Programme (No. FP7/2007-2013) under REA grant agreement No. 302005 and by project TerMic (Grant No. FIS2014-52486-R, Spanish Government) and also acknowledges helpful discussions with A. G. Grushin. A. W. R. acknowledges financial support from the U.S. National Science Foundation under Grant No. DMR-1454836. R. P. acknowledges the support of the U.S. Department of Energy, Office of Basic Energy Sciences, Division of Materials Sciences and Engineering under Award No. DE-SC0008176. R. P. thanks V. Adrian Parsegian, Roger H. French, Wai-Yim Ching, Nicole F. Steinmetz, and Jaime C. Hopkins for their input in preparing this review.

REFERENCES

Adler, S. L., 1962, Phys. Rev. **126**, 413.
Adzic, N., and R. Podgornik, 2014, Eur. Phys. J. E **37**, 49.
Adzic, N., and R. Podgornik, 2015, Phys. Rev. E **91**, 022715.
Ahlrichs, R., R. Penco, and G. Scoles, 1977, Chem. Phys. **19**, 119.
Akhmerov, A., and C. Beenakker, 2008, Phys. Rev. B **77**, 085423.
Ambrosetti, A., D. Alfe, R. A. DiStasio, Jr., and A. Tkatchenko, 2014, J. Phys. Chem. Lett. **5**, 849.
Ambrosetti, A., N. Ferri, R. A. DiStasio, Jr., and A. Tkatchenko, 2016, Science **351**, 1171.
Ambrosetti, A., A. M. Reilly, R. A. DiStasio, Jr., and A. Tkatchenko, 2014, J. Chem. Phys. **140**, 18A508.
Anderson, E., *et al.*, 1999, *LAPACK Users' Guide* (Society of Industrial and Applied Mathematics, Philadelphia), 3rd ed.
Ando, Y., 2013, J. Phys. Soc. Jpn. **82**, 102001.
Ashcroft, N. W., and N. D. Mermin, 1976, *Solid State Physics* (Holt, Reinhart & Winston, New York).
Atkins, P. R., Q. I. Dai, W. E. I. Sha, and W. C. Chew, 2013, Prog. Electromag. Research-PIER **142**, 615.
Autumn, K., and A. M. Peattie, 2002, Integr. Comp. Biol. **42**, 1081.
Autumn, K., M. Sitti, Y. A. Liang, A. M. Peattie, W. R. Hansen, S. Sponberg, T. W. Kenny, R. Fearing, J. N. Israelachvili, and R. J. Full, 2002, Proc. Natl. Acad. Sci. U.S.A. **99**, 12252.
Axilrod, B. M., and E. Teller, 1943, J. Chem. Phys. **11**, 299.
Bade, W. L., 1957, J. Chem. Phys. **27**, 1280.
Bajcsy, M., S. Hofferberth, V. Balic, T. Peyronel, M. Hafezi, A. Zibrov, V. Vuletic, and M. Lukin, 2009, Phys. Rev. Lett. **102**, 203902.
Balian, R., and B. Duplantier, 1977, Ann. Phys. (N.Y.) **104**, 300.
Balian, R., and B. Duplantier, 1978, Ann. Phys. (N.Y.) **112**, 165.
Bamidele, J., J. Brndiar, A. Gulans, L. Kantorovich, and I. Stich, 2013, J. Chem. Theory Comput. **9**, 5578.
Banishev, A. A., C.-C. Chang, R. Castillo-Garza, G. L. Klimchitskaya, V. M. Mostepanenko, and U. Mohideen, 2012, Phys. Rev. B **85**, 045436.
Banishev, A. A., C.-C. Chang, G. L. Klimchitskaya, V. M. Mostepanenko, and U. Mohideen, 2012, Phys. Rev. B **85**, 195422.
Banishev, A. A., G. L. Klimchitskaya, V. M. Mostepanenko, and U. Mohideen, 2013a, Phys. Rev. B **88**, 155410.
Banishev, A. A., G. L. Klimchitskaya, V. M. Mostepanenko, and U. Mohideen, 2013b, Phys. Rev. Lett. **110**, 137401.
Banishev, A. A., J. Wagner, T. Emig, R. Zandi, and U. Mohideen, 2013, Phys. Rev. Lett. **110**, 250403.
Banishev, A. A., J. Wagner, T. Emig, R. Zandi, and U. Mohideen, 2014, Phys. Rev. B **89**, 235436.
Banishev, A. A., H. Wen, J. Xu, R. K. Kawakami, G. L. Klimchitskaya, V. M. Mostepanenko, and U. Mohideen, 2013, Phys. Rev. B **87**, 205433.
Barash, Y. S., 1973, Izv. Vyssh. Uchebn. Zaved., Radiofiz. **16**, 1227.
Barash, Y. S., 1978, Izv. Vyssh. Uchebn. Zaved., Radiofiz. **21**, 1138.
Barash, Y. S., and V. L. Ginsburg, 1984, Sov. Phys. Usp. **27**, 467.

Barash, Y. S., and A. A. Kyasov, 1989, Sov. Phys. JETP **68**, 39.
Bartolo, D., and J. B. Fournier, 2003, Eur. Phys. J. E **11**, 141.
Barton, G., 1999, J. Phys. A **32**, 525.
Bar-Ziv, R., and S. A. Safran, 1993, Langmuir **9**, 2786.
Basov, D. N., M. M. Fogler, A. Lanzara, F. Wang, and Y. Zhang, 2014, Rev. Mod. Phys. **86**, 959.
Bay, S., P. Lambropoulos, and K. Mølmer, 1997, Phys. Rev. A **55**, 1485.
Behunin, R. O., *et al.*, 2014, Phys. Rev. A **90**, 062115.
Benali, A., L. Shulenburger, N. A. Romero, J. Kim, and O. A. von Lilienfel, 2014, J. Chem. Theory Comput. **10**, 3417.
Bender, H., C. Stehle, C. Zimmermann, S. Slama, J. Fiedler, S. Scheel, S. Y. Buhmann, and V. N. Marachevsky, 2014, Phys. Rev. X **4**, 011029.
Bendsoe, M. P., and O. Sigmund, 2003, *Topology Optimization* (Springer-Verlag, Berlin).
Benedict, L. X., N. G. Chopra, M. L. Cohen, A. Zettl, S. G. Louie, and V. H. Crespi, 1998, Chem. Phys. Lett. **286**, 490.
Ben-Yaakov, D., Y. Burak, D. Andelman, and S. A. Safran, 2007, Europhys. Lett. **79**, 48002.
Bergstrom, L., 1997, Adv. Colloid Interface Sci. **70**, 125.
Bergstrom, L., S. Stemme, T. Dahlfors, H. Arwin, and L. Odberg, 1999, Cellulose **6**, 1.
Bezerra, V. B., G. L. Klimchitskaya, U. Mohideen, V. M. Mostepanenko, and C. Romero, 2011, Phys. Rev. B **83**, 075417.
Bezerra, V. B., G. L. Klimchitskaya, V. M. Mostepanenko, and C. Romero, 2004, Phys. Rev. A **69**, 022119.
Bimonte, G., 2007, New J. Phys. **9**, 281.
Bimonte, G., 2009, Phys. Rev. A **79**, 042107.
Bimonte, G., 2014a, Phys. Rev. Lett. **113**, 240405.
Bimonte, G., 2014b, Phys. Rev. Lett. **112**, 240401.
Bimonte, G., 2015, Phys. Rev. B **91**, 205443.
Bimonte, G., T. Emig, R. L. Jaffe, and M. Kardar, 2012, Europhys. Lett. **97**, 50001.
Bimonte, G., D. López, and R. S. Decca, 2016, Phys. Rev. B **93**, 184434.
Bishop, K. J. M., C. E. Wilmer, S. Soh, and B. A. Grzybowski, 2009, Small **5**, 1600.
Bitbol, A.-F., A. Canaguier-Durand, A. Lambrecht, and S. Reynaud, 2013, Phys. Rev. B **87**, 045413.
Bitbol, A.-F., P. G. Dommersnes, and J.-B. Fournier, 2010, Phys. Rev. E **81**, 050903(R).
Blagov, E. V., G. L. Klimchitskaya, and V. M. Mostepanenko, 2005, Phys. Rev. B **71**, 235401.
Blagov, E. V., G. L. Klimchitskaya, and V. M. Mostepanenko, 2007, Phys. Rev. B **75**, 235413.
Blocki, J., J. Randrup, W. J. Swiatecki, and C. F. Tsang, 1977, Ann. Phys. (N.Y.) **105**, 427.
Bohm, D., and D. Pines, 1953, Phys. Rev. **92**, 609.
Bondarev, I. V., and P. Lambin, 2004, Solid State Commun. **132**, 203.
Bondarev, I. V., and P. Lambin, 2005, Phys. Rev. B **72**, 035451.
Bonnet, M., 1999, *Boundary Integral Equation Methods for Solids and Fluids* (Wiley, Chichester, England).
Bordag, M., 2006, Phys. Rev. D **73**, 125018.
Bordag, M., I. V. Fialkovsky, D. M. Gitman, and D. V. Vassilevich, 2009, Phys. Rev. B **80**, 245406.
Bordag, M., B. Geyer, G. Klimchitskaya, and V. M. Mostepanenko, 2006, Phys. Rev. B **74**, 205431.
Bordag, M., B. Geyer, G. L. Klimchitskaya, and V. M. Mostepanenko, 2000, Phys. Rev. Lett. **85**, 503.
Bordag, M., and N. R. Khusnutdinov, 2008, Phys. Rev. D **77**, 085026.
Bordag, M., G. L. Klimchitskaya, U. Mohideen, and V. M. Mostepanenko, 2009, *Advances in the Casimir effect* (Oxford University Press, Oxford, UK).
Bordag, M., G. L. Klimchitskaya, and V. M. Mostepanenko, 2012, Phys. Rev. B **86**, 165429.
Bordag, M., G. L. Klimchitskaya, V. M. Mostepanenko, and V. M. Petrov, 2015, Phys. Rev. D **91**, 045037.
Bordag, M., U. Mohideen, and V. M. Mostepanenko, 2001, Phys. Rep. **353**, 1.
Bordag, M., and D. V. Vassilevich, 2000, Phys. Lett. A **268**, 75.
Borkovec, M., B. Jonsson, and G. J. M. Koper, 2001, Surf. Colloid Sci. **16**, 99.
Borkovec, M., I. Szilagyi, I. Popa, M. Finessi, P. Sinha, P. Maroni, and G. Papastavrou, 2012, Adv. Colloid Interface Sci. **179–182**, 85.
Boström, M., V. Deniz, G. Franks, and B. W. Ninham, 2006, Adv. Colloid Interface Sci. **123–126**, 5.
Boström, M., and B. Ninham, 2006, Colloids Surf. A **291**, 24.
Boström, M., and B. E. Sernelius, 2000, Phys. Rev. Lett. **84**, 4757.
Boström, M., and B. E. Sernelius, 2012, Phys. Rev. A **85**, 012508.
Boström, M., F. W. Tavares, S. Finet, F. Skouri-Panet, A. Tardieu, and B. W. Ninham, 2005, Biophys. Chem. **117**, 217.
Boyd, J. P., 2001, *Chebychev and Fourier Spectral Methods* (Dover, New York), 2nd ed.
Boyer, T. H., 1968, Phys. Rev. **174**, 1764.
Boyer, T. H., 1974, Phys. Rev. A **9**, 2078.
Brandenburg, J. G., and S. Grimme, 2014, J. Phys. Chem. Lett. **5**, 1785.
Bressi, G., G. Carugno, R. Onofrio, and G. Ruoso, 2002, Phys. Rev. Lett. **88**, 041804.
Brevick, I., and G. Einevoll, 1988, Phys. Rev. D **37**, 2977.
Brey, L., and H. A. Fertig, 2006, Phys. Rev. B **73**, 235411.
Broer, W., G. Palasantzas, J. Knoester, and V. B. Svetovoy, 2012, Phys. Rev. B **85**, 155410.
Broer, W., G. Palasantzas, J. Knoester, and V. B. Svetovoy, 2013, Phys. Rev. B **87**, 125413.
Brown-Hayes, M., D. A. R. Davit, F. D. Mazzitelli, W. J. Kim, and R. Onofrio, 2005, Phys. Rev. A **72**, 052102.
Bučko, T., S. Lebegué, J. G. Angyan, and J. Hafner, 2014, J. Chem. Phys. **141**, 034114.
Bučko, T., S. Lebegué, J. Hafner, and J. G. Angyan, 2013a, J. Chem. Theory Comput. **9**, 4293.
Bučko, T., S. Lebegué, J. Hafner, and J. G. Angyan, 2013b, Phys. Rev. B **87**, 064110.
Buhmann, S., 2012a, *Dispersion Forces II: Many-Body Effects, Excited Atoms, Finite Temperature and Quantum Friction* (Springer-Verlag, Berlin).
Buhmann, S. Y., 2012b, *Dispersion Forces I: Macroscopic Quantum Electrodynamics and Ground-State Casimir, Casimir-Polder and van der Waals Forces* (Springer-Verlag, Berlin).
Buhmann, S. Y., L. Knöll, D.-G. Welsch, and H. T. Dung, 2004, Phys. Rev. A **70**, 052117.
Buhmann, S. Y., and D.-G. Welsch, 2007, Prog. Quantum Electron. **31**, 51.
Buks, E., and M. L. Roukes, 2001, Phys. Rev. B **63**, 033402.
Büscher, R., and T. Emig, 2004, Phys. Rev. A **69**, 062101.
Canaguier-Durand, A., P. A. M. Neto, A. Lambrecht, and S. Reynaud, 2010, Phys. Rev. Lett. **104**, 040403.
Capasso, F., J. N. Munday, D. Iannuzzi, and H. B. Chan, 2007, IEEE J. Sel. Top. Quantum Electron. **13**, 400.
Carrasco, J., A. Hodgson, and A. Michaelides, 2012, Nat. Mater. **11**, 667.
Casimir, H. B. G., 1948, Proc. K. Ned. Akad. Wet., Ser. B **51**, 793.
Casimir, H. B. G., and D. Polder, 1948, Phys. Rev. **73**, 360.

Cayssol, J., 2013, C.R. Phys. **14**, 760.
Chaichian, M., G. L. Klimchitskaya, V. M. Mostepanenko, and A. Tureanu, 2012, Phys. Rev. A **86**, 012515.
Chan, H. B., V. A. Aksyuk, R. N. Kleiman, D. J. Bishop, and F. Capasso, 2001, Science **291**, 1941.
Chan, H. B., Y. Bao, J. Zou, R. A. Cirelli, F. Klemens, W. M. Mansfield, and C. S. Pai, 2008, Phys. Rev. Lett. **101**, 030401.
Chang, C.-C., A. A. Banishev, G. L. Klimchitskaya, V. M. Mostepanenko, and U. Mohideen, 2011, Phys. Rev. Lett. **107**, 090403.
Chang, C.-C., A. A. Banishev, G. L. Klimchitskaya, V. M. Mostepanenko, and U. Mohideen, 2012, Phys. Rev. B **85**, 165443.
Charlier, J. C., X. Blase, and S. Roche, 2007, Rev. Mod. Phys. **79**, 677.
Chen, F., U. Mohideen, G. L. Klimchitskaya, and V. M. Mostepanenko, 2002, Phys. Rev. Lett. **88**, 101801.
Chen, F., U. Mohideen, G. L. Klimchitskaya, and V. M. Mostepanenko, 2005, Phys. Rev. A **72**, 020101(R).
Chen, L., and S. Wan, 2011, Phys. Rev. B **84**, 075149.
Chen, L., and S. Wan, 2012, Phys. Rev. B **85**, 115102.
Chen, X., and J. C. H. Spence, 2011, Phys. Status Solidi B **248**, 2064.
Chen, Y. L., *et al.*, 2009, Science **325**, 178.
Cheng, X., U. A. Gurkan, C. J. Dehen, M. P. Tate, H. W. Hillhouse, G. J. Simpson, and O. Akkus, 2008, Biomaterials **29**, 3278.
Chew, W. C., J. Jian-Ming, E. Michielssen, and S. Jiming, 2001, *Fast and Efficient Algorithms in Computational Electromagnetics* (Artech, Norwood, MA).
Chew, W. C., J. M. Jin, E. Michelssen, and J. M. Song, 1997, IEEE Trans. Antennas Propag. **45**, 533.
Chiu, H.-C., G. L. Klimchitskaya, V. N. Marachevsky, V. M. Mostepanenko, and U. Mohideen, 2009, Phys. Rev. B **80**, 121402(R).
Chiu, H.-C., G. L. Klimchitskaya, V. N. Marachevsky, V. M. Mostepanenko, and U. Mohideen, 2010, Phys. Rev. B **81**, 115417.
Churkin, Y. V., A. B. Fedortsov, G. L. Klimchistkaya, and V. A. Yurova, 2011, Int. J. Mod. Phys. A **26**, 3958.
Churkin, Y. V., A. B. Fedortsov, G. L. Klimchitskaya, and V. A. Yurova, 2010, Phys. Rev. B **82**, 165433.
Cole, M. W., D. Velegol, H.-Y. Kim, and A. A. Lucas, 2009, Mol. Simul. **35**, 849.
Contreras-Reyes, A. M., R. Guérout, P. A. M. Neto, D. A. R. Dalvit, A. Lambrecht, and S. Reynaud, 2010, Phys. Rev. A **82**, 052517.
Cooper, V. R., 2010, Phys. Rev. B **81**, 161104.
Cooper, V. R., L. Kong, and D. C. Langreth, 2010, Phys. Procedia **3**, 1417.
Cuervo, A., P. D. Dans, J. L. Carrascosa, M. Orozco, G. Gomila, and L. Fumagalli, 2014, Proc. Natl. Acad. Sci. U.S.A. **111**, E3624.
Cysne, T., W. J. M. Kort-Kamp, D. Oliver, F. A. Pinheiro, F. S. S. Rosa, and C. Farina, 2014, Phys. Rev. A **90**, 052511.
Dagastine, R. R., D. C. Prieve, and L. R. White, 2000, J. Colloid Interface Sci. **231**, 351.
Dalvit, D. A. R., and S. K. Lamoreaux, 2009, Phys. Rev. Lett. **102**, 189304.
Dalvit, D. A. R., F. C. Lombardo, F. D. Mazzitelli, and R. Onofrio, 2006, Phys. Rev. A **74**, 020101(R).
Dalvit, D. A. R., P. Milonni, D. Roberts, and F. S. S. Rosa, 2011, *Casimir Physics*, Lecture Notes in Physics (Springer-Verlag, Berlin/Heidelberg).
Das Sarma, S., S. Adam, E. H. Hwang, and E. Rossi, 2011, Rev. Mod. Phys. **83**, 407.
Das Sarma, S., E. Hwang, and W. Tse, 2007, Phys. Rev. B **75**, 121406.
Das Sarma, S., E. Hwang, and L. Zheng, 1996, Phys. Rev. B **54**, 8057.
David, F., 2004, *Statistical Mechanics of Membranes and Surfaces* (World Scientific, Singapore), 2nd ed.
Davids, P. S., F. Intravaia, and D. A. R. Dalvit, 2014, Opt. Express **22**, 12424.
Davids, P. S., F. Intravaia, F. S. S. Rosa, and D. A. R. Dalvit, 2010, Phys. Rev. A **82**, 062111.
Dean, D., J. Dobnikar, A. Naji, and R. Podgornik, 2014, *Electrostatics of Soft and Disordered Matter* (Pan Stanford Publishing, Singapore).
Dean, D. S., V. A. Parsegian, and R. Podgornik, 2015, J. Phys. Condens. Matter **27**, 214004.
Decca, R. S., D. Lopez, E. Fischbach, G. L. Klimchitskaya, D. E. Krause, and V. M. Mostepanenko, 2005, Ann. Phys. (Amsterdam) **318**, 37.
Decca, R. S., D. Lopez, E. Fischbach, and D. E. Krause, 2003, Phys. Rev. Lett. **91**, 050402.
Decca, R. S., D. Lopez, G. L. Klimchitskaya, and V. M. Mostepanenko, 2007, Phys. Rev. D **75**, 077101.
de Man, S., K. Heeck, and D. Iannuzzi, 2010, Phys. Rev. A **82**, 062512.
de Man, S., K. Heeck, R. J. Wijngaarden, and D. Iannuzzi, 2009, Phys. Rev. Lett. **103**, 040402.
Demery, V., D. S. Dean, and R. Podgornik, 2012, J. Chem. Phys. **137**, 174903.
Deserno, M., 2015, Chem. Phys. Lipids **185**, 11.
Despoja, V., M. Sunjic, and L. Marusic, 2007, Phys. Rev. B **75**, 045422.
Despoja, V., M. Sunjic, and L. Marusic, 2011, Phys. Rev. B **83**, 165421.
Dillon, A. C., K. M. Jones, T. A. Bekkedahl, C. H. Kiang, D. S. Bethune, and M. J. Heben, 1997, Nature (London) **386**, 377.
Dion, M., H. Rydberg, E. Schröder, D. C. Langreth, and B. I. Lundqvist, 2004, Phys. Rev. Lett. **92**, 246401.
DiStasio, Jr., R. A., V. V. Gobre, and A. Tkatchenko, 2014, J. Phys. Condens. Matter **26**, 213202.
DiStasio, Jr., R. A.,, O. A. von Lilienfeld, and A. Tkatchenko, 2012, Proc. Natl. Acad. Sci. U.S.A. **109**, 14791.
Dobson, J. F., 2011, Surf. Sci. **605**, 1621.
Dobson, J. F., and P. B. Dinte, 1996, Phys. Rev. Lett. **76**, 1780.
Dobson, J. F., and T. Gould, 2012, J. Phys. Condens. Matter **24**, 073201.
Dobson, J. F., T. Gould, and I. Klich, 2009, Phys. Rev. A **80**, 012506.
Dobson, J. F., T. Gould, and G. Vignale, 2014, Phys. Rev. X **4**, 021040.
Dobson, J. F., A. White, and A. Rubio, 2006, Phys. Rev. Lett. **96**, 073201.
Dommersnes, P. G., and J.-B. Fournier, 1999a, Europhys. Lett. **46**, 256.
Dommersnes, P. G., and J.-B. Fournier, 1999b, Eur. Phys. J. B **12**, 9.
Donchev, A. G., 2006, J. Chem. Phys. **125**, 074713.
Dresselhaus, M. S., G. Dresselhaus, R. Saito, and A. Jorio, 2007, Annu. Rev. Phys. Chem. **58**, 719.
Drosdoff, D., I. V. Bondarev, A. Widom, R. Podgornik, and L. M. Woods, 2016, Phys. Rev. X (to be published).
Drosdoff, D., A. D. Phan, L. M. Woods, I. V. Bondarev, and J. F. Dobson, 2012, Eur. Phys. J. B **85**, 365.
Drosdoff, D., and L. M. Woods, 2010, Phys. Rev. B **82**, 155459.
Drosdoff, D., and L. M. Woods, 2011, Phys. Rev. A **84**, 062501.
Drosdoff, D., and L. M. Woods, 2014, Phys. Rev. Lett. **112**, 025501.

Dryden, D. M., J. C. Hopkins, L. K. Denoyer, L. Poudel, N. F. Steinmetz, W.-Y. Ching, R. Podgornik, V. A. Parsegian, and R. H. French, 2015, Langmuir **31**, 10145.
Dzyaloshinskii, I., E. Lifshitz, and L. Pitaevskii, 1961, Adv. Phys. **10**, 165.
Ebbesen, T., H. Lezec, H. Ghaemi, T. Thio, and P. Wolff, 1998, Nature (London) **391**, 667.
Eberlein, C., and R. Zi, 2011, Phys. Rev. A **83**, 052514.
Eberlein, C., and R. Zi, 2012, Phys. Rev. A **86**, 062507.
Eckhardt, W., 1984, Phys. Rev. A **29**, 1991.
Edwards, S. A., and D. R. M. Williams, 2004, Phys. Rev. Lett. **92**, 248303.
Edwards, S. F., and A. Lenard, 1962, J. Math. Phys. (N.Y.) **3**, 778.
Eifler, J., P. Rulis, R. Tai, and W.-Y. Ching, 2014, Polymers **6**, 491.
Elbaum, M., and M. Schick, 1991, Phys. Rev. Lett. **66**, 1713.
Ellingsen, S., S. Y. Buhmann, and S. Scheel, 2010, Phys. Rev. A **82**, 032516.
Elstner, M., and P. Hobza, 2001, J. Chem. Phys. **114**, 5149.
Emig, T., 2003, Europhys. Lett. **62**, 466.
Emig, T., **2008**, J. Stat. Mech., P04007.
Emig, T., N. Graham, L. R. Jaffe, and M. Kardar, 2009, Phys. Rev. A **79**, 054901.
Emig, T., N. Graham, R. L. Jaffe, and M. Kardar, 2007, Phys. Rev. Lett. **99**, 170403.
Emig, T., A. Hanke, R. Golestanian, and M. Kardar, 2003, Phys. Rev. A **67**, 022114.
Emig, T., R. L. Jaffe, M. Kardar, and A. Scardicchio, 2006, Phys. Rev. Lett. **96**, 080403.
Esquivel-Sirvent, R., G. H. Cocoletzi, and M. Palomino-Ovando, 2010, J. Appl. Phys. **108**, 114101.
Esquivel-Sirvent, R., and G. C. Schatz, 2013, J. Phys. Chem. C **117**, 5492.
Esquivel-Sirvent, R., C. Villareal, W. L. Mochan, A. M. Contreras-Reyes, and V. B. Svetovoy, 2006, J. Phys. A **39**, 6323.
Essin, A., J. Moore, and D. Vanderbilt, 2009, Phys. Rev. Lett. **102**, 146805.
Falkovsky, L. A., and A. A. Varlamov, 2007, Eur. Phys. J. B **56**, 281.
Farnum, M., and C. Zukoski, 1999, Biophys. J. **76**, 2716.
Feiler, A. A., L. Bergstrom, and M. W. Rutland, 2008, Langmuir **24**, 2274.
Fernari, R., S. Scheel, and P. L. Knight, 2007, Phys. Rev. A **75**, 062905.
Fetter, A., and J. Walecka, 1971, *Quantum Theory of Many-particle Systems* (McGraw Hill, San Francisco).
Fialkovsky, I. V., V. N. Marachevsky, and D. V. Vassilevich, 2011, Phys. Rev. B **84**, 035446.
Fleck, C. C., and R. R. Netz, 2007, Eur. Phys. J. E **22**, 261.
Ford, L. H., 1993, Phys. Rev. A **48**, 2962.
Fosco, C. D., F. C. Lombardo, and F. D. Mazzitelli, 2012, Phys. Rev. D **85**, 125037.
Foulkes, W. M. C., L. Mitáš, R. J. Needs, and G. Rajagopal, 2001, Rev. Mod. Phys. **73**, 33.
Freitag, M., T. Low, W. J. Zhu, H. G. Yan, F. N. Xia, and P. Avouris, 2013, Nat. Commun. **4**, 1951.
French, R. H., *et al.*, 2010, Rev. Mod. Phys. **82**, 1887.
Freund, L. B., 2013, Proc. Natl. Acad. Sci. U.S.A. **110**, 2047.
Freysoldt, C., B. Grabowski, T. Hickel, J. Neugebauer, G. Kresse, A. Janotti, and C. G. Van de Walle, 2014, Rev. Mod. Phys. **86**, 253.
Gangadharaiah, S., A. Farid, and A. M. Mishchenko, 2008, Phys. Rev. Lett. **100**, 166802.
Gao, W., and A. Tkatchenko, 2013, Phys. Rev. Lett. **111**, 045501.
Garcia-Vidal, F. J., L. Martín-Moreno, and J. B. Pendry, 2005, J. Opt. A **7**, S97.
Garrett, J. L., D. Somers, and J. N. Munday, 2015, J. Phys. Condens. Matter **27**, 214012.
Geim, A. K., and I. V. Grigorieva, 2013, Nature (London) **499**, 419.
Gell-Mann, M., and K. A. Brueckner, 1957, Phys. Rev. **106**, 364.
Genet, C., A. Lambrecht, and S. Reynaud, 2003, Phys. Rev. A **67**, 043811.
Gerlach, E., 1971, Phys. Rev. B **4**, 393.
Geyer, B., G. L. Klimchitskaya, and V. M. Mostepanenko, 2005, Phys. Rev. D **72**, 085009.
Geyer, B., G. L. Klimchitskaya, and V. M. Mostepanenko, 2010, Phys. Rev. B **81**, 104101.
Gies, H., and K. Klingmuller, 2006a, Phys. Rev. Lett. **96**, 220401.
Gies, H., and K. Klingmuller, 2006b, Phys. Rev. D **74**, 045002.
Gies, H., K. Langfeld, and L. Moyaerts, **2003**, J. High Energy Phys. 6, 018.
Goban, A., K. S. Choi, D. J. Alton, D. Ding, C. Lacroute, M. Pototschnig, T. Thiele, N. P. Stern, and H. J. Kimble, 2012, Phys. Rev. Lett. **109**, 033603.
Goban, A., *et al.*, 2014, Nat. Commun. **5**, 3808.
Gobre, V. V., and A. Tkatchenko, 2013, Nat. Commun. **4**, 2341.
Golestanian, R., 2000, Phys. Rev. E **62**, 5242.
Golestanian, R., 2009, Phys. Rev. A **80**, 012519.
Golestanian, R., M. Goulian, and M. Kardar, 1996a, Phys. Rev. E **54**, 6725.
Golestanian, R., M. Goulian, and M. Kardar, 1996b, Europhys. Lett. **33**, 241.
Gómez-Santos, G., 2009, Phys. Rev. B **80**, 245424.
Goodsell, A., T. Ristroph, J. Golovchenko, and L. V. Hau, 2010, Phys. Rev. Lett. **104**, 133002.
Gould, T., J. F. Dobson, and S. Lebegué, 2013, Phys. Rev. B **87**, 165422.
Gould, T., E. Gray, and J. Dobson, 2009, Phys. Rev. B **79**, 113402.
Gould, T., S. Lebegué, and J. Dobson, 2013, J. Phys. Condens. Matter **25**, 445010.
Gould, T., K. Simpkins, and J. F. Dobson, 2008, Phys. Rev. B **77**, 165134.
Goulian, M., R. Bruinsma, and P. Pincus, 1993, Europhys. Lett. **22**, 145.
Graham, N., M. Quandt, and H. Weigel, 2009, *Spectral Methods in Quantum Field Theory* (Springer-Verlag, Berlin).
Grimme, S., 2004, J. Comput. Chem. **25**, 1463.
Grimme, S., 2006, J. Comput. Chem. **27**, 1787.
Grimme, S., 2012, Chem. Eur. J. **18**, 9955.
Grimme, S., J. Antony, S. Ehrlich, and H. Krieg, 2010, J. Chem. Phys. **132**, 154104.
Grisenti, R. E., W. Schöllkopf, J. P. Toennies, G. C. Hegerfeldt, and T. Köhler, 1999, Phys. Rev. Lett. **83**, 1755.
Grushin, A. G., 2012, Phys. Rev. D **86**, 045001.
Grushin, A. G., and A. Cortijo, 2011, Phys. Rev. Lett. **106**, 020403.
Grushin, A. G., and F. de Juan, 2012, Phys. Rev. B **86**, 075126.
Grushin, A. G., T. Neupert, C. Chamon, and C. Mudry, 2012, Phys. Rev. B **86**, 205125.
Grushin, A. G., P. Rodriguez-Lopez, and A. Cortijo, 2011, Phys. Rev. B **84**, 045119.
Guérout, R., J. Lussange, H. B. Chan, A. Lambrecht, and S. Reynaud, 2013, Phys. Rev. A **87**, 052514.
Gunnarsson, O., and B. I. Lundqvist, 1976, Phys. Rev. B **13**, 4274.
Hanson, G. W., 2008, J. Appl. Phys. **103**, 064302.
Harihara, K., M. Kociak, S. Bandow, T. Nakahara, K. Itoh, Y. Saito, and S. Iijima, 2006, Phys. Rev. B **73**, 195420.
Hasan, M. Z., and C. L. Kane, 2010, Rev. Mod. Phys. **82**, 3045.
Henkel, C., and K. Joulain, 2005, Europhys. Lett. **72**, 929.

Hepburn, J., and G. Scoles, 1975, Chem. Phys. Lett. **36**, 451.
Hertzberg, M. P., R. L. Jaffe, M. Kardar, and A. Scardicchio, 2007, Phys. Rev. D **76**, 045016.
Hollertz, R., H. Arwin, B. Faure, Y. Zhang, L. Bergstrom, and L. Wagberg, 2013, Cellul. Chem. Technol. **20**, 1639.
Holm, C., P. Kekicheff, and R. Podgornik, 2001, *Electrostatic Effects in Soft Matter and Biophysics* (Kluwer Academic, Dordrecht).
Hopkins, J. C., R. Podgornik, W.-Y. Ching, R. H. French, and V. A. Parsegian, 2015, J. Phys. Chem. C **119**, 19083.
Høye, J. S., I. Brevik, S. A. Ellingsen, and J. B. Aarseth, 2007, Phys. Rev. E **75**, 051127.
Hsu, P. Y., L. Ge, X. Li, A. Y. Stark, C. Wesdemiotis, P. H. Niewiarowski, and A. Dhinojwala, 2011, J. R. Soc. Interface **9**, 657.
Huan, T., M. Amsler, R. Sabatini, V. Tuoc, N. Le, L. Woods, N. Marzari, and S. Goedecker, 2013, Phys. Rev. B **88**, 024108.
Hung, C.-L., S. M. Meenehan, D. E. Chang, O. Painter, and H. J. Kimble, 2013, New J. Phys. **15**, 083026.
Iannuzzi, D., and F. Capasso, 2003, Phys. Rev. Lett. **91**, 029101.
Iannuzzi, D., M. Lisanti, J. N. Munday, and F. Capasso, 2005, Solid State Commun. **135**, 618.
Incardone, R., T. Fukuta, S. Tanaka, T. Petrosky, L. Rizzuto, and R. Passante, 2014, Phys. Rev. A **89**, 062117.
Intravaia, F., and R. Behunin, 2012, Phys. Rev. A **86**, 062517.
Intravaia, F., P. S. Davids, R. S. Decca, V. A. Aksyuk, D. López, and D. A. R. Dalvit, 2012, Phys. Rev. A **86**, 042101.
Intravaia, F., S. Koev, I. W. Jung, A. A. Talin, P. S. Davids, R. S. Decca, A. Aksyuk, D. A. R. Dalvit, and D. Lopez, 2013, Nat. Commun. **4**, 2515.
Intravaia, F., and A. Lambrecht, 2005, Phys. Rev. Lett. **94**, 110404.
Israelachvili, J. N., 1991, *Intermolecular and Surface Forces* (Academic Press, London).
Ito, H., T. Nakata, K. Sasaki, M. Ohtsu, K. I. Lee, and W. Jhe, 1996, Phys. Rev. Lett. **76**, 4500.
Jackson, J. D., 1998, *Classical Electrodynamics* (Wiley, New York), 3rd ed.
Jaekel, M. T., and S. Reynaud, 1991, J. Phys. I (France) **1**, 1395.
Jeonga, H. E., and K. Y. Suh, 2009, Nano Today **4**, 335.
Jin, J., 2002, *The Finite Element Method in Electromagnetics* (Wiley, New York), 2nd ed.
Jin, M. H., X. J. Feng, L. Feng, T. L. Sun, J. Zhai, T. J. Li, and L. Jiang, 2005, Adv. Mater. **17**, 1977.
Joannopoulos, J. D., S. G. Johnson, J. N. Winn, and R. Meade, 2008, *Photonic Crystals: Molding the Flow of Light* (Princeton University Press, Princeton, NJ).
John, S., 1987, Phys. Rev. Lett. **58**, 2486.
Johnson, E. R., and A. D. Becke, 2005, J. Chem. Phys. **123**, 024101.
Judd, T., R. Scott, A. Martin, B. Kaczmarek, and T. Fromhold, 2011, New J. Phys. **13**, 083020.
Jurecka, P., J. Sponer, J. Cerny, and P. Hobza, 2006, Phys. Chem. Chem. Phys. **8**, 1985.
Kaltak, M., J. Klimeś, and G. Kresse, 2014, Phys. Rev. B **90**, 054115.
Kanduc, M., M. Trulsson, A. Naji, Y. Burak, J. Forsman, and R. Podgornik, 2008, Phys. Rev. E **78**, 061105.
Kardar, M., and R. Golestanian, 1999, Rev. Mod. Phys. **71**, 1233.
Kats, E. I., 1978, Sov. Phys. JETP **47**, 1205.
Kaur, K., J. Kaur, B. Arora, and B. Sahoo, 2014, Phys. Rev. B **90**, 245405.
Kenneth, O., and I. Klich, 2006, Phys. Rev. Lett. **97**, 160401.
Kenneth, O., and I. Klich, 2008, Phys. Rev. B **78**, 014103.
Kenneth, O., I. Klich, A. Mann, and M. Revzen, 2002, Phys. Rev. Lett. **89**, 033001.
Khusnutdinov, N., R. Kashparov, and L. M. Woods, 2015, Phys. Rev. D **92**, 045002.
Khusnutdinov, N. R., D. Drosdoff, and L. M. Woods, 2014, Phys. Rev. D **89**, 085033.
Kim, W. J., A. O. Sushkov, D. A. R. Dalvit, and S. K. Lamoreaux, 2009, Phys. Rev. Lett. **103**, 060401.
Kim, W. J., A. O. Sushkov, D. A. R. Dalvit, and S. K. Lamoreaux, 2010, Phys. Rev. A **81**, 022505.
Kirkwood, J., and J. Shumaker, 1952, Proc. Natl. Acad. Sci. U.S.A. **38**, 863.
Kitaev, A., 2009, AIP Conf. Proc. **1134**, 22.
Kittel, C., 1986, *Introduction to Solid State Physics* (Wiley, New York), 6th ed.
Klich, K., and O. Kenneth, 2009, J. Phys. Conf. Ser. **161**, 012020.
Klimchitskaya, G. L., E. V. Blagov, and V. M. Mostepanenko, 2008, J. Phys. A **41**, 164012.
Klimchitskaya, G. L., U. Mohideen, and V. M. Mostepananko, 2009, Rev. Mod. Phys. **81**, 1827.
Klimchitskaya, G. L., U. Mohideen, and V. M. Mostepanenko, 2000, Phys. Rev. A **61**, 062107.
Klimchitskaya, G. L., U. Mohideen, and V. M. Mostepanenko, 2014, Phys. Rev. B **89**, 115419.
Klimchitskaya, G. L., and V. M. Mostepanenko, 2013, Phys. Rev. B **87**, 075439.
Klimchitskaya, G. L., and V. M. Mostepanenko, 2014, Phys. Rev. A **89**, 052512.
Klimchitskaya, G. L., and V. M. Mostepanenko, 2015a, Phys. Rev. A **92**, 042109.
Klimchitskaya, G. L., and V. M. Mostepanenko, 2015b, Phys. Rev. B **91**, 045412.
Klimchitskaya, G. L., V. M. Mostepanenko, and B. E. Sernelius, 2014, Phys. Rev. B **89**, 125407.
Klimeš, J., D. R. Bowler, and A. Michaelides, 2010, J. Phys. Condens. Matter **22**, 022201.
Klimeš, J., D. R. Bowler, and A. Michaelides, 2011, Phys. Rev. B **83**, 195131.
Klimeš, J., and A. Michaelides, 2012, J. Chem. Phys. **137**, 120901.
Koide, A., 1976, J. Phys. B **9**, 3173.
Kollmitzer, B., P. Heftberger, R. Podgornik, J. F. Nagle, and G. Pabst, 2015, Biophys. J. **108**, 2833.
Kornilovitch, P. E., 2013, J. Phys. Condens. Matter **25**, 035102.
Korolev, K. S., and D. R. Nelson, 2008, Phys. Rev. E **77**, 051702.
Kotov, V. N., B. Uchoa, V. M. Pereira, F. Guinea, and A. H. Castro Neto, 2012, Rev. Mod. Phys. **84**, 1067.
Kronik, L., and A. Tkatchenko, 2014, Acc. Chem. Res. **47**, 3208.
Kuzmenko, A., E. van Heumen, F. Carbone, and D. van der Marel, 2008, Phys. Rev. Lett. **100**, 117401.
Lambrecht, A., M.-T. Jaekel, and S. Reynaud, 1997, Phys. Lett. A **225**, 188.
Lambrecht, A., P. A. Maia Neto, and S. Reynaud, 2006, New J. Phys. **8**, 243.
Lambrecht, A., P. A. Maia Neto, and S. Reynaud, 2008, J. Phys. A **41**, 164004.
Lambrecht, A., and V. N. Marachevsky, 2008, Phys. Rev. Lett. **101**, 160403.
Lamoreaux, S. K., 1997, Phys. Rev. Lett. **78**, 5.
Lamoreaux, S. K., 2005, Rep. Prog. Phys. **68**, 201.
Langreth, D. C., and J. P. Perdew, 1977, Phys. Rev. B **15**, 2884.
Lau, A. W. C., D. B. Lukatsky, P. Pincus, and S. A. Safran, 2001, Phys. Rev. E **64**, 031507.
Lau, A. W. C., D. B. Lukatsky, P. Pincus, and S. A. Safran, 2002, Phys. Rev. E **65**, 051502.
Lau, A. W. C., and P. Pincus, 1999, Eur. Phys. J. B **10**, 175.

Lau, A. W. C., and P. Pincus, 2002, Phys. Rev. E **66**, 041501.
Lebegué, S., J. Harl, T. Gould, J. G. Angyan, G. Kresse, and J. F. Dobson, 2010, Phys. Rev. Lett. **105**, 196401.
Leckband, D., and J. Israelachvili, 2001, Q. Rev. Biophys. **34**, 105.
Leckband, D., and S. Sivasankar, 1999, Colloids Surf. B **14**, 83.
Lee, K., E. D. Murray, L. Kong, B. I. Lundqvist, and D. C. Langreth, 2010, Phys. Rev. B **82**, 081101(R).
Lee, M., 2014, *Remarkable Natural Material Surfaces and Their Engineering Potential* (Springer International Publishing, Switzerland).
Lee, S., and W. M. Sigmund, 2001, J. Colloid Interface Sci. **243**, 365.
Lee, S., and W. M. Sigmund, 2002, Colloids Surf. A **204**, 43.
Leek, P. J., J. M. Fink, A. Blais, R. Bianchetti, M. Goepl, J. M. Gambetta, D. I. Schuster, L. Frunzio, R. J. Schoelkopf, and A. Wallraff, 2007, Science **318**, 1889.
Leonhardt, U., 2006, Science **312**, 1777.
Leonhardt, U., and T. G. Philbin, 2007, New J. Phys. **9**, 254.
Levin, M., A. P. McCauley, A. W. Rodriguez, M. T. Homer Reid, and S. G. Johnson, 2010, Phys. Rev. Lett. **105**, 090403.
Li, L., C. Li, Z. Zhang, and E. Alexov, 2013, J. Chem. Theory Comput. **9**, 2126.
Li, L.-W., M.-S. Leong, T.-S. Yeo, and P.-S. Kooi, 2000, J. Electromagn. Waves Appl. **14**, 961.
Li, Z. Q., E. A. Henriksen, Z. Jian, Z. Hao, M. C. Martin, P. Kim, H. L. Stormer, and D. S. Basov, 2008, Nat. Phys. **4**, 532.
Lifshitz, E. M., 1956, Sov. Phys. JETP **2**, 73.
Lifshitz, E. M., and L. P. Pitaevskii, 1980, *Statistical Physics* (Pergamon, Oxford), Pt. 2.
Lin, H.-K., R. Zandi, U. Mohideen, and L. P. Pryadko, 2011, Phys. Rev. Lett. **107**, 228104.
Lipowsky, R., 1991, Nature (London) **349**, 475.
Liu, C.-X., X.-L. Qi, H.-J. Zhang, X. Dai, Z. Fang, and S.-C. Zhang, 2010, Phys. Rev. B **82**, 045122.
Liu, M., X. Yin, E. Ulin-Avila, B. Geng, T. Zentgraf, J. Long, F. Wang, and X. Zhang, 2011, Nature (London) **474**, 64.
Liu, R.-F., J. G. Angyan, and J. F. Dobson, 2011, J. Chem. Phys. **134**, 114106.
Liu, W., J. Carrasco, B. Santra, A. Michaelides, M. Scheffler, and A. Tkatchenko, 2012, Phys. Rev. B **86**, 245405.
Liu, W., S. N. Filimonov, J. Carrasco, and A. Tkatchenko, 2013, Nat. Commun. **4**, 2569.
Liu, W., A. Tkatchenko, and M. Scheffler, 2014, Acc. Chem. Res. **47**, 3369.
London, F., 1930, Z. Phys. Chem., Abt. B **11**, 222.
Loskill, P., H. Hahl, T. Faidt, S. Grandthyll, F. Muller, and K. Jacobs, 2012, Adv. Colloid Interface Sci. **179–182**, 107.
Loskill, P., J. Puthoff, M. Wilkinson, K. Mecke, K. Jacobs, and K. Autumn, 2012, J. R. Soc. Interface **10**, 20120587.
Lu, B.-S., A. Naji, and R. Podgornik, 2015, J. Chem. Phys. **142**, 214904.
Lu, B.-S., and R. Podgornik, 2015, Phys. Rev. E **92**, 022112.
Lu, B.-S., and R. Podgornik, 2016, J. Chem. Phys. **145**, 044707.
Lund, M., and B. Jonsson, 2013, Q. Rev. Biophys. **46**, 265.
Luo, Y., R. Zhao, and J. B. Pendry, 2014, Proc. Natl. Acad. Sci. U.S.A. **111**, 18422.
Ma, L., J. Wang, and F. Ding, 2013, ChemPhysChem **14**, 47.
Machta, B. B., S. L. Veatch, and J. P. Sethna, 2012, Phys. Rev. Lett. **109**, 138101.
Maggs, A. C., and R. Podgornik, 2014, Europhys. Lett. **108**, 68003.
Maghrebi, M. F., S. J. Rahi, T. Emig, N. Graham, R. L. Jaffe, and M. Kardar, 2011, Proc. Natl. Acad. Sci. U.S.A. **108**, 6867.
Mahanty, J., and B. Ninham, 1976, *Dispersion Forces* (Academic Press, London).
Maia Neto, P. A., A. Lambrecht, and S. Reynaud, 2008, Phys. Rev. A **78**, 012115.
Maier, S. A., 2007, *Plasmonics: Fundamentals and Applications* (Springer, New York).
Markovich, T., D. Andelman, and R. Podgornik, 2014, Europhys. Lett. **106**, 16002.
Marom, N., R. A. DiStasio, Jr., V. Atalla, S. Levchenko, A. M. Reilly, J. R. Chelikowsky, L. Leiserowitz, and A. Tkatchenko, 2013, Angew. Chem., Int. Ed. Engl. **52**, 6629.
Martinez, J., and M. Jalil, 2013, J. Appl. Phys. **113**, 204302.
Mayer, J. E., 1933, J. Chem. Phys. **1**, 270.
Mazzitelli, F. D., D. A. R. Dalvit, and F. C. Lombardo, 2006, New J. Phys. **8**, 240.
McCauley, A. P., A. W. Rodriguez, J. D. Joannopoulos, and S. G. Johnson, 2010, Phys. Rev. A **81**, 012119.
McCauley, A. P., A. W. Rodriguez, M. T. H. Reid, and S. G. Johnson, 2011, arXiv:1105.0404.
McCauley, A. P., F. S. S. Rosa, A. W. Rodriguez, J. D. Joannopoulos, D. A. R. Dalvit, and S. G. Johnson, 2011, Phys. Rev. A **83**, 052503.
McCauley, A. P., R. Zhao, M. T. H. Reid, A. W. Rodriguez, J. Zhou, F. S. S. Rosa, J. D. Joannopoulos, D. A. R. Dalvit, C. M. Soukoulis, and S. G. Johnson, 2010, Phys. Rev. B **82**, 165108.
Messina, R., D. A. R. Dalvit, P. A. M. Neto, A. Lambrecht, and S. Reynaud, 2009, Phys. Rev. A **80**, 022119.
Messina, R., P. A. Maia Neto, B. Guizal, and M. Antezza, 2015, Phys. Rev. A **92**, 062504.
Meurk, A., P. F. Luckham, and L. Bergstrom, 1997, Langmuir **13**, 3896.
Mikhailov, S. A., and K. Ziegler, 2007, Phys. Rev. Lett. **99**, 016803.
Milling, A., P. Mulvaney, and I. Larson, 1996, J. Colloid Interface Sci. **180**, 460.
Milonni, P. W., 1993, *The Quantum Vacuum: An Introduction to Quantum Electrodynamics* (Academic Press, San Diego).
Milton, K. A., 2004, J. Phys. A **37**, R209.
Milton, K. A., E. K. Abalo, P. Parashar, and N. Pourtolami, 2011, Phys. Rev. A **83**, 062507.
Milton, K. A., E. K. Abalo, P. Parashar, N. Pourtolami, I. Brevik, and S. Ellingsen, 2012, J. Phys. A **45**, 374006.
Milton, K. A., L. L. DeRaad, Jr., and J. Schwinger, 1978, Ann. Phys. (N.Y.) **115**, 388.
Milton, K. A., P. Parashar, and J. Wagner, 2008, Phys. Rev. Lett. **101**, 160402.
Milton, K. A., P. Parashar, J. Wagner, and C. Pelaez, 2010, J. Vac. Sci. Technol. B **28**, C4A8.
Milton, K. A., and J. Wagner, 2008, J. Phys. A **41**, 155402.
Milton, K. A., J. Wagner, P. Parashar, and I. Brevik, 2010, Phys. Rev. D **81**, 065007.
Mintmire, J., B. I. Dunlap, and C. T. White, 1992, Phys. Rev. Lett. **68**, 631.
Misquitta, A. J., R. Maezono, N. D. Drummond, A. J. Stone, and R. Needs, 2014, Phys. Rev. B **89**, 045140.
Misquitta, A. J., J. Spencer, A. J. Stone, and A. Alavi, 2010, Phys. Rev. B **82**, 075312.
Mochan, W. L., and C. Villarreal, 2006, New J. Phys. **8**, 242.
Modrzejewski, M., G. Chałasinski, and M. M. Szczesniak, 2014, J. Chem. Theory Comput. **10**, 4297.
Moellmann, J., S. Ehrlich, R. Tonner, and S. Grimme, 2012, J. Phys. Condens. Matter **24**, 424206.
Mohideen, U., and A. Roy, 1998, Phys. Rev. Lett. **81**, 4549.
Moreno, G. A., D. A. R. Dalvit, and E. Calzetta, 2010, New J. Phys. **12**, 033009.

Moreno, G. A., R. Messina, D. A. R. Dalvit, A. Lambrecht, P. A. Maia Neto, and S. Reynaud, 2010, Phys. Rev. Lett. **105**, 210401.
Munday, J., F. Capasso, and V. A. Parsegian, 2009, Nature (London) **457**, 170.
Munday, J. N., and F. Capasso, 2007, Phys. Rev. A **75**, 060102(R).
Munday, J. N., D. Iannuzzi, Y. Barash, and F. Capasso, 2005, Phys. Rev. A **71**, 042102; **78**, 029906(E) (2008).
Nair, R. R., P. Blake, A. N. Grogorenko, K. S. Novoselov, T. J. Booth, T. Stauber, N. M. R. Peres, and A. K. Geim, 2008, Science **320**, 1308.
Naji, A., M. Kandu, J. Forsman, and R. Podgornik, 2013, J. Chem. Phys. **139**, 150901.
Nandi, N., K. Bhattacharyya, and B. Bagchi, 2000, Chem. Rev. **100**, 2013.
Narayanaswamy, A., and Y. Zheng, 2013, Phys. Rev. A **88**, 012502.
Neal, B. L., D. Asthagiri, and A. M. Lenhoff, 1998, Biophys. J. **75**, 2469.
Nel, A. E., L. Maedler, D. Velegol, T. Xia, E. M. V. Hoek, P. Somasundaran, F. Klaessig, V. Castranova, and M. Thompson, 2009, Nat. Mater. **8**, 543.
Neto, A. H. C., F. Guinea, N. M. R. Peres, K. S. Novoselov, and A. K. Geim, 2009, Rev. Mod. Phys. **81**, 109.
Netz, R. R., 1997, J. Phys. I (France) **7**, 833.
Netz, R. R., 2001a, Eur. Phys. J. E **5**, 557.
Netz, R. R., 2001b, Eur. Phys. J. E **5**, 189.
Netz, R. R., and H. Orland, 2000, Eur. Phys. J. E **1**, 203.
Neveau, D. M. L., R. P. Rand, V. A. Parsegian, and D. Gingell, 1977, Biophys. J. **18**, 209.
Nie, S., and S. Emory, 1997, Science **275**, 1102.
Nie, W., R. Zeng, Y. Lan, and S. Zhu, 2013, Phys. Rev. B **88**, 085421.
Ninham, B. W., and V. A. Parsegian, 1970, Biophys. J. **10**, 646.
Noruzifar, E., T. Emig, U. Mohideen, and R. Zandi, 2012, Phys. Rev. B **86**, 115449.
Noruzifar, E., T. Emig, and R. Zandi, 2011, Phys. Rev. A **84**, 042501.
Noruzifar, E., J. Wagner, and R. Zandi, 2013, Phys. Rev. E **88**, 042314.
Noto, A., R. Messina, B. Guizal, and M. Antezza, 2014, Phys. Rev. A **90**, 022120.
Novoselov, K. S., A. K. Geim, S. V. Morozov, D. Jiang, Y. Zhang, S. V. Dubonos, I. V. Grigorieva, and A. Firsov, 2004, Science **306**, 666.
Oberst, H., D. Kouznetsov, K. Shimizu, J. Fujita, and F. Shimizu, 2005, Phys. Rev. Lett. **94**, 013203.
Obrecht, J. M., R. J. Wild, M. Antezza, L. P. Pitaevskii, S. Stringari, and E. A. Cornell, 2007, Phys. Rev. Lett. **98**, 063201.
Oskooi, A. F., D. Roundy, M. Ibanescu, P. Bermel, J. D. Joannopoulos, and S. G. Johnson, 2010, Comput. Phys. Commun. **181**, 687.
Otero-de-la Roza, A., and E. R. Johnson, 2012, J. Chem. Phys. **137**, 054103.
Otero-de-la Roza, A., and E. R. Johnson, 2013, J. Chem. Phys. **138**, 054103.
Ouvrard, C., and S. L. Price, 2004, Cryst. Growth Des. **4**, 1119.
Park, J. M., and T. C. Lubensky, 1996, J. Phys. I (France) **6**, 1217.
Parsegian, V. A., 2006, *Van der Waals Forces: A Handbook for Biologists, Chemists, Engineers, and Physicists* (Cambridge University Press, Cambridge, England).
Parsegian, V. A., and B. W. Ninham, 1969, Nature (London) **224**, 1197.
Parsegian, V. A., and Ninham, B. W., 1970, Biophys. J. **10**, 664.
Parsegian, V. A., and G. H. Weiss, 1972, J. Adhes. **3**, 259.
Pasichnyk, I., R. Everaers, and A. C. Maggs, 2008, J. Phys. Chem. B **112**, 1761.
Pasquali, S., and A. C. Maggs, 2008, J. Chem. Phys. **129**, 014703.
Pasquali, S., and A. C. Maggs, 2009, Phys. Rev. A **79**, 020102(R).
Pasquini, T. A., M. Saba, G.-B. Jo, Y. Shin, W. Ketterle, D. E. Pritchard, T. A. Savas, and N. Mulders, 2006, Phys. Rev. Lett. **97**, 093201.
Peccei, R., and H. Quinn, 1977, Phys. Rev. Lett. **38**, 1440.
Pendry, J. B., A. I. Fernandez-Dominguez, and R. Zhao, 2013, Nat. Phys. **9**, 518.
Pendry, J. B., A. J. Holden, D. J. Robbins, and W. J. Stewart, 1999, IEEE Trans. Microwave Theory Tech. **47**, 2075.
Pendry, J. B., L. Martin-Moreno, and F. J. Garcia-Vidal, 2004, Science **305**, 847.
Pendry, J. B., D. Schurig, and D. R. Smith, 2006, Science **312**, 1780.
Perdew, J. P., K. Burke, and M. Ernzerhof, 1996, Phys. Rev. Lett. **77**, 3865.
Pernice, W. H. P., M. Li, D. Garcia-Sanchez, and H. X. Tang, 2010, Opt. Express **18**, 12615.
Perreault, J. D., and A. D. Cronin, 2005, Phys. Rev. Lett. **95**, 133201.
Peterson, B., and S. Ström, 1974, Phys. Rev. D **10**, 2670.
Petrache, H. I., N. Gouliaev, S. Tristram-Nagle, R. Zhang, R. M. Suter, and J. Nagle, 1998, Phys. Rev. E **57**, 7014.
Petrache, H. I., T. Zemb, L. Belloni, and V. A. Parsegian, 2006, Proc. Natl. Acad. Sci. U.S.A. **103**, 7982.
Petrov, P., S. Machluf, S. Younis, R. Macaluso, T. David, B. Hadad, Y. Japha, M. Keil, E. Joselevich, and R. Folman, 2009, Phys. Rev. A **79**, 043403.
Phan, A. D., T. X. Hoang, T. L. Phan, and L. M. Woods, 2013, J. Chem. Phys. **139**, 184703.
Phan, A. D., L. M. Woods, D. Drosdoff, I. V. Bondarev, and N. A. Viet, 2012, Appl. Phys. Lett. **101**, 113118.
Philbin, T. G., and U. Leonhardt, 2008, Phys. Rev. A **78**, 042107.
Phillips, R., J. Kondev, and J. Theriot, 2008, *Physical Biology of the Cell* (Garland Science, New York).
Pinchuk, A., 2004, J. Quant. Spectr. & Rad. Trans. **85**, 211.
Pinchuk, A. O., and V. I. Vysotskii, 1999, Bioelectrochem. Bioenerg. **48**, 329.
Pinchuk, A. O., and V. I. Vysotskii, 2001, Phys. Rev. E **63**, 031904.
Pitaevskii, L. P., 2008, Phys. Rev. Lett. **101**, 163202.
Pitaevskii, L. P., 2009, Phys. Rev. Lett. **102**, 189302.
Podgornik, R., 1990, J. Phys. A **23**, 275.
Podgornik, R., R. H. French, and V. A. Parsegian, 2006, J. Chem. Phys. **124**, 044709.
Podgornik, R., and B. Zeks, 1988, J. Chem. Soc., Faraday Trans. 2 **84**, 611.
Polimeridis, A. G., M. T. H. Reid, S. G. Johnson, J. K. White, and A. W. Rodriguez, 2015, IEEE Trans. Antennas Propag. **63**, 611.
Popescu, A., L. M. Woods, and I. V. Bondarev, 2011, Phys. Rev. B **83**, 081406(R).
Poudel, L., P. Rulis, L. Liang, and W.-Y. Ching, 2014, Phys. Rev. E **90**, 022705.
Prausnitz, J., 2015, Biophys. J. **108**, 453.
Qi, X.-L., T. L. Hughes, and S.-C. Zhang, 2008, Phys. Rev. B **78**, 195424.
Qi, X.-L., R. Li, J. Zang, and S.-C. Zhang, 2009, Science **323**, 1184.
Qi, X.-L., and S.-C. Zhang, 2011, Rev. Mod. Phys. **83**, 1057.
Rahi, S. J., T. Emig, N. Graham, R. L. Jaffe, and M. Kardar, 2009, Phys. Rev. D **80**, 085021.
Rahi, S. J., T. Emig, and R. L. Jaffe, 2011, Lect. Notes Phys. **834**, 129.
Rahi, S. J., M. Kardar, and T. Emig, 2010, Phys. Rev. Lett. **105**, 070404.
Rahi, S. J., A. W. Rodriguez, T. Emig, R. L. Jaffe, S. G. Johnson, and M. Kardar, 2008, Phys. Rev. A **77**, 030101(R).

Rajter, R., R. H. French, W. Ching, R. Podgornik, and V. A. Parsegian, 2013, RSC Adv. **3**, 823.
Rajter, R. F., R. Podgornik, V. A. Parsegian, R. H. French, and W. Y. Ching, 2007, Phys. Rev. B **76**, 045417.
Rapcewicz, K., and N. W. Ashcroft, 1991, Phys. Rev. B **44**, 4032(R).
Rehr, J. J., E. Zaremba, and W. Kohn, 1975, Phys. Rev. B **12**, 2062.
Reid, H., J. White, and S. G. Johnson, 2011, Phys. Rev. A **84**, 010503(R).
Reid, M. T. H., 2012, http://homerreid.dyndns.org/scuff-EM/.
Reid, M. T. H., A. W. Rodriguez, and S. G. Johnson, 2013, Proc. IEEE **101**, 531.
Reid, M. T. H., A. W. Rodriguez, J. White, and S. G. Johnson, 2009, Phys. Rev. Lett. **103**, 040401.
Reid, M. T. H., J. White, and S. G. Johnson, 2013, Phys. Rev. A **88**, 022514.
Reilly, A. M., and A. Tkatchenko, 2013a, J. Chem. Phys. **139**, 024705.
Reilly, A. M., and A. Tkatchenko, 2013b, J. Phys. Chem. Lett. **4**, 1028.
Reilly, A. M., and A. Tkatchenko, 2014, Phys. Rev. Lett. **113**, 055701.
Rezac, J., K. E. Riley, and P. Hobza, 2011, J. Chem. Theory Comput. **7**, 2427.
Ribeiro, S., and S. Scheel, 2013a, Phys. Rev. A **88**, 052521.
Ribeiro, S., and S. Scheel, 2013b, Phys. Rev. A **88**, 042519.
Richardson, D. D., and J. Mahanty, 1977, J. Phys. C **10**, 3971.
Rodrigues, R. B., P. A. Maia Neto, A. Lambrecht, and S. Reynaud, 2006, Phys. Rev. Lett. **96**, 100402.
Rodriguez, A., M. Ibanescu, D. Iannuzzi, F. Capasso, J. D. Joannopoulos, and S. G. Johnson, 2007, Phys. Rev. Lett. **99**, 080401.
Rodriguez, A., M. Ibanescu, D. Iannuzzi, J. D. Joannopoulos, and S. G. Johnson, 2007, Phys. Rev. A **76**, 032106.
Rodriguez, A. W., F. Capasso, and S. G. Johnson, 2011, Nat. Photonics **5**, 211.
Rodriguez, A. W., P. C. Hui, D. N. Woolf, S. G. Johnson, M. Loncar, and F. Capasso, 2015, Ann. Phys. (Berlin) **527**, 45.
Rodriguez, A. W., J. D. Joannopoulos, and S. G. Johnson, 2008, Phys. Rev. A **77**, 062107.
Rodriguez, A. W., A. P. McCauley, J. D. Joannopoulos, and S. G. Johnson, 2009, Phys. Rev. A **80**, 012115.
Rodriguez, A. W., A. P. McCauley, D. Woolf, F. Capasso, J. D. Joannopoulos, and S. G. Johnson, 2010, Phys. Rev. Lett. **104**, 160402.
Rodriguez, A. W., J. Munday, D. Davlit, F. Capasso, J. D. Joannopoulos, and S. G. Johnson, 2008, Phys. Rev. Lett. **101**, 190404.
Rodriguez, A. W., D. Woolf, P.-C. Hui, E. Iwase, A. P. McCauley, F. Capasso, M. Loncar, and S. G. Johnson, 2011, Appl. Phys. Lett. **98**, 194105.
Rodriguez, A. W., D. Woolf, A. P. McCauley, F. Capasso, and S. G. Johnson, 2010, Phys. Rev. Lett. **105**, 060401.
Rodriguez-Lopez, P., 2009, Phys. Rev. E **80**, 061128.
Rodriguez-Lopez, P., 2011, Phys. Rev. B **84**, 165409.
Rodriguez-Lopez, P., and T. Emig, 2012, Phys. Rev. A **85**, 032510.
Rodriguez-Lopez, P., and A. G. Grushin, 2014, Phys. Rev. Lett. **112**, 056804.
Rodriguez-Lopez, P., W. J. M. Kort-Kamp, D. A. R. Dalvit, and L. M. Woods, 2016, arXiv:1609.05193.
Rodriguez-Lopez, P., S. J. Rahi, and T. Emig, 2009, Phys. Rev. A **80**, 022519.
Rodriguez-Reyes, J. C. F., C. G. F. Siler, W. Liu, A. Tkatchenko, C. M. Friend, and R. J. Madix, 2014, J. Am. Chem. Soc. **136**, 13333.
Rosa, F. S. S., 2009, J. Phys. Conf. Ser. **161**, 012039.
Rosa, F. S. S., D. A. R. Dalvit, and P. W. Milonni, 2008a, Phys. Rev. A **78**, 032117.
Rosa, F. S. S., D. A. R. Dalvit, and P. W. Milonni, 2008b, Phys. Rev. Lett. **100**, 183602.
Roth, C. M., and A. M. Lenhoff, 1996, J. Colloid Interface Sci. **179**, 637.
Roth, C. M., B. L. Neal, and A. M. Lenhoff, 1996, Biophys. J. **70**, 977.
Roy, A., C. Y. Lin, and U. Mohideen, 1999, Phys. Rev. D **60**, 111101.
Ruiz, V. G., W. Liu, E. Zojer, M. Scheffler, and A. Tkatchenko, 2012, Phys. Rev. Lett. **108**, 146103.
Ruzsinsky, A., J. Perdew, J. Tao, G. Csonka, and J. Pitarke, 2012, Phys. Rev. Lett. **109**, 233203.
Ryu, S., and T. Takayanagi, 2010, Phys. Lett. B **693**, 175.
Saito, R., G. Dresselhaus, and M. S. Dresselhaus, 1998, *Physical Properties of Carbon Nanotubes* (Imperial College Press, London).
Salis, A., and B. W. Ninham, 2014, Chem. Soc. Rev. **43**, 7358.
Santra, B., J. Klimeš, D. Alfe, A. Tkatchenko, B. Slater, A. Michaelides, R. Car, and M. Scheffler, 2011, Phys. Rev. Lett. **107**, 185701.
Sarabadani, J., A. Naji, R. Asgari, and R. Podgornik, 2011, Phys. Rev. B **84**, 155407.
Sasaki, K., K. Kato, Y. Tokura, and T. Sogawa, 2011, Phys. Rev. B **84**, 085458.
Sato, T., and H. Nakai, 2009, J. Chem. Phys. **131**, 224104.
Sato, T., and H. Nakai, 2010, J. Chem. Phys. **133**, 194101.
Saville, D. A., J. Chun, J.-L. Li, H. C. Schniepp, R. Car, and I. A. Aksay, 2006, Phys. Rev. Lett. **96**, 018301.
Schimelman, J. B., D. M. Dryden, L. Poudel, R. Podgornik, V. A. Parsegian, L. K. Denoyer, R. H. French, N. F. Steinmetz, and W.-Y. Ching, 2015, Phys. Chem. Chem. Phys. **17**, 4589.
Schmiedmayer, J., R. Folman, and T. Calarco, 2002, J. Mod. Opt. **49**, 1375.
Schnyder, A. P., S. Ryu, A. Furusaki, and A. W. W. Ludwig, 2008, Phys. Rev. B **78**, 195125.
Sedighi, M., V. B. Svetovoy, W. H. Broer, and G. Palasantzas, 2014, Phys. Rev. B **89**, 195440.
Sedmik, R., I. Vasiljevich, and M. Tajmar, 2007, J. Comput.-Aided Mater. Des. **14**, 119.
Semenoff, G., 1984, Phys. Rev. Lett. **53**, 2449.
Sernelius, B. E., 2011, Europhys. Lett. **95**, 57003.
Sernelius, B. E., 2012, Phys. Rev. B **85**, 195427.
Sernelius, B. E., 2015, J. Phys. Condens. Matter **27**, 214017.
Serry, F. M., D. Walliser, and G. J. Maclay, 1995, J. Microelectromech. Syst. **4**, 193.
Serry, F. M., D. Walliser, and G. J. Maclay, 1998, J. Appl. Phys. **84**, 2501.
Shalaev, V. M., 2007, Nat. Photonics **1**, 41.
Shao, C.-G., A.-H. Tong, and J. Luo, 2005, Phys. Rev. A **72**, 022102.
Sharma, A., P. Harnish, S. Sylvester, V. N. Kotov, and A. H. C. Castro Neto, 2014, Phys. Rev. B **89**, 235425.
Shelby, R. A., D. R. Smith, and S. Schultz, 2001, Science **292**, 77.
Shtogun, Y. V., and L. M. Woods, 2010, J. Phys. Chem. Lett. **1**, 1356.
Siber, A., R. F. Rajter, R. H. French, W. Y. Ching, V. A. Parsegian, and R. Podgornik, 2009, Phys. Rev. B **80**, 165414.
Silaghi, S. D., M. Friedrich, C. Cober, N. Esser, W. Braun, and D. R. T. Zahn, 2005, Phys. Status Solidi B **242**, 3047.
Silveirinha, M. G., 2010, Phys. Rev. B **82**, 085101.
Silveirinha, M. G., and S. I. Maslovski, 2010, Phys. Rev. Lett. **105**, 189301.
Silvestrelli, P. L., 2013, J. Chem. Phys. **139**, 054106.

Simpson, W. M. R., and U. Leonhardt, 2015, *Forces of the Quantum Vacuum: An Introduction to Casimir Physics* (World Scientific Publishing Co., New York).

Singh, G., K. E. Bremmell, H. J. Griesser, and P. Kingshott, 2015, Soft Matter **11**, 3188.

Sodemann, I., and M. Fogler, 2012, Phys. Rev. B **86**, 115408.

Song, X., 2002, J. Chem. Phys. **116**, 9359.

Song, X., and X. Zhao, 2004, J. Chem. Phys. **120**, 2005.

Sonmezoglu, S., and O. Sonmezoglu, 2011, Mater. Sci. Eng., C **31**, 1619.

Sontz, P. A., N. B. Muren, and J. K. Barton, 2012, Acc. Chem. Res. **45**, 1792.

Sparnaay, M. J., 1958, Physica (Utrecht) **24**, 751.

Spataru, C., M. A. Cazalilla, A. Rubio, L. X. Benedict, P. M. Echenique, and S. G. Louie, 2001, Phys. Rev. Lett. **87**, 246405.

Spataru, C., S. Ismail-Beigi, L. X. Benedict, and S. G. Louie, 2004, Phys. Rev. Lett. **92**, 077402.

Spataru, C., S. Ismail-Beigi, R. Capaz, and S. G. Louie, 2005, Phys. Rev. Lett. **95**, 247402.

Stark, A. Y., I. Badge, N. A. Wucinich, T. W. Sullivan, P. H. Niewiarowski, and A. Dhinojwala, 2013, Proc. Natl. Acad. Sci. U.S.A. **110**, 6340.

Stark, L., D. M. Dryden, K. Peterson, R. H. French, and A. Dhinojwala, 2015, J. R. Soc. Interface **12**, 20150464.

Stedman, T., D. Drosdoff, and L. M. Woods, 2014, Phys. Rev. A **89**, 012509.

Stehle, C., H. Bender, C. Zimmermann, D. Kern, M. Fleischer, and S. Slama, 2011, Nat. Photonics **5**, 494.

Steinmann, S., and C. Corminboeuf, 2011, J. Chem. Theory Comput. **7**, 3567.

Stone, H. A., and S. Kim, 2001, AIChE J. **47**, 1250.

Strikwerda, J., 1989, *Finite Difference Schemes and Partial Differential Equations* (Wadsworth and Brooks/Cole, Pacific Grove, CA).

Sun, J., B. Xiao, Y. Fang, R. Haunschild, P. Hao, A. Ruzsinszky, G. Csonka, G. Scuseria, and J. Perdew, 2013, Phys. Rev. Lett. **111**, 106401.

Sushkov, A. O., W. J. Kim, D. A. R. Dalvit, and S. K. Lamoreaux, 2011, Nat. Phys. **7**, 230.

Svetovoy, V., Z. Moktadir, M. Elwenspoek, and H. Mizuta, 2011, Europhys. Lett. **96**, 14006.

Taflove, A., and S. C. Hagness, 2000, *Computational Electrodynamics: The Finite-Difference Time-Domain Method* (Artech, Norwood, MA).

Tai, C. T., 1994, *Dyadic Green Functions in Electromagnetic Theory* (IEEE Press, Piscataway, NJ).

Tajmar, M., 2004, Int. J. Mod. Phys. C **15**, 1387.

Takatani, T., E. G. Hohenstein, M. Malagoli, M. S. Marshall, and C. D. Sherrill, 2010, J. Chem. Phys. **132**, 144104.

Tang, K., and J. P. Toennies, 1984, J. Chem. Phys. **80**, 3726.

Tang, L., J. Zhou, H. Chan, M. Nikolic, and A. W. Rodriguez, 2015, Bull. Am. Phys. Soc. **60**, Q16.00012 [http://meetings.aps.org/Meeting/MAR15/Session/Q16.12].

Tao, J., and J. P. Perdew, 2014, J. Chem. Phys. **141**, 141101.

Tao, J., J. P. Perdew, and A. Ruzsinszky, 2010, Phys. Rev. B **81**, 233102.

Tasaki, S., K. Maekawa, and T. Yamabe, 1998, Phys. Rev. B **57**, 9301.

Tkatchenko, A., 2015, Adv. Funct. Mater. **25**, 2054.

Tkatchenko, A., D. Alfè, and K. S. Kim, 2012, J. Chem. Theory Comput. **8**, 4317.

Tkatchenko, A., A. Ambrosetti, and R. A. DiStasio, Jr., 2013, J. Chem. Phys. **138**, 074106.

Tkatchenko, A., R. A. DiStasio, Jr., M. Head-Gordon, and M. Scheffler, 2009, J. Chem. Phys. **131**, 094106.

Tkatchenko, A., R. A. DiStasio, Jr., R. Car, and M. Scheffler, 2012, Phys. Rev. Lett. **108**, 236402.

Tkatchenko, A., L. Romaner, O. T. Hofmann, E. Zojer, C. Ambrosch-Draxl, and M. Scheffler, 2010, MRS Bull. **35**, 435.

Tkatchenko, A., and M. Scheffler, 2009, Phys. Rev. Lett. **102**, 073005.

Tomaš, M. S., 2002, Phys. Rev. A **66**, 052103.

Torricelli, G., P. J. van Zwol, O. Shpak, C. Binns, G. Palasantzas, B. J. Kooi, V. B. Svetovoy, and M. Wutting, 2010, Phys. Rev. A **82**, 010101(R).

Torricelli, G., P. J. van Zwol, O. Shpak, G. Palasantzas, V. B. Svetovoy, C. Binns, B. J. Kooi, P. Jost, and M. Wutting, 2012, Adv. Funct. Mater. **22**, 3729.

Tristram-Nagle, S., and J. F. Nagle, 2004, Chem. Phys. Lipids **127**, 3.

Trondle, M., S. Kondrat, A. Gambassi, L. Harnau, and S. Dietrich, 2010, J. Chem. Phys. **133**, 074702.

Tse, W.-K., and A. H. MacDonald, 2010, Phys. Rev. Lett. **105**, 057401.

Tse, W.-K., and A. H. MacDonald, 2011, Phys. Rev. B **84**, 205327.

Tse, W.-K., and A. H. MacDonald, 2012, Phys. Rev. Lett. **109**, 236806.

Tsoi, S., P. Dev, A. L. Friedman, R. Stine, J. T. Robinson, T. L. Reinecke, and P. E. Sheehan, 2014, ACS Nano **8**, 12410.

van Enk, S. J., 1995a, J. Mod. Opt. **42**, 321.

van Enk, S. J., 1995b, Phys. Rev. A **52**, 2569.

van Kampen, N. G., B. R. Nijober, and K. Schram, 1968, Phys. Lett. **26A**, 307.

van Zwol, P. J., G. Palasantzas, and J. T. M. De Hosson, 2008, Phys. Rev. B **77**, 075412.

van Zwol, P. J., G. Palasantzas, and J. T. M. De Hosson, 2009, Phys. Rev. B **79**, 195428.

Veble, G., and R. Podgornik, 2007, Eur. Phys. J. E **23**, 275.

Veble, G., and R. Podgornik, 2009, Phys. Rev. B **80**, 075422.

Veselago, V. G., 1968, Sov. Phys. Usp. **10**, 509.

Voet, D., W. Gratzer, R. Cox, and P. Doty, 1963, Biopolymers **1**, 193.

Vydrov, O., and T. Van Voorhis, 2009, Phys. Rev. Lett. **103**, 063004.

Vydrov, O., and T. Van Voorhis, 2010, Phys. Rev. A **81**, 062708.

Vydrov, O. A., and T. Van Voorhis, 2012, J. Chem. Theory Comput. **8**, 1929.

Wagner, C., N. Fournier, V. Ruiz, C. Li, K. Mullen, M. Rohlfing, A. Tkatchenko, R. Temirov, and F. Tautz, 2014, Nat. Commun. **5**, 5568.

Wallace, P., 1947, Phys. Rev. **71**, 622.

Wang, F., G. Dukovic, L. Brus, and T. Heinz, 2005, Science **308**, 838.

Weber, A., and H. Gies, 2010a, Phys. Rev. D **82**, 125019.

Weber, A., and H. Gies, 2010b, Phys. Rev. Lett. **105**, 040403.

Weikel, T., 2003, Eur. Phys. J. E **12**, 265.

Welding, T. O., A. M. Black-Schaffer, and A. V. Balatsky, 2014, Adv. Phys. **63**, 1.

Wilczek, F., 1987, Phys. Rev. Lett. **58**, 1799.

Wilen, L. A., J. S. Wettlaufer, M. Elbaum, and M. Schick, 1995, Phys. Rev. B **52**, 12426.

Wilson, J. H., A. A. Allocca, and V. M. Galistki, 2015, Phys. Rev. B **91**, 235115.

Wiser, N., 1963, Phys. Rev. **129**, 62.

Woods, L. M., A. Popescu, D. Drosdoff, and I. V. Bondarev, 2013, Chem. Phys. **413**, 116.

Wu, Q., and W. Yang, 2002, J. Chem. Phys. **116**, 515.

Wu, X., M. C. Vargas, S. Nayak, S. Lotrich, and G. Scoles, 2001, J. Chem. Phys. **115**, 8748.

Xiong, J., and W. C. Chew, 2009, Appl. Phys. Lett. **95**, 154102.

Xiong, J. L., M. S. Tong, P. Atkins, and W. C. Chew, 2010, Phys. Lett. A **374**, 2517.
Yablonovitch, E., 1987, Phys. Rev. Lett. **58**, 2059.
Yablonovitch, E., T. J. Gmitter, and K. M. Leung, 1991, Phys. Rev. Lett. **67**, 2295.
Yamarty, C., and S. McNamara, 2009, IEEE Int. Conf. Nano/Micro Eng. Mol. Syst., 645.
Yannopapas, V., and N. V. Vitanov, 2009, Phys. Rev. Lett. **103**, 120401.
Yasar, S., R. Podgornik, J. Valle-Orero, M. R. Johnson, and V. A. Parsegian, 2015, Sci. Rep. **4**, 6877.
Yaziev, O., 2010, Rep. Prog. Phys. **73**, 056501.
Yolcu, C., and M. Deserno, 2012, Phys. Rev. E **86**, 031906.
Yolcu, C., I. Z. Rothstein, and M. Deserno, 2011, Europhys. Lett. **96**, 20003.
Young, K. L., M. B. Ross, M. G. Blaber, M. Rycenga, M. R. Jones, C. Zhang, A. J. Senesi, B. Lee, G. C. Schatz, and C. A. Mirkin, 2014, Adv. Mater. **26**, 653.
Yu, J., S. Chary, S. Das, J. Tamelier, N. S. Pesika, K. L. Turner, and J. N. Israelachvili, 2011, Adv. Funct. Mater. **21**, 3010.
Zacharia, R., H. Ulbricht, and T. Hertel, 2004, Phys. Rev. B **69**, 155406.
Zaheer, S., A. W. Rodriguez, S. G. Johnson, and R. L. Jaffe, 2007, Phys. Rev. A **76**, 063816.
Zalar, A., D. Tepfer, S. Hoffmann, J. Kenney, and S. Leach, 2007, Int. J. Astrobiol. **6**, 229.
Zhang, G.-X., A. Tkatchenko, J. Paier, H. Appel, and M. Scheffler, 2011, Phys. Rev. Lett. **107**, 245501.
Zhang, H.-J., C.-X. Liu, X.-L. Qi, X. Dai, Z. Fang, and S.-C. Zhang, 2009, Nat. Phys. **5**, 438.
Zhang, Y., and W. Yang, 1998, Phys. Rev. Lett. **80**, 890.
Zhao, B. S., S. A. Schulz, S. A. Meek, G. Meijer, and W. Schöllkopf, 2008, Phys. Rev. A **78**, 010902.
Zhao, R., J. Zhou, T. Koschny, E. N. Economou, and C. M. Soukoulis, 2009, Phys. Rev. Lett. **103**, 103602.
Zhao, R., J. Zhou, T. Koschny, E. N. Economou, and C. M. Soukoulis, 2010, Phys. Rev. Lett. **105**, 189302.
Zhao, Y., and D. G. Truhlar, 2008, Theor. Chem. Acc. **120**, 215.
Zheng, J., J. J. Birktoft, Y. Chen, T. Wang, R. Sha, P. E. Constantinou, S. L. Ginell, C. Mao, and N. C. Seeman, 2009, Nature (London) **461**, 74.
Zheng, Y., and T. Ando, 2002, Phys. Rev. B **65**, 245420.
Zho, J., Z. Marcet, A. W. Rodriguez, M. T. H. Reid, A. P. McCauley, I. I. Kravchenko, T. Lu, Y. Bao, S. G. Johnson, and H. B. Chan, 2013, Nat. Commun. **4**, 1845.
Zhou, F., and L. Spruch, 1995, Phys. Rev. A **52**, 297.
Zimmerli, U., M. Parrinello, and P. Koumotsakos, 2004, J. Chem. Phys. **120**, 2693.